SERA
Seismology and Earthquake Engineering
Research Infrastructure Alliance for Europe

DELIVERABLE

D26.4 Methods for Estimating Site Effects in Risk Assessments

Work package	WP26 (JRA4: Risk Modelling Framework for Europe)
Lead	EUCE
Authors	Helen Crowley, EUCE Graeme Weatherill, GFZ Evi Riga, AUTH Kyriazis Pitilakis, AUTH Agathe Roullé, BRGM Bruno Tourlière, BRGM Anne Lemoine, BRGM Cécile Gracianne Hidalgo, BRGM
Reviewers	Management Board
Approval	Management Board
Status	Final
Dissemination level	Public
Delivery deadline	30.04.2019
Submission date	30.04.2019
Intranet path	DOCUMENTS/DELIVERABLES/SERA_D26.4_Site_Amplification_Risk_Assessment

This project has received funding from the European Union's Horizon 2020 research and innovation programme under grant agreement No 730900.

Table of Contents

Summary 4
1 Introduction 5
2 Harmonised Geology and Topography at European Scale 6
2.1 Harmonised geological map using OneGeology and Promine 6
2.1.1 Step one: simplified coding of the ProMine geological map 6
2.1.2 Step two: coding improvement from OG data 7
2.1.3 Step three – Stratigraphic coding 10
2.1.4 Step four: constitution of the final harmonized geological map 10
2.2 Topography 12
3 Sources of Measured V_{S30} Data Across Europe 13
4 Correlation of V_{S30} with topography and geology 16
4.1 Correlation between topography and V_{S30} 16
4.1.1 Wald and Allen methodology 16
4.1.2 Evaluations, limitations and perspectives 20
4.2 Correlation between geology and V_{S30} 21
4.2.1 An attempt to build a SERA geology-based model 23
4.2.2 Alternative geology-based model 26
4.2.3 Limitations and perspectives 27
5 Correlation of $\delta S2S_S$ with proxies (topography and geology), observed and measured V_{S30} 29
5.1 Fitting an amplification model to $\delta S2SS$ 30
5.2 Incorporating geology into site amplification models 33
5.3 Regional site amplification without V_{S30} 37
5.4 Potential for modelling site amplification at European scale 40
6 Nonlinear site amplification model for site classes 44
6.1 Site amplification data 44
6.2 Description of soil classification scheme 46
6.3 Elastic response spectra and nonlinear soil amplification factors 49
7 Implementation and Comparison of Site Amplification Models 52
7.1 OpenQuake-engine implementations 52
7.1.1 Technical Considerations in the OpenQuake-engine implementation 52
7.1.2 Site Amplification According to Design Code Factors 53
7.1.3 Site amplification from generalised amplification models 54
7.1.4 Site amplification from inferred proxy models for Europe 55
7.2 Comparison of models – scenario earthquake 56
7.3 Comparison of models – PSHA 63
8 Conclusions 67

9 Acknowledgements 68
10 References 68
Contact 72

Summary

This deliverable summarises the research undertaken by the partners of the site amplification working group of SERA (comprising BRGM, AUTH and GFZ as the main partners) that have each investigated different methods for including site amplification within a seismic risk assessment. EUCE has managed the activities of the group, as the leader of the SERA JRA4 work package. BRGM and GFZ have focused on European scale site amplification, with BRGM putting together proxy datasets on geology and topography and looking at their correlation with V_{S30}, and GFZ considering how these proxy datasets correlate with the site term in a new shallow crustal ground motion model, and how uncertainties related to site amplification should be propagated in the risk assessment. AUTH have focused on a nonlinear site amplification model that can be used for local scale risk assessment, when more detailed information is available to characterize the site. All methods are presented herein together with some preliminary comparisons in terms of the impact of different amplification models on the spectra from scenario earthquakes as well as hazard curves. However, further testing of the methods, within the European seismic risk framework, is planned to continue during the final 12 months of the project.

1 Introduction

As part of the development of a seismic risk modelling framework for Europe (see Deliverable D26.7: Crowley et al., 2019), models of site characterisation and amplification that can be integrated into a probabilistic seismic hazard and risk assessment (PSHRA) at different scales (local to continental) are needed.

Since the beginning of the SERA project, the partners working on this interface between seismic hazard and risk have decided to develop and apply an efficient and practical approach that goes beyond the use of topography to infer the 30-m averaged shear-wave velocity, V_{S30} (e.g. Wald and Allen, 2007), given the shortcomings that have been identified for this approach, especially in stable continental regions (e.g. Lemoine et al., 2012). Recent studies have also inferred site properties from quantities including surface geology (Wills and Clahan, 2006; Vilanova et al., 2018), surface morphology (Iwahashi and Pike, 2007), geotechnical descriptors (Seyhan and Stewart, 2014) and hybrid methods (Ahdi et al., 2017). Furthermore, there is evidence that including additional parameters that are available at the local scale, such as depth to bedrock geology features and fundamental period (T_0), leads to a better estimation of the site effects than V_{S30} alone (e.g. Derras et al., 2017), considering also that the latter is still a proxy for site amplification.

This deliverable investigates the use of both topography and geology as proxies for site characterisation at the continental scale. The next chapter of the deliverable describes how harmonised Europe-wide proxy datasets of geology and topography have been developed. The correlation of these proxies with V_{S30} is first investigated in Chapter 4 (such that the latter could be used as input to ground-motion models with inferred V_{S30} site models), and then Chapter 5 presents a new shallow crustal ground motion model with a geologically-calibrated slope amplification model (thus bypassing the use of V_{S30} within the ground-motion modelling). At the local scale, a nonlinear site amplification model is proposed in Chapter 6 that characterises the site using both V_{S30} and T_0 and provides amplification factors that are calibrated using strong motion simulations (and thus extends beyond available ground motion data which often does not does show significant nonlinearity). The latter approach is more geared towards use within seismic design codes, but it has been integrated within a seismic risk framework herein (using the OpenQuake-engine) such that it can be directly compared with the aforementioned proxy-based regional approaches (as presented in Chapter 7). The final chapter of this deliverable summarises the topics that could benefit from further research and testing.

2 Harmonised Geology and Topography at European Scale

This chapter of the deliverable describes how harmonised Europe-wide proxy datasets of geology and topography have been developed.

2.1 Harmonised geological map using OneGeology and Promine

An initial task required by the site amplification working group (and undertaken by BRGM) was to create a geological map devoted to the SERA project with a simplified lithology and stratigraphy. The 1:1 500 000 scale map from the European funded project ProMine (2009-2012) has been used as the basic map because of its good level of information in solid geology and its completeness over the majority of the SERA geographical scope. However, that map is not very accurate for recent formations, essentially in northeastern Europe and so, when it was possible, the information has been completed by the information provided by the « OneGeology » (OG) 1:1 000 000 scale map. In summary, here are the main characteristics of the two available geological maps over Europe:

- EGDI map (from OneGeology-Europe project, 2016)
  - ✓ 1:1 M scale
  - ✓ Harmonized map of lithological and stratigraphic information delivered the geological surveys of 21 countries using INSPIRE data models
  - ✓ Focused on outcropping superficial formations
  - ✓ Not complete for SERA extent: 15 countries missing (from which Austria, Greece, Iceland, Switzerland, and most of the Balkan countries)
  - ✓ http://www.europe-geology.eu/metadata
- Promine map (2012)
  - ✓ 1:1,5 M map
  - ✓ Lithological and stratigraphic information based on main geological events (Caledonian, variscan and alpine orogenies)
  - ✓ For mineral resources purpose: focus on solid geology
  - ✓ Not complete for SERA extent but with a better coverage than EGDI map: Iceland is missing
  - ✓ http://promine.gtk.fi/

2.1.1 Step one: simplified coding of the ProMine geological map

To create a litho-stratigraphic map over Europe, the first step consisted in creating a simplified lithological coding from the lithological descriptions contained in the ProMine attribute table. When several lithologies are described, BRGM have decided to consider only the first one, regarded as the dominant one. Table 1 summarizes the final lithological codes and the corresponding lithologies.

Some remarks about the simplified lithological codes:

- COAL is related to coal basin meaning mainly detrital rocks interlayed by coal layers;
- SALT corresponds to formations containing salty layers (gypsum, salt);
- MUD corresponds to unconsolidated formations essentially present in France and Germany that can be related to alluviums;
- SDMT corresponds to undifferentiated mainly poorly consolidated sediments;
- TILL means glacial formations;
- METAM vs. SCHST: schists (rocks of low metamorphic grade) has been differentiated from higher metamorphic grade rock like micaschists, gneisses or migmatites;
- PLTE (Pelite in ProMine) and CLST (Clastic rocks in OG) could be considered as a unique family of rocks.

Table 1: Simplified lithological codes and corresponding geological descriptions.

Simplified Code	Legend	Simplified Code	Legend
ALLU	Alluvium	PLTE	Pelites, shales
CARB	Carbonaceous formations (Peat)	SAGR	Sands and Gravels
CGRT	Conglomerates	SALT	Formations with salts
CHLK	Chalk	SAND	Sands
CLAY	Clay	SCHST	Schists and slates
CLST	Clastic Rocks	SDMT	Undifferentiated sediments
COAL	Coal basins	SFOR	Soils and/or Loess
FELSIC	Felsic igneous rocks	SILT	Silts
FLINT	Formations with dominant flints	SSTN	Sandstones
IMPCT	Impactite	TECTO	Tectonic breccias and mylonites
LAKES	Lakes	TILL	Tills
LMST	Limestone and dolomites	UMAFIC	Ultramafic igneous rocks
MAFIC	Mafic igneous rocks	UNCS	Unconsolidated formations
MARL	Marls	VOLC	Volcanic formations
METAM	Metamorphic rocks (from micaschists to migmatites)	WASTE	Anthropic formations
MUD	Mud – unconsolidated sediments		

2.1.2 Step two: coding improvement from OG data

In the ProMine map, recent geological formations are generally poorly described, e.g. the 'undifferentiated sediments' of Northern Germany and Poland (e.g. beige areas in Figure 1), whereas in the OG map, those areas are more detailed.

To improve that, BRGM have decided to replace the simplified code « SDMT» (undifferentiated sediments) of Promine map by the simplified codes coming from the OG map as shown in Figure 2.

Even though no information is added in Turkey (due to lack of information in OG map), the map is significantly improved in Germany and Poland.

The replacement of the simplified ProMine coding by the simplified OG coding was done by a Union operation and selection/copy in the corresponding attribute (Simp attribute in ArcGIS file).

Furthermore, that operation has updated the lithological coding of Atlantic islands (Azores, Madeira and Canary Islands). The junction between the two maps is globally correct even if some sharp limits can be observed, especially in Northern Europe as shown in Figure 3.

The final European lithological map is presented in Figure 4.

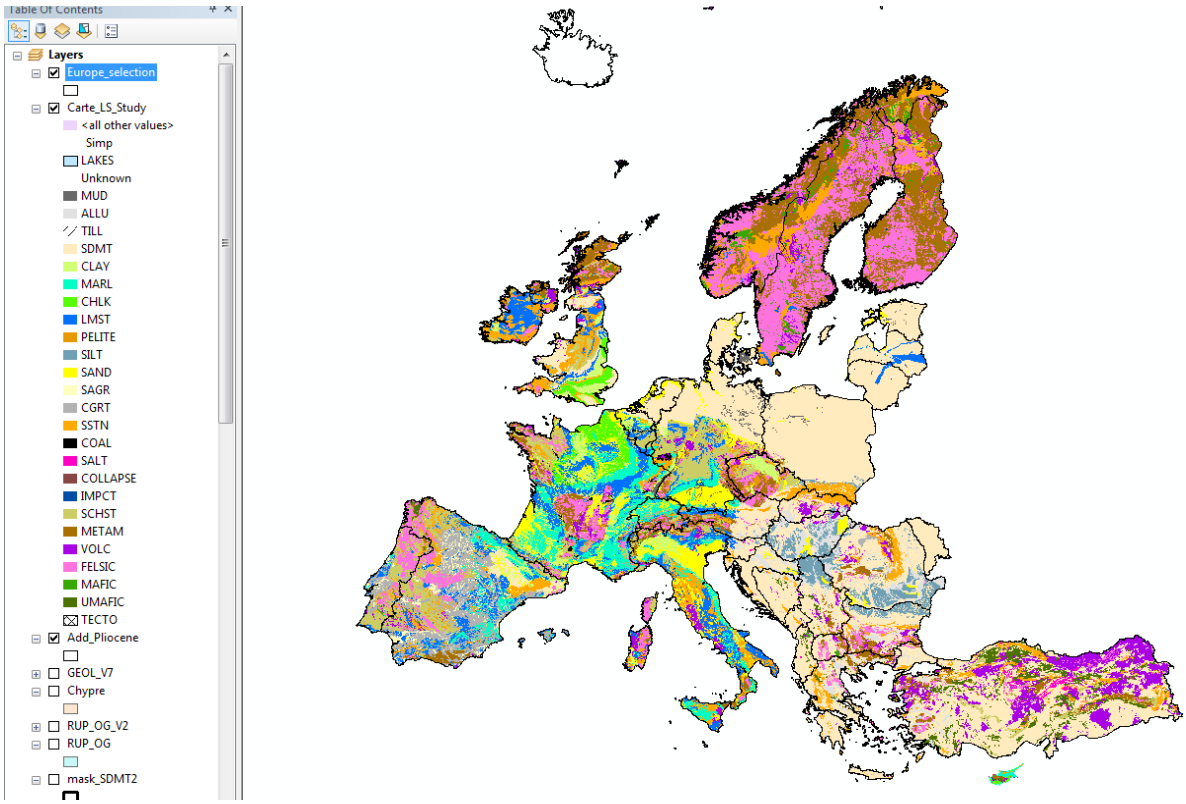

Figure 1: simplified lithological coding of the ProMine Map

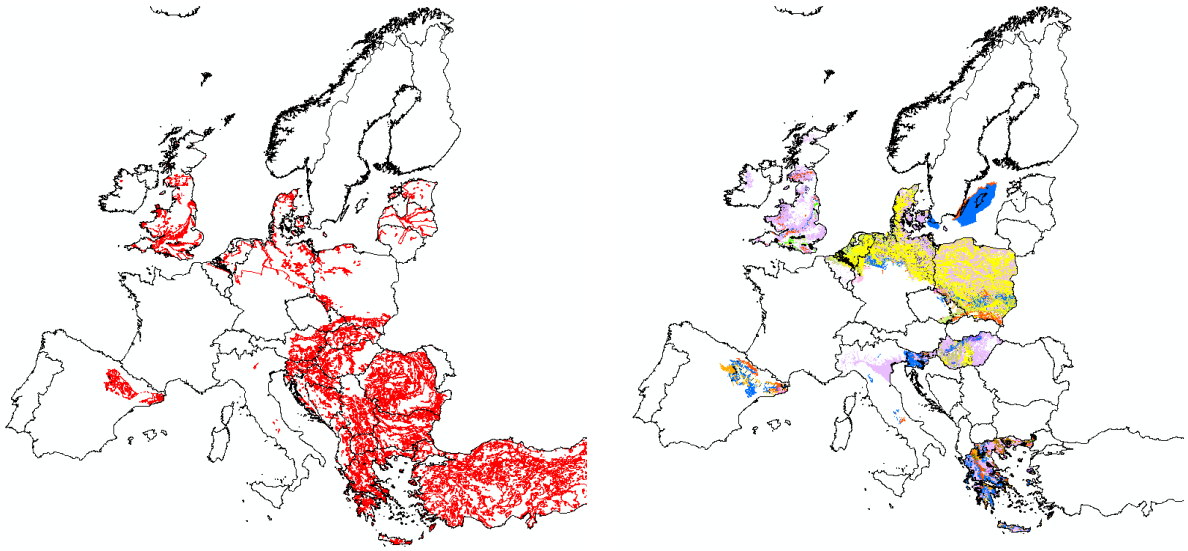

Extension of SDMT polygons on the ProMine map.

Replacement of the SDMT code by the lithological information from the OG map.

Figure 2 : selection of SDMT simplified code zones of Promine map (in red) and replacement by the OG simplified coded polygons where they are superimposed.

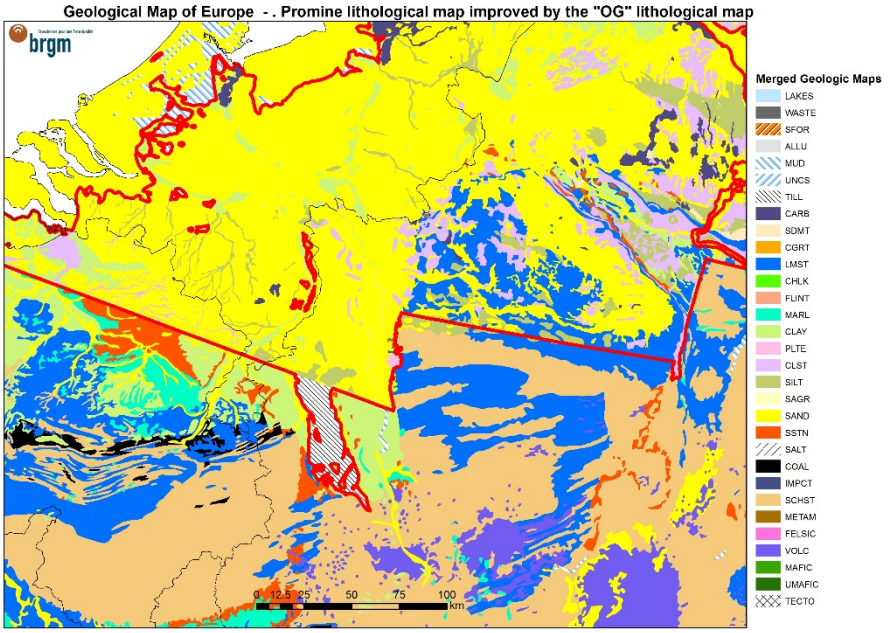

Figure 3: Example of contact between ProMine simplifed code (south of red line) and OG simplified codes (north of red line)

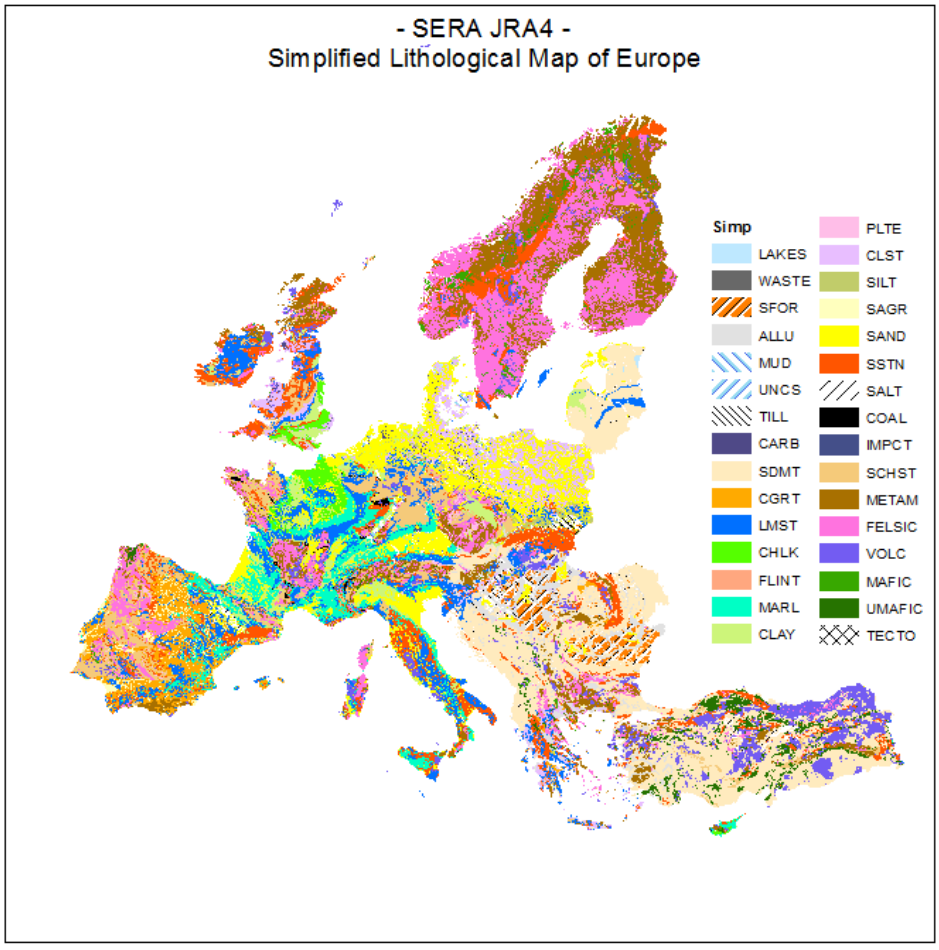

Figure 4: Final lithological map after union between ProMine polygons and OG polygons.

2.1.3 Step three – Stratigraphic coding

As much as possible, stratigraphic coding has been detailed for quaternary and tertiary formations, those formations being considered as potentially less consolidated, so prone to site effects, than the older ones. Before the Tertiary, only Epoch or Era are considered. Table 2 and Figure 5 present the final stratigraphic classification and deduced European stratigraphic map.

Table 2: Stratigraphic coding

Strati	Epoch	Era	Era_simp
UK	UNKNOWN	UNKNOWN	UK
PH	PHANEROZOIC	PHANEROZOIC	PH
CN	CENOZOIC	CENOZOIC	CN
HC	HOLOCENE	HOLOCENE	HO
PC	PLEISTOCENE	CENOZOIC	CN
PL	PLIOCENE	CENOZOIC	CN
MC	MIOCENE	CENOZOIC	CN
NG	NEOGENE	CENOZOIC	CN
OL	OLIGOCENE	CENOZOIC	CN
EC	EOCENE	CENOZOIC	CN
PG	PALEOGENE	CENOZOIC	CN
CR	CRETACEOUS	MESOZOIC	MS
JR	JURASSIC	MESOZOIC	MS
TR	TRIAS	MESOZOIC	MS
PZ	PALEOZOIC	PALEOZOIC	PZ
PK	PRECAMBRIAN	PRECAMBRIAN	PK

2.1.4 Step four: constitution of the final harmonized geological map

Finally, lithological and stratigraphic codes are stored as attributes in a dbf database associated to the Geol_V7 polygons shapefiles. These data were sent to the other SERA site amplification working group partners in November 2018 (shapefile format). In summary, the final litho-stratigraphic data is described as follows:

- Lithological classes:
  - ✓ mainly based on ProMine map, with the primary lithology (if more)
  - ✓ completed by OG information for superficial formations when available (e.g. undetermined sediments)
  - ✓ some lithologies were added if not existing in ProMine map (e.g. Clastic Rocks)
  - ✓ 33 final classes
- Stratigraphic classes:
  - ✓ Detailed for Quaternary and Tertiary deposits
  - ✓ For ancient periods, only information on Epoch or Era
  - ✓ 16 final classes
- Litho-stratigraphic information
  - ✓ Combine lithological and stratigraphic class (ex. HO-ALLU=Holocene Alluvium)
  - ✓ 140 final classes

It is noted that the OG and ProMine scopes did not include Iceland, so that this country is not covered by our maps. This gap will attempt to be filled in future research.

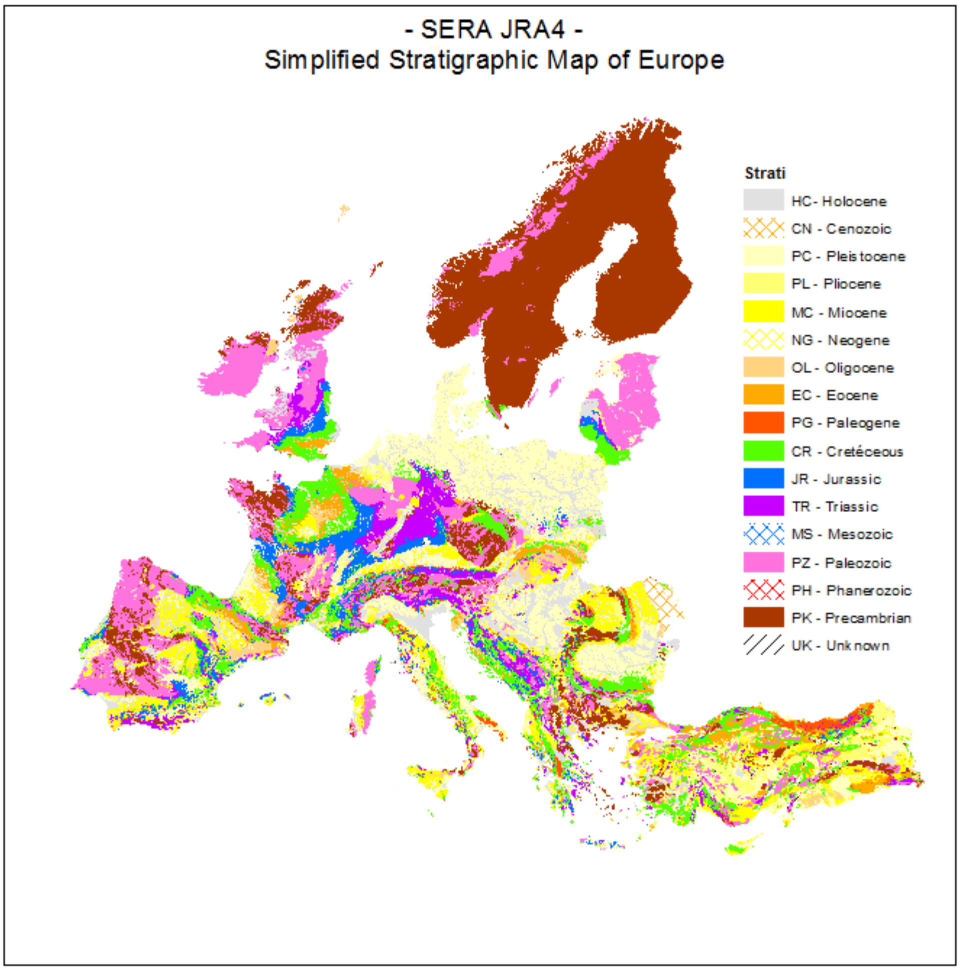

Figure 5: Final stratigraphic map.

Table 1: Extract of the final database containing lithological and stratigraphic codes.

GEOL_V7

FID	Shape *	Simp	Strati	LTH_STR	ERA	ERA_simp
1381	Polygon	CLAY	PL	PL-CLAY	CENOZOIC	CN
1381	Polygon	CLAY	PL	PL-CLAY	CENOZOIC	CN
1381	Polygon	CLAY	PL	PL-CLAY	CENOZOIC	CN
1381	Polygon	CLAY	PL	PL-CLAY	CENOZOIC	CN
1381	Polygon	CLAY	PL	PL-CLAY	CENOZOIC	CN
1381	Polygon	CLAY	PL	PL-CLAY	CENOZOIC	CN
1381	Polygon	CLAY	PL	PL-CLAY	CENOZOIC	CN
1381	Polygon	CLAY	PL	PL-CLAY	CENOZOIC	CN
1381	Polygon	CLAY	PL	PL-CLAY	CENOZOIC	CN
1382	Polygon	CLAY	PL	PL-CLAY	CENOZOIC	CN
1382	Polygon	CLAY	PL	PL-CLAY	CENOZOIC	CN
1382	Polygon	CLAY	PL	PL-CLAY	CENOZOIC	CN
1382	Polygon	CLAY	PL	PL-CLAY	CENOZOIC	CN
1382	Polygon	CLAY	PL	PL-CLAY	CENOZOIC	CN
1382	Polygon	CLAY	PL	PL-CLAY	CENOZOIC	CN
1382	Polygon	CLAY	PL	PL-CLAY	CENOZOIC	CN
1382	Polygon	CLAY	PL	PL-CLAY	CENOZOIC	CN
1382	Polygon	CLAY	PL	PL-CLAY	CENOZOIC	CN
1382	Polygon	CLAY	PL	PL-CLAY	CENOZOIC	CN
1383	Polygon	CLAY	PL	PL-CLAY	CENOZOIC	CN
1383	Polygon	CLAY	PL	PL-CLAY	CENOZOIC	CN
1383	Polygon	CLAY	PZ	PZ-CLAY	PALEOZOIC	PZ
1383	Polygon	CLAY	PZ	PZ-CLAY	PALEOZOIC	PZ
1383	Polygon	CLAY	PZ	PZ-CLAY	PALEOZOIC	PZ
1383	Polygon	CLAY	PZ	PZ-CLAY	PALEOZOIC	PZ
1383	Polygon	CLAY	PZ	PZ-CLAY	PALEOZOIC	PZ
1383	Polygon	CLAY	PZ	PZ-CLAY	PALEOZOIC	PZ
1383	Polygon	CLAY	PZ	PZ-CLAY	PALEOZOIC	PZ
1383	Polygon	CLAY	PZ	PZ-CLAY	PALEOZOIC	PZ
1384	Polygon	CLAY	PZ	PZ-CLAY	PALEOZOIC	PZ

2.2 Topography

A number of different global topographic data sets are currently publicly available. The Wald and Allen (2007) study that correlated topography with V_{S30} was built on slope calculations based on SRTM30, a 30 arc-second (~1000 m) land topography data set (Farr and Kobrick, 2000). It is a near-global digital elevation model (DEM) combining data from the Shuttle Radar Topography Mission and the U.S. Geological Survey's GTOPO30 data set. Over the years, upgrading and integration of different data sets led to different releases and improved resolution. For example, NASA SRTM Global 1 arc second grid is now available (Version 3.0, SRTMGL1, about 30 meters resolution). SRTM data sets also include the global 3 arc-second (~90 m) sub-sampled product, derived from the 1 arc second product (SRTMGL3).

However, Allen and Wald (2009) tested higher than 30 arc second resolution data as input for site classification from topographic slopes. They did not find evidence of statistical improvement of accuracy for site classification maps, as neither did Roullé et al. (2010) for France.

For consistency on one hand with the Wald and Allen (2007) approach, and on the other hand with the geological maps at continental scale, we choose to keep a 30 arc second resolution for topography.

Another global 30 arc-second DEM is also available: GEBCO_2014. This is a global terrain model for ocean and land, based on SRTM_Plus (v5) data set (Becker et al., 2009). It includes bathymetric compilations in different areas, and land topography is based on SRTM30 (v2.0, Farr et al., 2007).

3 Sources of Measured V_{S30} Data Across Europe

This chapter summarises the data set of measured V_{S30} that has been compiled for the purposes of testing the correlation between V_{S30} and the proxy datasets for regional site amplification.

An effort has been made to collect all publicly available data on site characterization (with measured V_{S30} values) at a European scale. An initial proposal was Engineering Strong Motion (ESM) database (Luzi et al., 2016a; 2016b) would provide a good source of data for this purpose. However, an initial analysis of this database (DB) showed that only 469 measured V_{S30} values were available in this DB, mainly from Greece, Italy and Turkey. This very poor spatial coverage induced a strong spatial bias in the analysis and was not enough to build a reliable slope-V_{S30} or geology-V_{S30} correlation for Europe. A complementary collection effort was thus performed between December 2018 and February 2019, which led to a complete database of 1626 measured V_{S30} values all over Europe. The different contributions came from (see Figure 6):

- The ESM DB describing site characterization for European Strong Motion stations (Luzi et al., 2016; 2016b);
- SHARE data from Switzerland (contributor: ETHZ) and France (contributor: BRGM) described in Lemoine et al. (2012) and Roullé et al. (2010);
- Portuguese data used in the geologically based V_{S30} site-condition model of Vilanova et al. (2018);
- Dutch data from the site characterization of Groningen gas field (Noorlandt et al., 2018);
- Greek data used for inferring V_{S30} values from geologic- and terrain-base proxies (Stewart et al., 2014);
- Turkish data from the National Strong Motion project of Turkey and from a microzonation study on the city if Istanbul (Yilmaz et al., 2014).

Different methods were used for V_{S30} measurements depending mainly on the operator responsible for the acquisition (Figure 7 and Figure 8), including:

- Active seismic methods:
  - Refraction;
  - Active Surface Wave (e.g. MASW, SASW);
- Passive seismic methods:
  - Passive Surface Wave (e.g. Array measurements, Remi);
- Combination of active and passive methods
- Geotechnical methods (e.g. SCPT)
- Borehole methods (e.g. Downhole, Crosshole, PS Logging)
- Combination of borehole method and passive seismic methods.

The distribution of V_{S30} values in terms of acquisition methods shows that most of the data come from active seismic acquisition (MASW), which represents 44% of the dataset, and from borehole methods, which represents 33% of the dataset.

The use of different acquisition methods for estimating VS profiles can give rise to uncertainties, but the recent papers of Garofalo et al. (2016a and 2016b) showed that it does not induce significant variation in V_{S30} estimation and this it has not been considered further in the methods proposed herein.

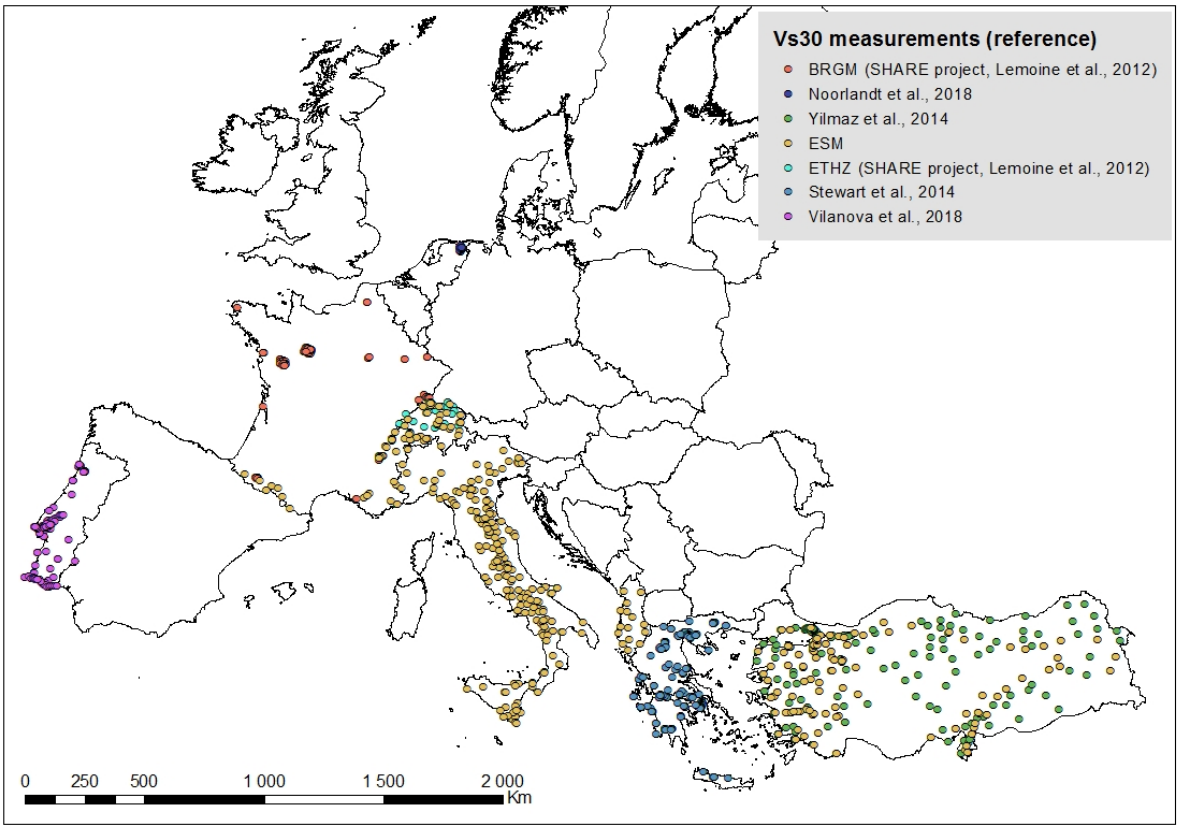

Figure 6: Location of the measured V_{S30} values used in SERA project for inferring a European correlation between slope/geology and V_{S30}.

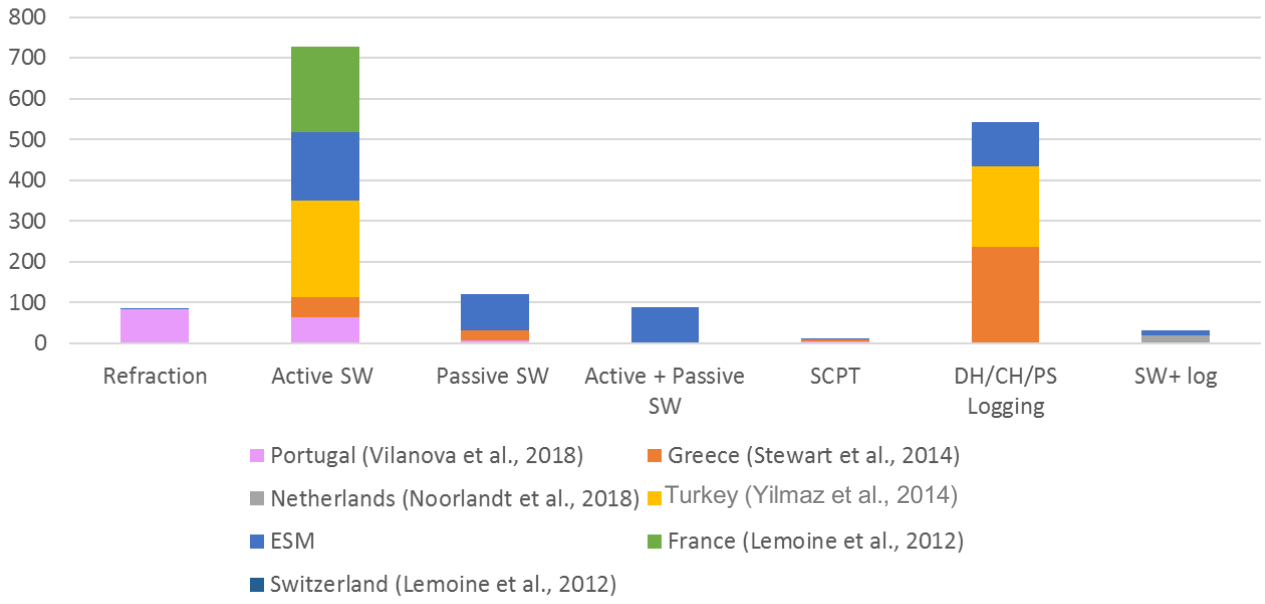

Figure 7: V_{S30} dataset of SERA project: acquisition methods and providers.

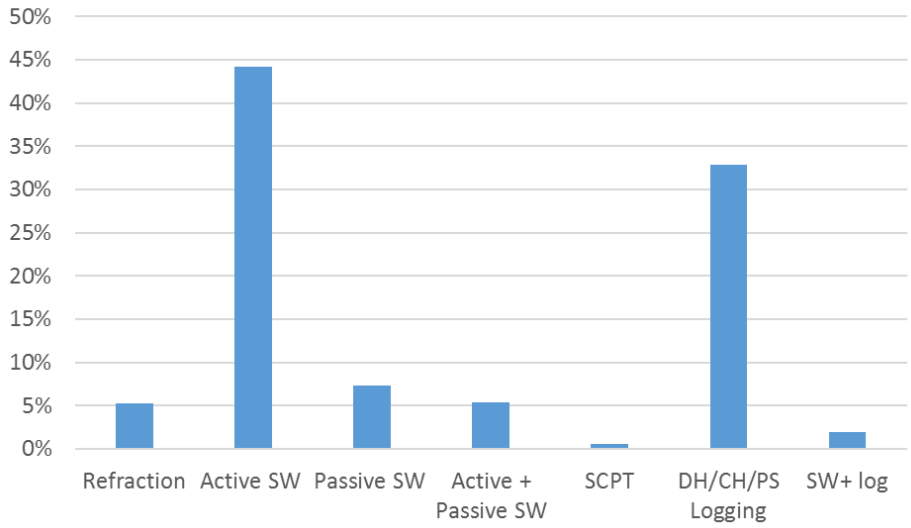

Figure 8: V_{S30} dataset of SERA project: distribution of the data in terms of acquisition methods.

The measured V_{S30} distribution shows a homogeneous coverage of soft soils ranges (< 800 m/s) but very sparse information on rock sites (Figure 9). Finally, it is felt that the V_{S30} dataset collected for the SERA project is not sufficient to build an ad-hoc European correlation between geomorphological or geological criteria and V_{S30} ranges because of both poor spatial coverage and poor geological condition distribution. Further collection of measured V_{S30} data is thus recommended to allow further developments in this field to be made.

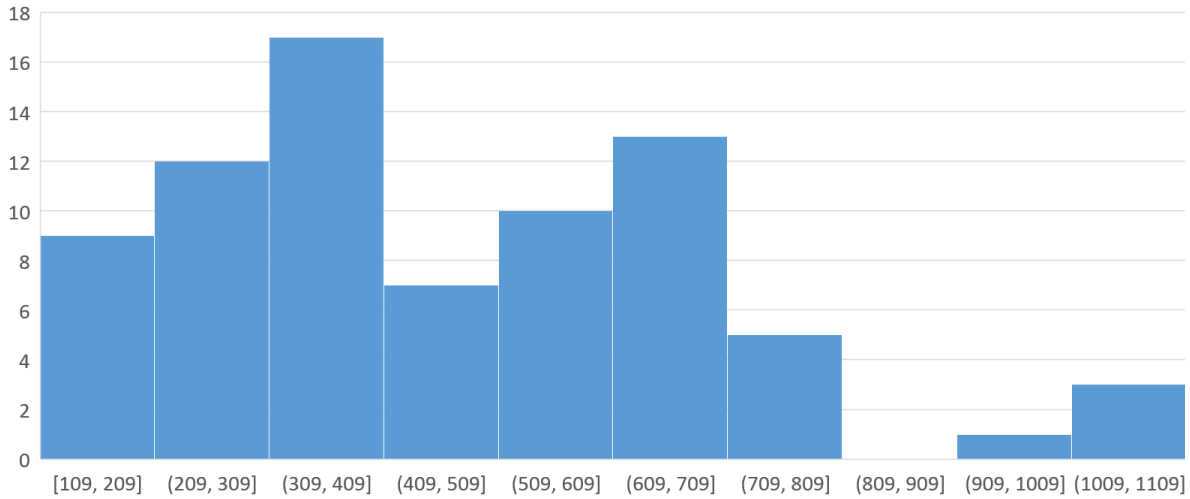

Figure 9: Measured V_{S30} distribution for data collected during SERA project.

4 Correlation of V_{S30} with topography and geology

Recent papers have developed alternative methodologies based on both geological and DEM information to derive site effects proxies (mainly V_{S30} parameter and EC8 soil classes) at regional scale:

- **Topographic gradient (slope) or other DEM-derived elements** (roughness, convexity, elevation, distance from moutain), e.g. Wald and Allen (2007) based only on slope criteria or Iwahashi and Pike (2007) based on multiple geomorphological criteria;
- **Surface geology**, e.g. Wills and Clahan (2006) in the United States, Lee and Tsaï (2008) in Taïwan, Mc Pherson et al. (2013) in Australia, Vilanova et al. (2018) for Portugal, Forte et al. (2017) and Di Capua et al. (2016) for Italy;
- **Hybrid methods** combining different information as terrain classes, lithostratigraphic criteria and DEM information (mainly slope), e.g. Stewart et al. (2014) Seyhan et al (2014) or Ahdi et al. (2017).

For the purposes of the SERA project, the aim was to obtain a V_{S30} map at European scale derived from existing input data. Two processes were applied to calculate the final maps described herein:

- The application of the DEM-based methodology of Wald and Allen (2007) as tested in SHARE project (Lemoine et al., 2012), taking into account the limitations of the methodology;
- The application of a geology-based methodology applying the V_{S30}-lithostratigraphic correlation developed by Vilanova et al. (2018).

Two other processes have been investigated but require further testing in the upcoming months:

- An EC8 map derived from geology for which each lithology described in Section 2.1.1 will be classified in terms of EC8 soil class through the V_{S30} information collected in SERA and expert judgment;
- A DEM-based binary map derived from a morphological analysis, which tends to identify deposit zones (alluvial plains) where site effects are prone to occur.

4.1 Correlation between topography and V_{S30}

4.1.1 Wald and Allen methodology

The first step was to build a map of ranges of V_{S30} from a widely used methodology based on DEM global data developed by Wald and Allen (2007). The latter proposed a simple methodology in order to infer easily NEHRP site-amplification factors from topographic slope calculation. From V_{S30} data sets, they defined correlations between V_{S30} ranges and slope ranges both for active tectonic and stable continental areas. After calculation of topographic slope using GMT command “grdgradient” (Wessel and Smith, 1991), V_{S30} are assigned to all sites using defined correlations. This method is not consistent for specific geological contexts, e.g. flat volcanic rock plateaus.

As discussed before, a 30 arc-second DEM has been used to infer V_{S30} ranges values for Europe from slope data using the Wald and Allen (2007) methodology. Nevertheless, as discussed in Lemoine et al. (2012), topographic slopes derived from land terrain model only are associated to artifacts in coastal areas. As an illustration, Figure 10 shows the artifacts slope values observed in slope values deduced from SRTM30 land DEM and Figure 11 shows that all the outliers slope value sites associated with V_{S30} SERA dataset (orange dots) are located in coastal areas. BRGM therefore decided to use the

GEBCO_2014 DEM introduced in Section 2.2 and the topographic slope was calculated using the same algorithm as Wald and Allen (2007), i.e., GMT's "grdgradient".

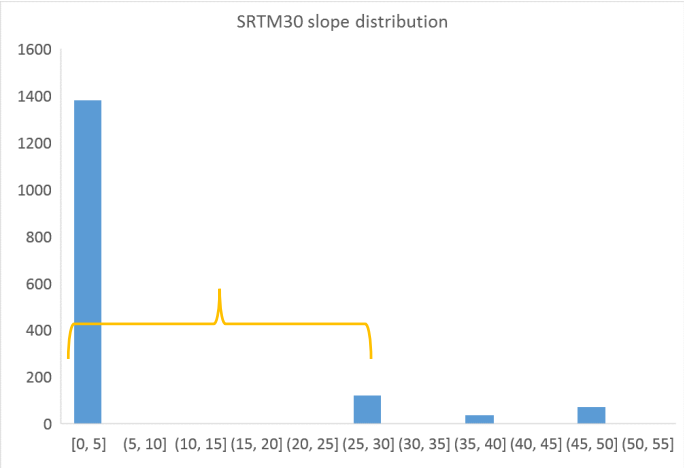

Figure 10: SRTM30 slope distribution for Europe. In orange: outlier with a gradient value superior to 1 m/m.

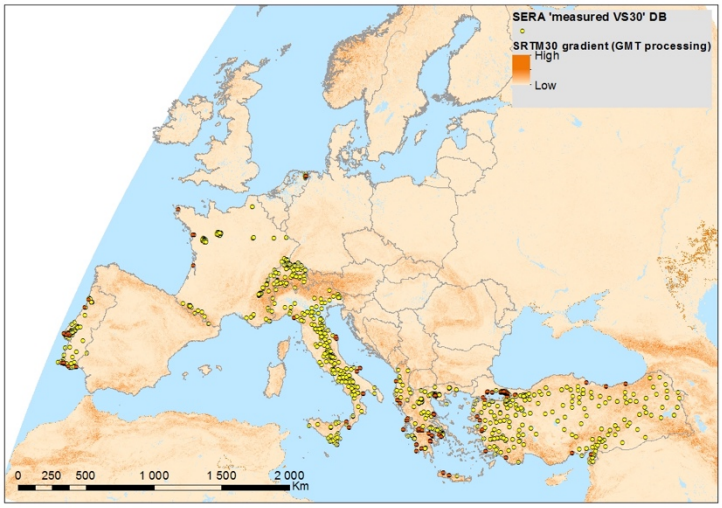

Figure 11: Location of the measured VS30 data (coloured dots) superimposed with the SRTM30 gradient calculated from GMT process. Orange dots correspond to outliers (on coastal sites) and yellow dots correspond to sites with regular slope values.

Ranges of V_{S30} values were calculated for both stable continental and active tectonic areas by applying the Wald and Allen (2007) correlations (Figure 12 and Figure 13). The next step was to separate stable continent areas and active tectonic ones. The distinction was done using the SHARE tectonic classification, modified from Delavaud et al. (2012). Turkey, which was not fully covered by the SHARE zonation, was considered as an active tectonic area for the whole country (Figure 14). A final merged map was built (Figure 15) providing V_{S30} ranges for the whole Europe. Iceland is included in the GIS file, even though, for visibility reasons, it was not plotted on Figure 15.

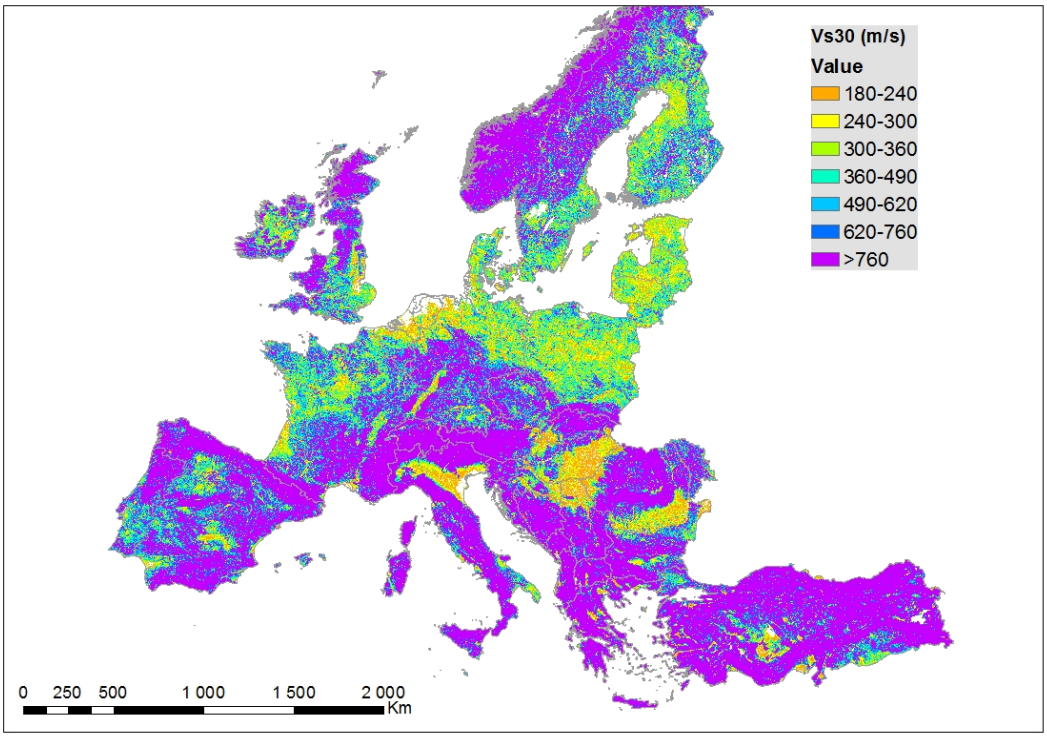

Figure 12: V_{S30} distribution over Europe inferred from Wald and Allen V_{S30}/slope correlation for stable continental and calculated on GEBCO DEM.

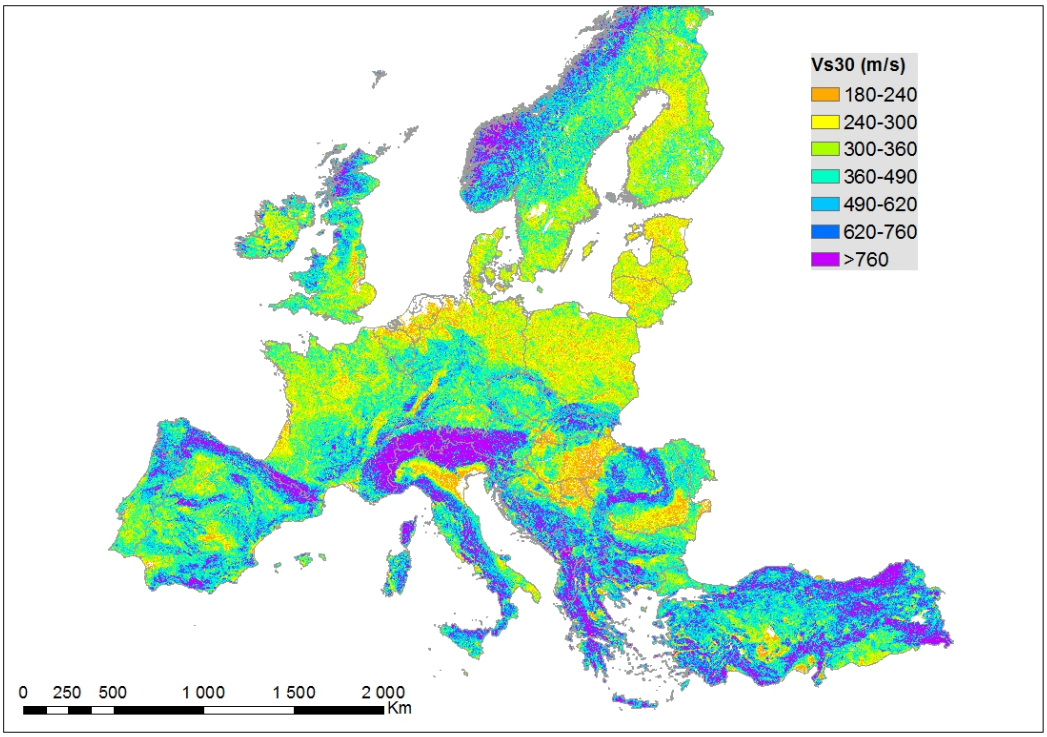

Figure 13: V_{S30} distribution over Europe inferred from Wald and Allen V_{S30}/slope correlation for active tectonic areas and calculated on GEBCO DEM.

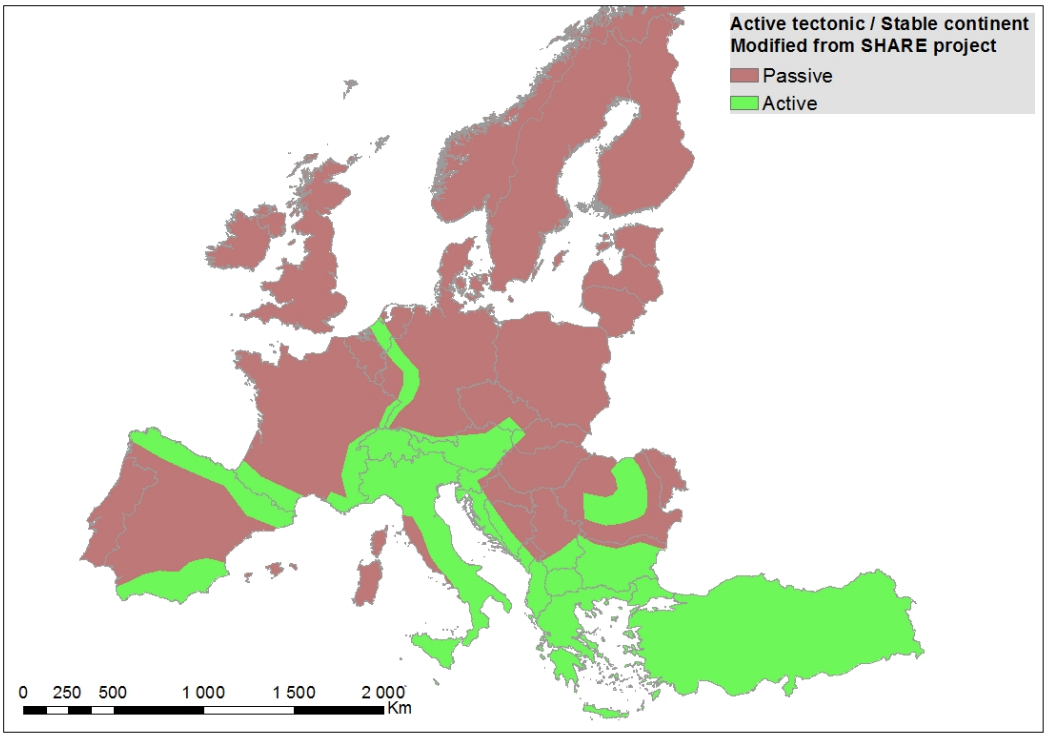

Figure 14: Identification of active tectonic areas (green) and stable continental areas (brown) from SHARE seismotectonic zonation.

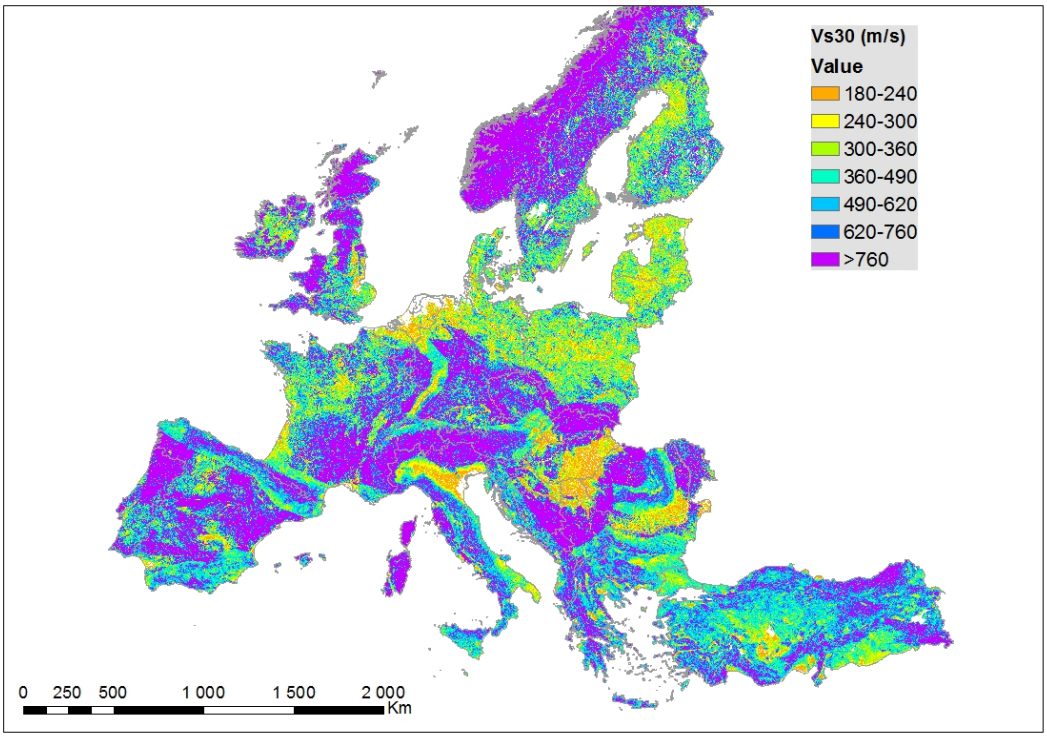

Figure 15: Final ranges of V_{S30} over Europe inferred from Wald and Allen V_{S30}/slope correlations for active and stable areas. The final map was built merging information from stable and active tectonic areas (Figure 12 and Figure 13) using the classification described in Figure 14.

4.1.2 Evaluations, limitations and perspectives

In order to evaluate the reliability of Figure 15, a comparison between the V_{S30} data presented in Chapter 3 and slope is shown in Figure 16, and is overlain with several models comparing the natural logarithm of slope to the natural logarithm of V_{S30}: i) the model of Allen & Wald (2009) for active regions (interpolated to a continuous scale), ii) the model of Wald & Allen (2007) for stable regions (interpolated to a continuous scale), iii) non-parametric LOESS regression.

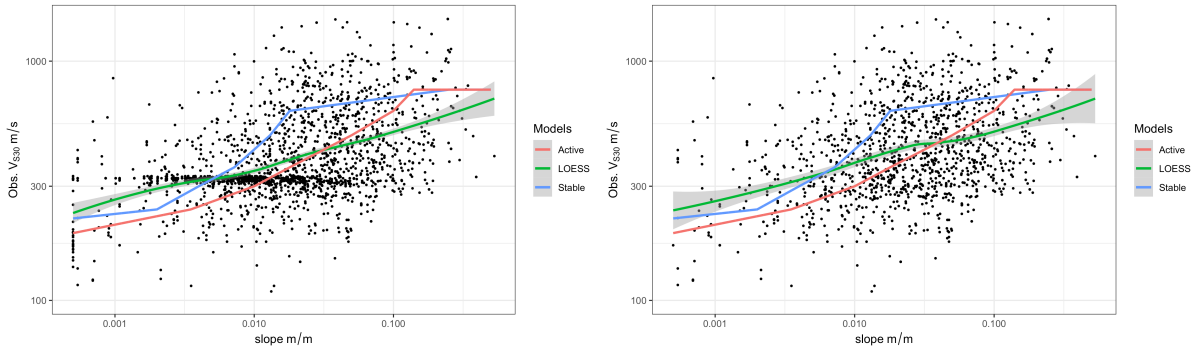

Figure 16: Comparison of observed V_{S30} against slope for i) the entire data set (left) and ii) the data set without the Groningen and Cologne subsets (right). Relations between V_{S30} and slope are shown for active regions (red) (Allen & Wald, 2009) and stable regions (blue) (Wald & Allen, 2007), and a non-parametric LOESS regression fit shown as a green line.

The results show that for the whole data set there is a sampling bias from two data sources: Cologne, where a range of slope values are found but the majority of the sites are on Pleistocene rock with V_{S30} in the 300 m/s to 330 m/s range, and Groningen, where all of the sites are on Pleistocene Sand, with slopes too flat for the algorithm to correctly constrain given the resolution of the DEM. Comparisons on Figure 16 are thus shown with and without the Cologne and Groningen data. Regardless of the data set, the LOESS regression model would suggest a flatter scaling between slope and V_{S30} in the European data than that predicted by either the active or stable craton models, though both fall within the range of the data.

Another consideration that should be made when evaluating Figure 15 is that slope values are strongly dependent on DEM models, as shown on Figure 17, and in Roullé et al. (2010). Hence, V_{S30}-slope correlations should be built for each resolution and version of input DEM and those correlations would be relevant only for representative V_{S30} data sets. It is also noted that the map does not account for the exclusion of specific geological units (e.g. flat volcanic plateaus), as recommended by Wald and Allen (2007). Moreover, the boundary between active and stable areas are sharp which could probably induce singularities in the resulting risk maps. This first model of ranges of V_{S30} shown in Figure 15 thus needs further adaptation to the European context and this first attempt to provide a V_{S30} range map for all Europe must be carefully considered by end-users. It must not be considered as a recommended European site effect map, but as one of the many investigations carried out in the study presented herein.

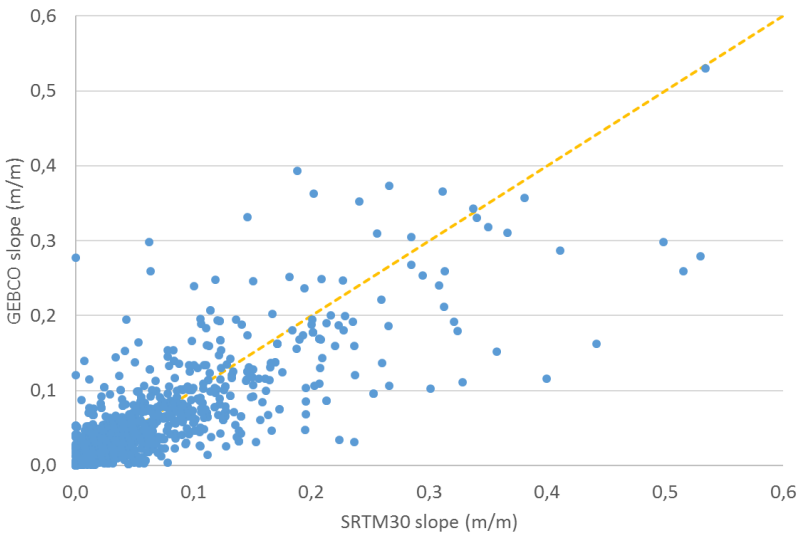

Figure 17: Comparison between slope values (m/m) between SRTM30 & GEBCO_2014 DEM data for SERA VS30 DB. The dotted line represents the 1:1 reference corresponding to GEBCO slope = SRTM30 slope.

4.2 Correlation between geology and V_{S30}

As an initial evaluation of the correlation between geology, slope and V_{S30}, the correlation presented previously in Figure 16 (without Groningen and Cologne) has been decomposed into geological unit, as shown in Figure 18. From this figure it is difficult to determine a clear trend or tendency in the scaling. Holocene and Cenozoic environments provide the most data and show similar correlations, albeit with Cenozoic sites sampling more densely the higher slope conditions and Holocene sites the flatter environments. Neither Pre-Cambrian nor Ultra-Mafic units are sufficiently well-sampled to determine any correlation between slope and V_{S30}, though the LOESS regression would suggest no discernible correlation regardless. Likewise, a seemingly flat trend is observed in the Paleozoic category too. A possible conclusion that may be drawn, albeit a weak one, is that the two models (active and stable) seem to capture the body of the data in the Pleistocene, Holocene and Mesozoic rocks, though they seem to over-estimate the V_{S30} in Cenozoic conditions.

The geological data set contains a simple stratigraphic classification of each unit, and whilst many stratigraphic units contain too few observations of V_{S30} for a robust comparison, the decomposition of the trends by stratigraphic unit in Figure 19 can provide some insight into which conditions the V_{S30}-slope relations may be better or poorly suited for. Environments typical of harder rock tend to show a very weak, or even absent, correlation between slope and V_{S30}. These include felsic, metamorphic (METAM), shist (SCHST), ultra-mafic (UMAFIC) and volcanic (VOLC) environments. Better agreement can be seen for consolidated sediment environments such as sand and gravel (SAGR), sand (SAND), clastic rocks (CLST) and conglomerates (CGRT). Sites on very soft sedimentary environments (alluvium [ALLU] and sediment [SDMT]) are typified by lower V_{S30} values, and in many cases show poor correlation with slope, mostly suggesting that slope-based V_{S30} estimates would overestimate V_{S30}. Areas of low V_{S30} on steeper slope may in reality correspond to small sedimentary layers in upland valleys that are not well captured from the resolution of the DEM. For example, several alluvium sites were identified in the western extent of the Anatolian plateau, which would be characterised by relatively shallow layers of fluvial sediment overlaying hard rock.

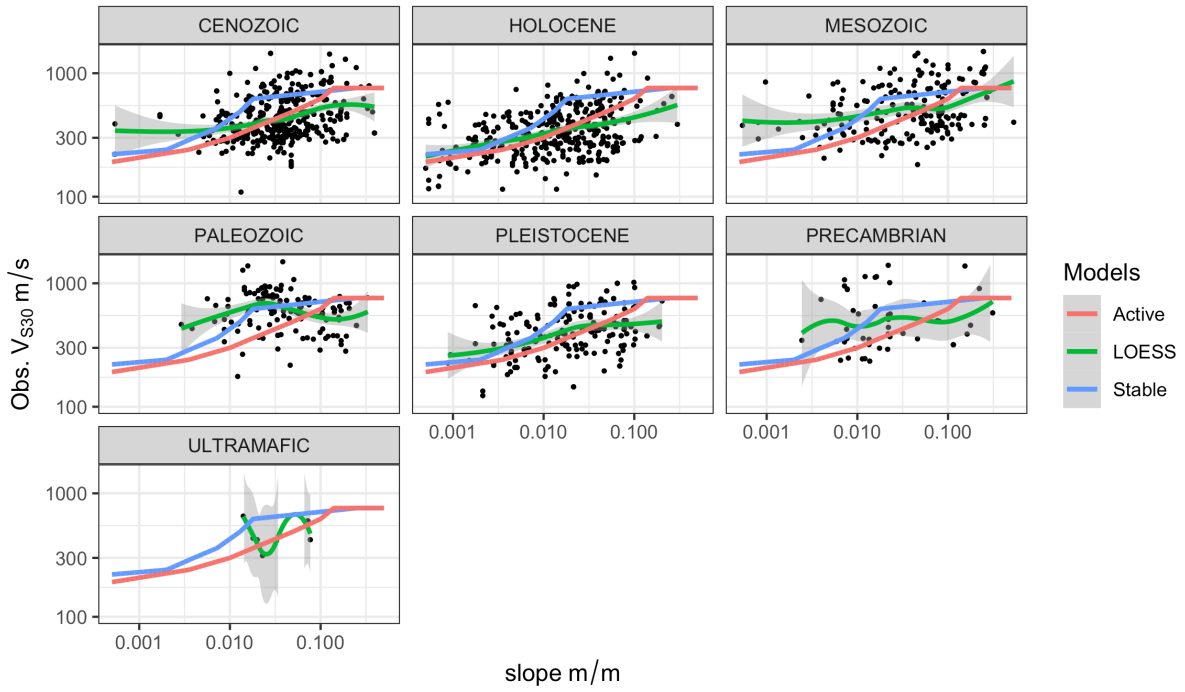

Figure 18: Relation between topographic slope and measured V_{S30} per geological era, with fitted model descriptions as Figure 16 (excluding data from Groningen and Cologne)

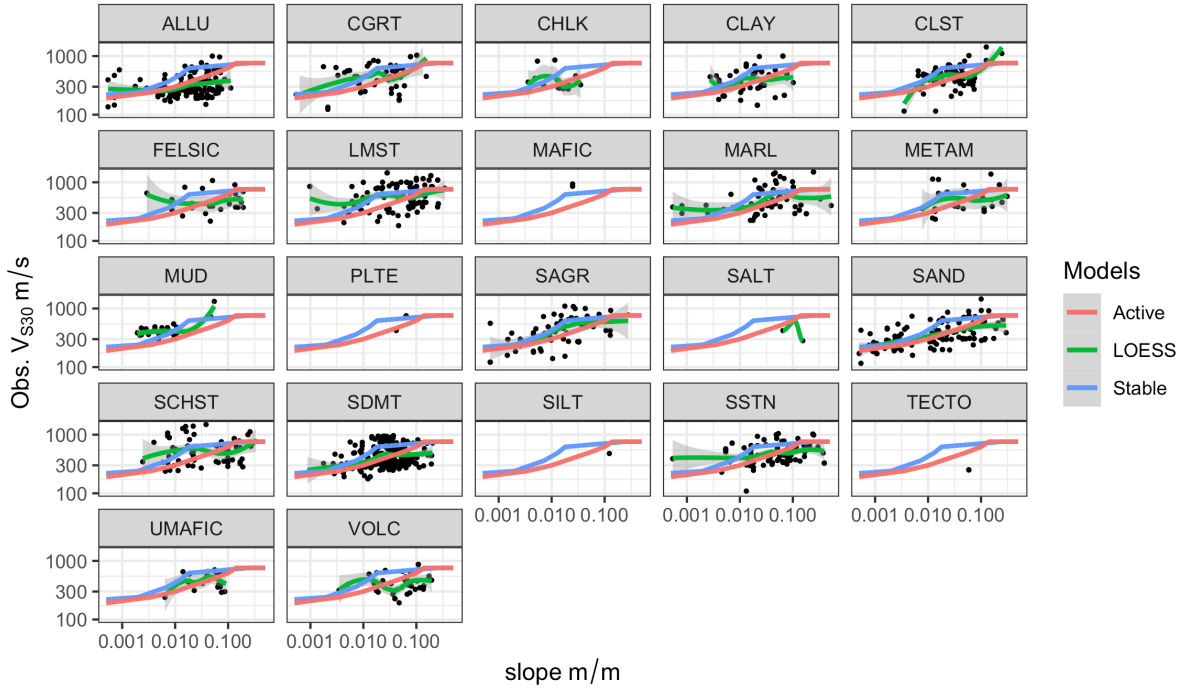

Figure 19: Relation between topographic slope and measured V_{S30} per stratigraphic unit, with fitted model description as Figure 16.

The composite dataset of V_{S30} and slope observations compiled within this study mostly extends the previous data of Lemoine et al., (2012). With the exception of some special case regions, this new data demonstrates that at a broad scale there may be a reasonable agreement in the general slope and V_{S30} trends compared to previous studies, but that the predictive performance of slope to V_{S30} models is highly dependent on the geological and stratigraphic unit. This conclusion agrees with that of recent analyses (Thompson et al., 2014; Vilanova et al., 2018) and concurs with Lemoine et al., (2012). This

naturally highlights the limitations of applying existing models to infer V_{S30} from topography for the purpose of defining a regional V_{S30} model and demonstrates why further refinement from geology is beneficial for improving the estimates. Nevertheless, it is evident that for Europe not all geological or stratigraphic units are sufficiently sampled within the data set to enable robust estimates of calibration factors. Further acquisition of V_{S30} observations would be necessary improve such correlations, or else extension of the data set to encompass other regions of the world. Such developments should be a target of future investigation.

In the meantime, an initial attempt has been made to build a SERA geology-based model using the following scheme:

- Classification of geological data based on lithology and stratigraphy information;
- Building correlations between geological units and V_{S30} distribution from measured V_S profiles (punctual data);
- Spatializing information to obtain V_{S30} maps and/or EC8 maps.

4.2.1 An attempt to build a SERA geology-based model

In SERA, BRGM have attempted to build a geology-based model for V_{S30} estimation as described in the literature using the measured V_{S30} data collected, especially during the project. The first step of the study consisted in exploring the V_{S30} dataset collected in the SERA framework. The spatial distribution of the data is quite poor with more than 80% of the data coming from active tectonic areas (Italy, Greece, Turkey, the Alps and the Pyrenees) as shown in Figure 6. This poor spatial distribution of the V_{S30} data induces a bias in the analysis since some geological units will be underrepresented in the dataset as, for example, geologies from stable areas in Western and Northern Europe (Figure 20). However, the spatial analysis (Figure 21) shows that an extrapolation of the V_{S30} information (coloured polygons) to all the geological polygons characterized by a similar lithology (grey polygons) will lead to a rather good spatial coverage of V_{S30} information all over Europe.

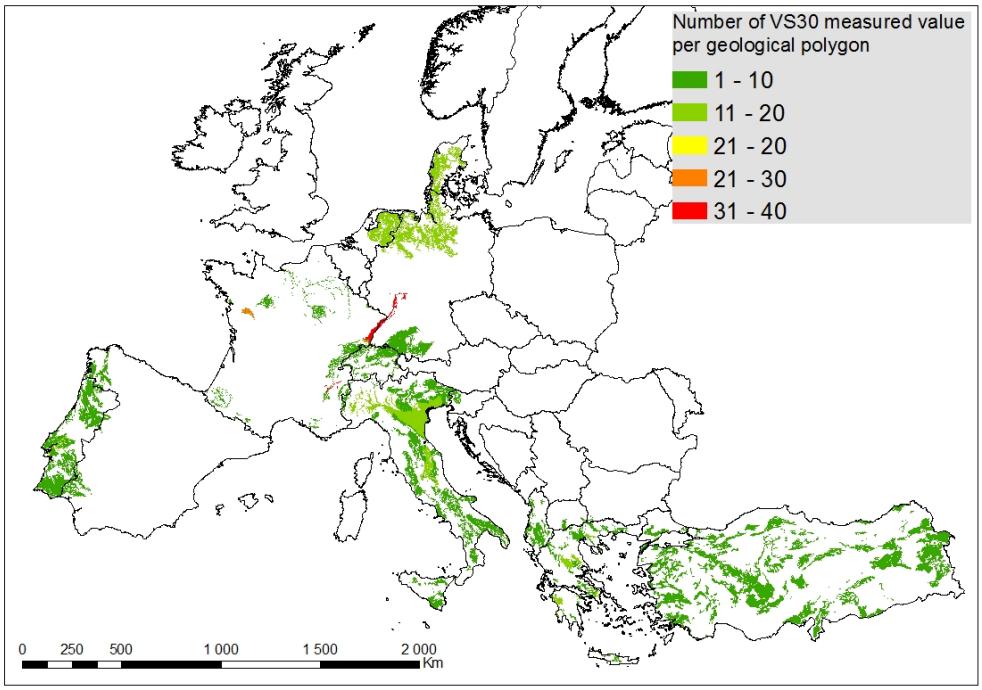

Figure 20: Spatial distribution of V_{S30} measured data regarding lithological information. Colours represent the number of V_{S30} data available in each geological polygon.

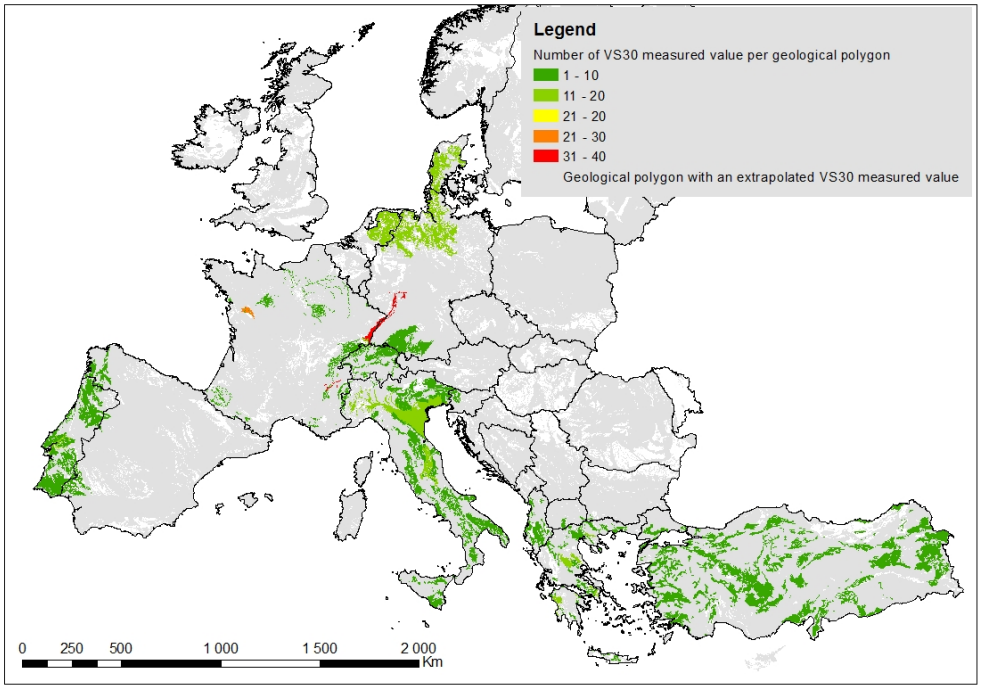

Figure 21: Spatial distribution of V_{S30} measured data regarding lithological information. Colours represent the number of V_{S30} data available in each geological polygon (same as in Figure 20). Grey areas represent geological polygons where V_{S30} information is available by extrapolating the V_{S30} information available in similar lithology (coloured polygons).

BRGM then analysed the V_{S30} distribution values for each lithology described in Section 2.1.1. Figure 22 and Table 3 shows that, for soft soils, median V_{S30} values are roughly between 250 and 450 m/s, corresponding to EC8 soil classes B to C, as expected. On the contrary, results for stiff soils to rock are quite unexpected since they show quite low V_{S30} values with median values between 324 and 555 m/s (except for MAFIC code) and mean values between 390 and 666 m/s, corresponding mainly to EC8 soil class B instead of the expected soil class A. This can be due to:

- Poor geological classification at station site since geology is based on a 1:1 500 000 scale map, which is not precise enough for local analysis;
- Bias in V_{S30} sampling since site characterizations of strong-motion stations are generally devoted to soft soils. Our dataset is probably missing rock V_{S30} values due to a lack of V_S measurements in this kind of geologies.

Those limitations avoid us to build a geology-based V_{S30} model for all Europe since it will lead to an over-estimate of the ground motion amplification for soft to hard rock configurations.

Consequently, we decided i) to derive an alternative geology-based map from the work done in Portugal (Vilanova et al., 2018) and ii) to use our V_{S30} database for deriving an EC8 map for all Europe keeping V_{S30} information for soft soils and applying an expert classification for soft to hard rock (still in progress).

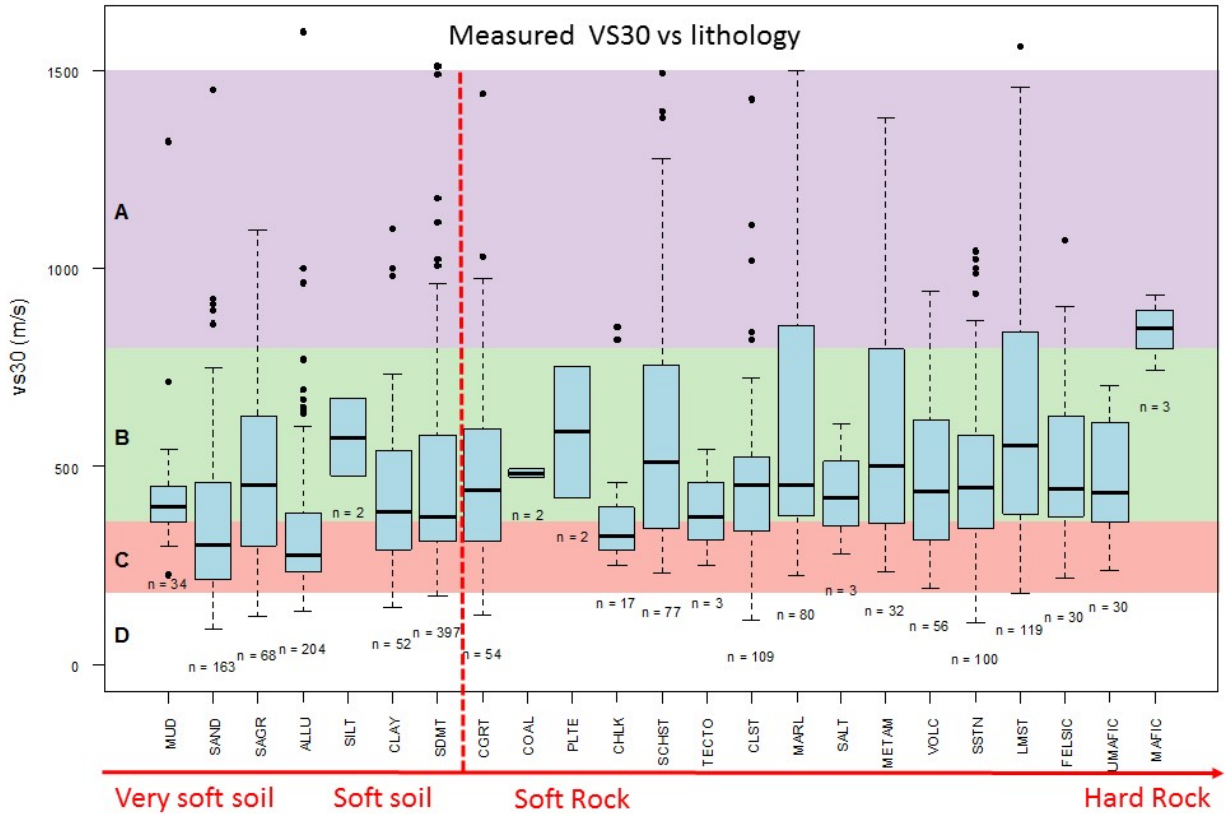

Figure 22: Boxplots showing the measured V_{S30} distribution for each lithological code of Section 2.1.1. The EC8 soil classes A, B, C and D are superimposed with colours (EC8 class A=purple, class B=green, class C=orange, Class D= white).

Table 3: Statistical values of V_{S30} for each lithology described in Section 2.1.1

Lithological codes	Statistical values / lithology				
	boxplot Q1	boxplot Q2 (median value)	boxplot Q3	Mean value	standard deviation
MUD	362	397	450	435	177
SAND	213	306	462	366	197
SAGR	301	454	627	483	236
ALLU	236	278	384	335	168
SILT	478	576	673	576	138
CLAY	293	390	542	438	208
SDMT	311	374	580	460	211
CGRT	311	442	594	474	240
COAL	473	485	496	485	16
PLTE	421	587	753	587	235
CHLK	290	324	398	393	176
SCHST	345	510	758	607	358
TECTO	314	376	460	390	147
CLST	338	454	525	465	203
MARL	378	455	859	673	477
SALT	351	420	514	436	163

METAM	358	501	798	666	503
VOLC	315	437	619	463	186
SSTN	346	447	582	485	192
LMST	380	555	843	659	376
FELSIC	375	446	628	499	197
UMAFIC	362	433	611	482	141
MAFIC	799	853	895	845	96

4.2.2 Alternative geology-based model

As the V_{S30} dataset collected in SERA framework was not sufficient to build our own geology-based model for estimating V_{S30}, we decided, in a pragmatic way, to use an existing model, built on a regional scale and to extrapolate it to all Europe. Several possibilities, developed in continental Europe, appeared:

- The model developed by Stewart et al. (2014) in Greece, which combined terrain type, surface geology (age) and surface gradient information. This model is not easily reproducible at European scale mainly due to the complexity of terrain classification;
- The model developed by Di Capua et al. (2016) based on surface geology (lithology) and considering additional critera such as geological age, consistency, and terrain structure. As for Greece, this model is not easily reproducible at European scale mainly due to i) a lack of harmonized surface geology at European scale and ii) to the complexity of terrain classification.
- The model developed by Vilanova and al. (2018) for Portugal, based mainly on a stratigraphic classification easily reproducible at the European scale using the stratigraphic codes of Section 2.1.3. This model was thus chosen herein.

Vilanova et al. (2018) built a geology-based model for estimating V_{S30} in Portugal from geological data at 1:500 000 to 1:50 000 scale and V_{S30} measurements. The final model is the following:

Table 4: Geology-based classification from Vilanova et al. (2018).

Name	Geological Unit	Mean VS30 value (log-averaged)	VS30 - sigma	VS30+sigma
F1	Igneous, metamorphic and old sedimentary rocks	829	523	1315
F2	Neogene and Pleistocene formations	470	329	672
F3	Holocene formations	237	144	392

Table 5: Correspondence between stratigraphic codes of Section 2.1.3 and the geology-based model classes of Table 4.

Stratigraphic code	Epoch	Era	Simplified Era	Vilanova model
UK	UNKNOWN	UNKNOWN	UK	F1
PH	PHANEROZOIC	PHANEROZOIC	PH	F1
CN	CENOZOIC	CENOZOIC	CN	F1
HC	HOLOCENE	HOLOCENE	HO	F3
PC	PLEISTOCENE	CENOZOIC	CN	F2
PL	PLIOCENE	CENOZOIC	CN	F2
MC	MIOCENE	CENOZOIC	CN	F2

NG	NEOGENE	CENOZOIC	CN	F1
OL	OLIGOCENE	CENOZOIC	CN	F1
EC	EOCENE	CENOZOIC	CN	F1
PG	PALEOGENE	CENOZOIC	CN	F1
CR	CRETACEOUS	MESOZOIC	MS	F1
JR	JURASSIC	MESOZOIC	MS	F1
TR	TRIAS	MESOZOIC	MS	F1
PZ	PALEOZOIC	PALEOZOIC	PZ	F1
PK	PRECAMBRIAN	PRECAMBRIAN	PK	F1

The resulting map of the geologically-based model from Vilanova et al. (2018) method is presented in Figure 23.

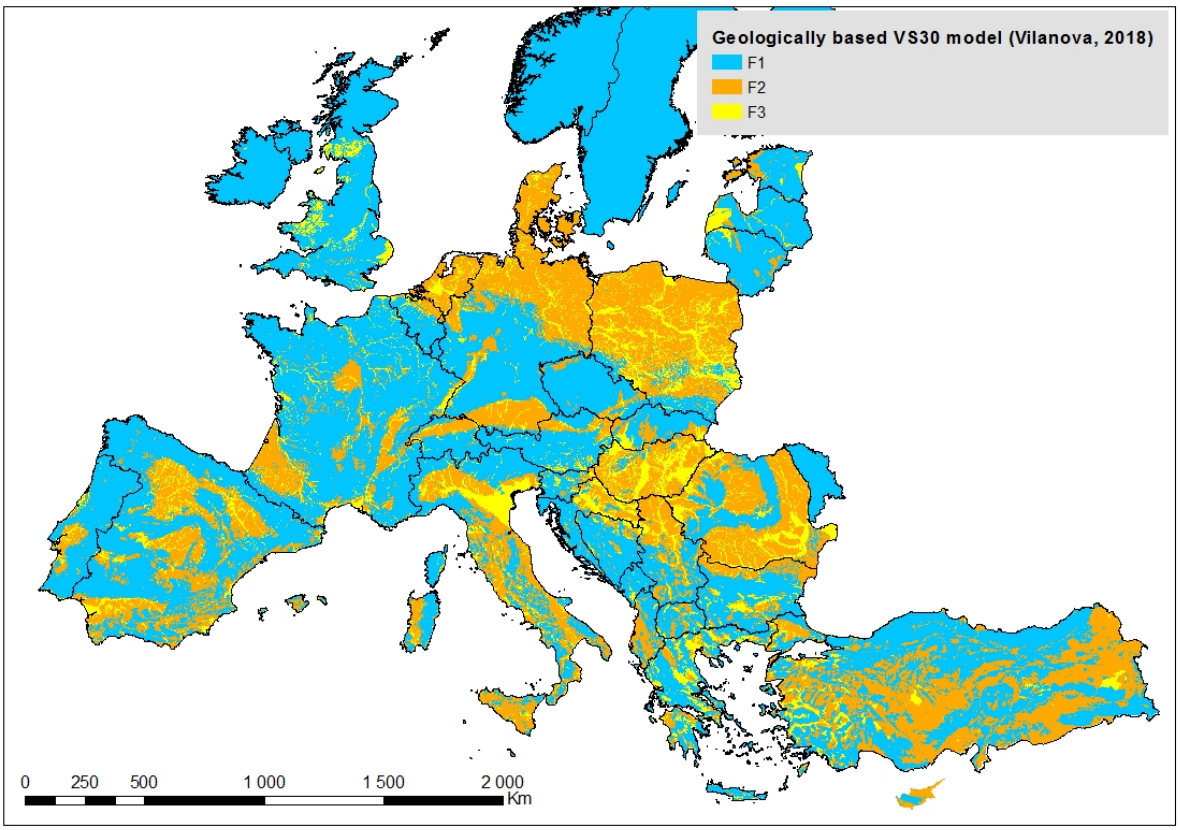

Figure 23: Geology-based model of Vilanova et al. (2018) extrapolated to all Europe.

4.2.3 Limitations and perspectives

BRGM faced problems to derive a correlation between geological criteria (lithology and/or stratigraphy) and V_{S30} during the SERA project due to:

- Discrepancy between local scale and continental scale information (in particular for surface geology);
- Lack of harmonized information on surface geology at European scale;
- Poor spatial and geomorphological (active/stable tectonic area) distribution of the 'measured V_{S30}' dataset.

To address the need for a geology-based model of V_{S30} for all Europe, BRGM decided, in a pragmatic way, to apply an existing model built in Portugal by the recent work of Vilanova et al. (2018) and easily reproducible at European scale. BRGM are still testing this solution, developed for a stable tectonic area, both at regional scale and statistically at European scale as it was done in SHARE project for the Wald and Allen methodology (Lemoine et al., 2012). This work is still under progress and will need to be compared to other methodologies during the last 12 months of the project.

5 Correlation of $\delta S2S_S$ with proxies (topography and geology), observed and measured V_{S30}

The development of a new shallow crustal ground motion model using the ESM flatfile has been carefully designed to permit deeper exploration of the site-to-site properties in European strong motion records than has been possible from previous models. A full description of this new shallow crustal ground motion model can be found in Deliverable 25.4 (Weatherill et al., 2019b) and Kotha et al., (2019 – *in preparation*). The general functional form of the model assumes the following:

$$\ln(PSA,T) = f_R\left(M_W, R_{JB}, h, T\right) + f_M(M_W, T) + \delta B_e(T) + \delta S2S_S(T) + \delta WS_{e,s}(T) \qquad [5.1]$$

where the fixed effect terms follow orthogonal normal distributions such that $\delta B_e(T) = \mathcal{N}(0, \tau(T))$, $\delta S2S_s(T) = \mathcal{N}(0, \phi_{S2S}(T))$ and $\delta WS_{e,s}(T) = \mathcal{N}(0, \phi_0(T))$. In contrast with many ground motion models, for which a linear or nonlinear amplification term is included within the fixed effects part of the random effects regression (Bates et al., 2015), the site term, $\delta S2S_S(T)$, is adopted as a random effect within the regression itself. This term represents the site-specific residual, which is determined from repeated recordings at the same site. Correspondingly, the total aleatory variability of the ground motion model is given by $\sigma_T^2 = \tau^2 + \phi_0^2 + \phi_{S2S}^2$

From the ESM flatfile, and considering only earthquakes of shallow origin, $\delta S2S_S(T)$ is estimated for a total of 1548 stations within the Euro-Mediterranean region (for short period motion), decreasing to 1464 for periods greater than 4 s. The spatial distribution of $\delta S2S_S(T)$ for PGA, Sa (0.2 s), Sa (1.0 s) and Sa (2.0 s) are shown in Figure 24.

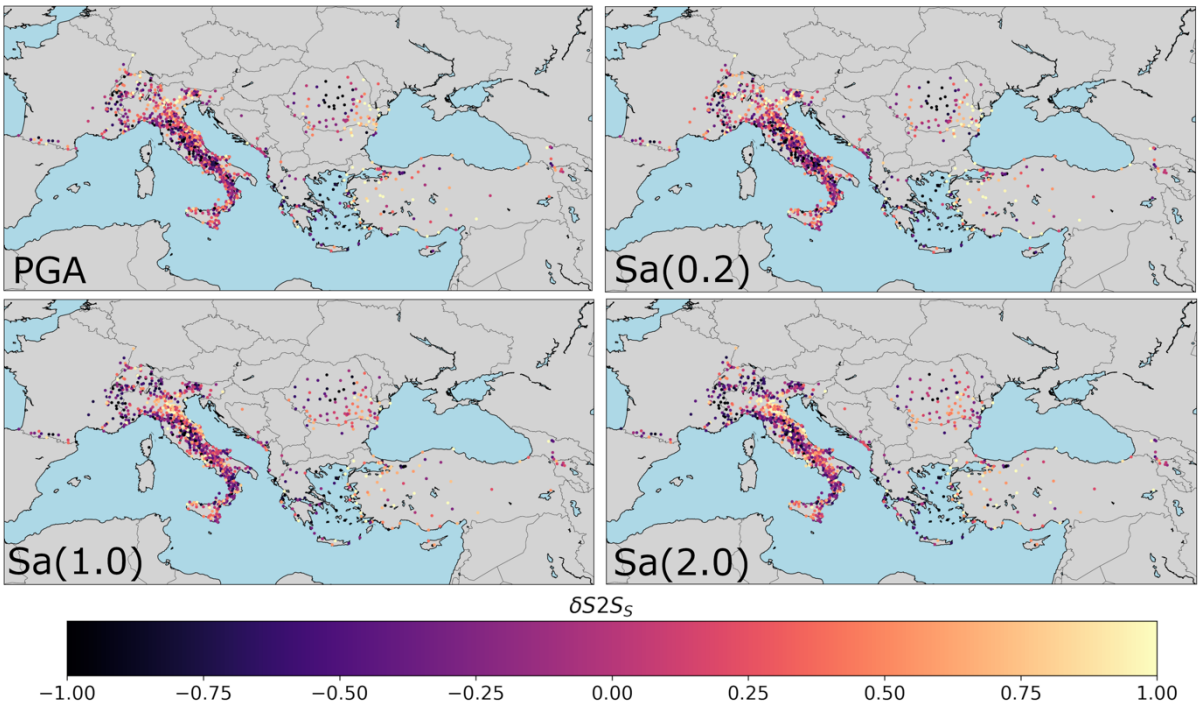

Figure 24: Variation in $\delta S2S_S(T)$ with site for the ESM database using the proposed SERA shallow crustal GMPE (Figure reproduced from SERA Deliverable 25.4, Weatherill et al., 2019b)

5.1 Fitting an amplification model to $\delta S2S_S$

For the calculation of seismic hazard on the reference Eurocode 8 rock site, it is necessary to determine the ground motion for V_{S30} of 800 m/s. From Figure 25, however, it can be seen that the number of sites for which V_{S30} is observed is substantially smaller than the number for which it is inferred from topographic slope via the method of Wald & Allen (2007). Only 363 of the 1588 stations found in the data set used for fitting the ground motion model have a measured V_{S30} value. The absence of a reported uncertainty on V_{S30} in the ESM flatfile would preclude the use of Bayesian methods for regression with uncertain parameters (e.g. Gehl et al., 2011; Stafford, 2014; Kuehn & Abrahamson, 2018). Instead, we prefer to characterise an amplification model, $f_S(V_{S30})$, with separate coefficients in the case that the site is on measured V_{S30} or inferred V_{S30}. For definition of seismic hazard on rock for Eurocode 8 purposes, it would be the measured V_{S30} form of the model that would be adopted, whilst the inferred form would be used in the case that the site information were inferred from topographic slope using the method of Wald & Allen (2007), or similar.

Figure 26 and Figure 27 show the correlation between $\delta S2S_S(T)$ and V_{S30} for the sites with measured V_{S30} and inferred V_{S30} respectively. Non-parametric regression using the LOESS methodology is highlighted in blue on both figures. Firstly, it can be seen clearly that the inferred V_{S30} dataset does not represent soft soil sites (V_{S30} < 300 m/s) to the same extent as the observed V_{S30} subset, albeit such values are sparse even then. Secondly, the inferred data does not predict such as strong trend between the two variables as the observed data, and the uncertainty is significantly greater.

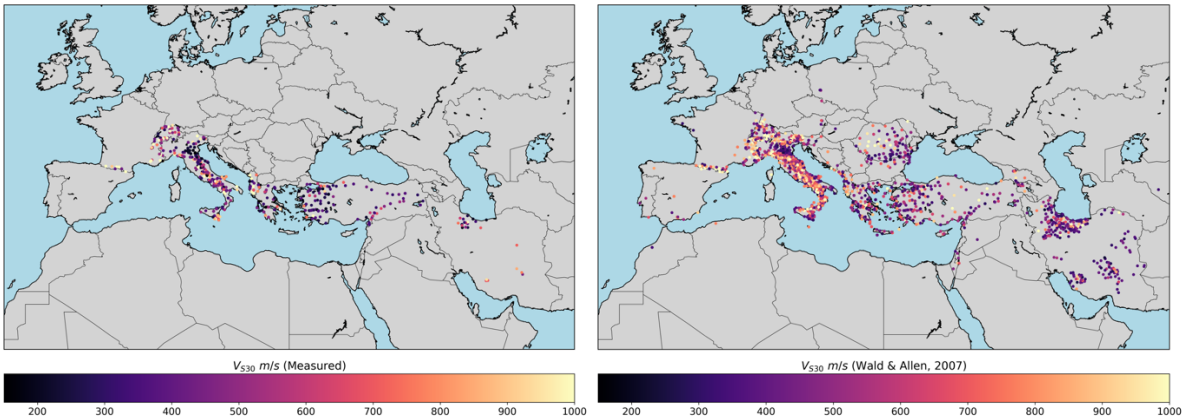

Figure 25: Density of stations in the ESM flatfile with measured VS30 (left) and with VS30 inferred using the methodology of Wald & Allen (2007) (Figures reproduced from SERA Deliverable 25.4, Weatherill et al., 2019b)

More ambiguous than the general amplification trend is the possibility of nonlinearity in the data. Here $\delta S2S_S(T)$ is limited in its capacity to resolve nonlinear amplification trends as it is, by definition, a linear site offset term. Given this and the small proportion of sites on softer soils it is reasonable to expect that little sign of nonlinearity can be seen in the data. In Figure 26, however, it is unclear if this is necessarily true. The non-parametric regression for short periods shows a trend that is not atypical of nonlinear behaviour, with small amplifications present at high frequencies on very soft soil. This is because of the notably lower $\delta S2S_S(T)$ for sites with V_{S30} < 200 m/s, which diverge from the linear trend. Nevertheless, such trend is present in the non-parametric plots only because of the lower $\delta S2S_S(T)$ at three sites. Taking into account the large error-bars on the regression, and noting that for PGA a linear trend would not fall outside the 5th to 95th percentile bands, one could not say with confidence that a nonlinear amplification trend is present.

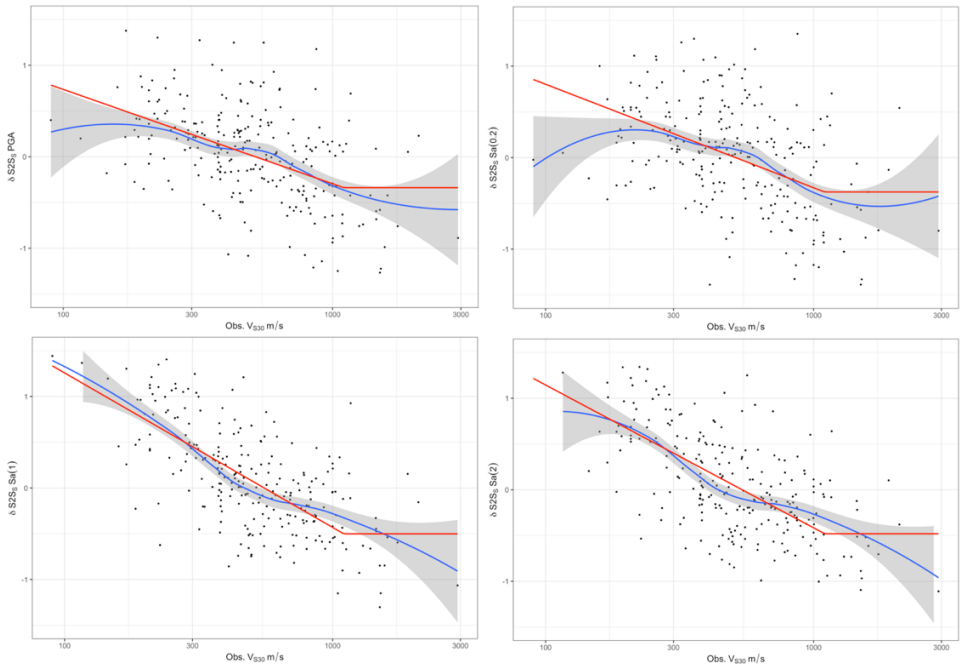

Figure 26: Correlation between $\delta S2S_S$ and observed V_{S30} for PGA (top left), Sa (0.2 s) (top right), Sa (1.0 s) (bottom left) and Sa (2.0 s) (bottom right) with non-parametric LOESS regression fit shown in blue and the $f_S(V_{S30})$ fitted model in red. (Figure reproduced from SERA Deliverable 25.4, Weatherill et al., 2019b)

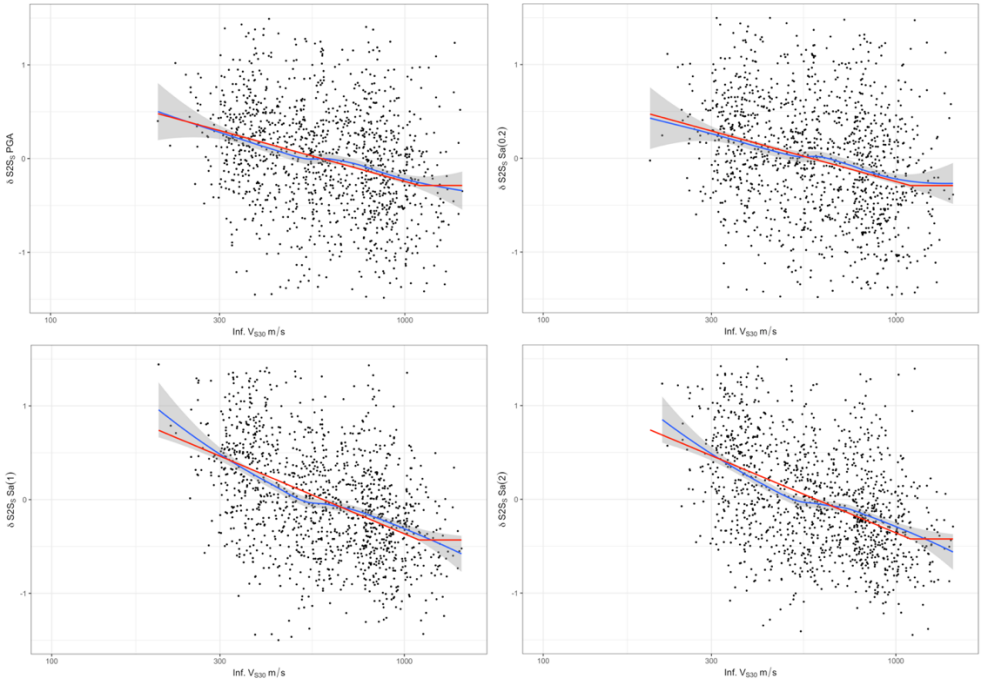

Figure 27: As Figure 26 for the inferred V_{S30} data set (Figure reproduced from SERA Deliverable 25.4, Weatherill et al., 2019b)

Assuming then that a linear amplification model is more suitable to capture the distribution in $\delta S2S_S(T)$ with either observed or inferred V_{S30}, a two-segment piecewise linear model is fit to each of the two subsets such that:

$$f_S(V_{S30}) = \begin{cases} c_0(T) + c_1(T) \cdot \ln V_{S30} \\ c_0(T) + c_1(T) \cdot \ln V_C \end{cases} + \varepsilon \quad \begin{matrix} \text{for } V_{S30} \leq V_C \\ \text{for } V_{S30} > V_C \end{matrix} \qquad [5.2]$$

Where $c_0$and $c_1$are fit in the regression and V_C is a constant above which amplification is held fixed, and ε is the residual term described by a Gaussian distribution with $\mathcal{N}(0, \phi_S)$. Exploration of the regression with V_C as a free parameter demonstrated that the resulting estimates did not vary substantially with period. Therefore V_C is held fixed at 1100 m/s. The fits $f_S(V_{S30})$ using the $\delta S2S_S$ values are shown in the red lines in Figure 26 and Figure 27. It can be seen that the fitted model matches the non-parametric regression well, with the only notable divergence in the very soft soil range at high frequencies, which may be indicative of nonlinearity.

A comparison of the amplification, with respect to V_{S30} 800 m/s, of the fitted models is made against three ground motion models derived from the previous European strong motion data set RESORCE (Akkar et al., 2014, Bindi et al., 2014; Derras et al. 2014), which is shown in Figure 28. These three models are particularly pertinent as they are fit to the same dataset, but each characterises site amplification differently. Akkar et al. (2014) adopts a nonlinear amplification model, Bindi et al., (2014) a linear model and Derras et al., (2014) is fit using a neural network approach and can therefore be considered to have a non-parametric amplification model.

The comparisons against the RESORCE GMPEs seem to show the following results. Firstly, it can be seen that the level of amplification predicted from the observed V_{S30} model and the inferred V_{S30} model is perhaps surprisingly similar, diverging only notably at certain periods on very soft soil sites. Above V_{S30} values of approximately 500 – 600 m/s the degree of predicted amplification is similar, or more accurately, the amplification predicted from Equation 5.2 would seem to be consistent with the range of amplifications found in existing models. The main divergence comes at lower V_{S30} values, in which we see the new amplification models predicting higher values at short periods and gradually transitioning to lower values at longer periods. To what extent this is an artefact of the function itself or the data set to which it is fit remains unclear. The ESM substantially increases the number of sites with measured V_{S30} in comparison to the preceding RESORCE database, with some revised characterisations of V_{S30} for some stations in Italy, Greece and Turkey.

Although the use of inferred or observed V_{S30} does not appear to have a strong influence in the amplification factor, it is more influential in the characterisation of the uncertainty. Figure 29 shows the total aleatory variability predicted by the present model with respect to those derived from the RESORCE database. Here is can be seen that the use of inferred V_{S30} results in a higher total standard deviation (σ_T) by a factor of about 0.06 – 0.08 natural log units. This increase is more pertinent for seismic hazard and risk analysis, potentially resulting in a higher seismic hazard in the cases where V_{S30} is inferred from topography.

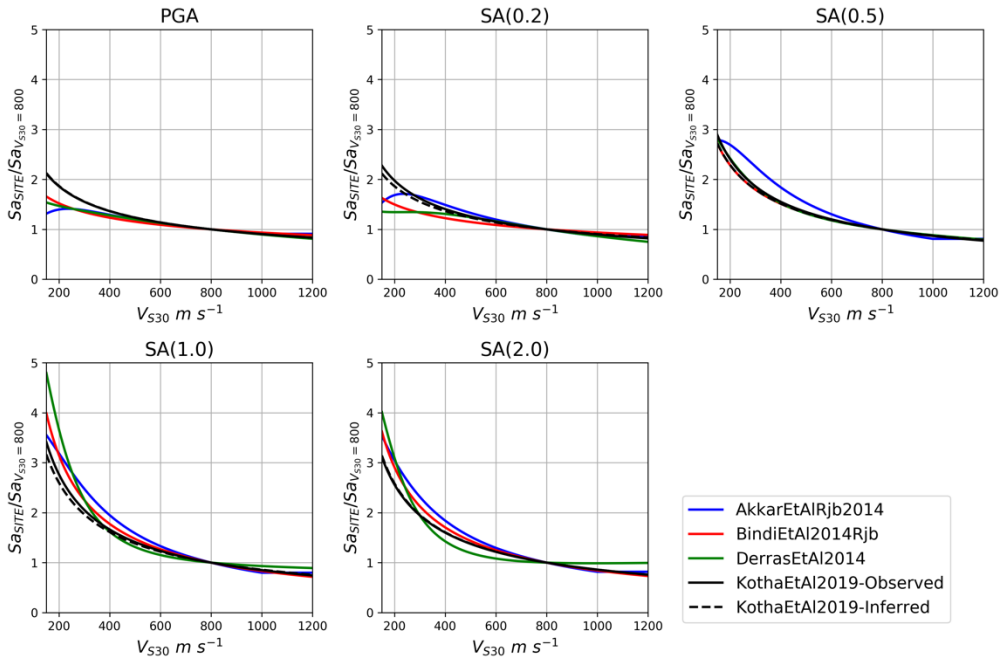

Figure 28: Comparison of amplification (with respect to V_{S30} 800 m/s) with velocity for the RESORCE GMM set (Akkar et al., 2014; Bindi et al., 2014; Derras et al., 2014) and the proposed SERA model (Figure reproduced from reproduced from SERA Deliverable 25.4, Weatherill et al., 2019b)

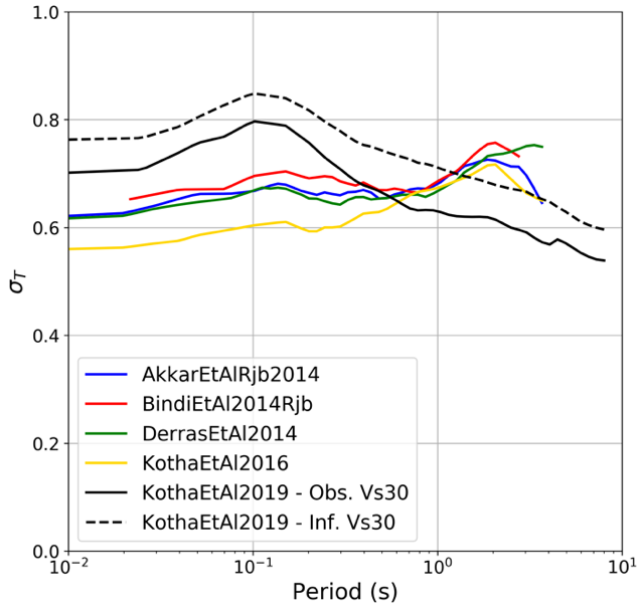

Figure 29: Scaling of the total aleatory variability with period for the RESORCE GMMs plus Kotha et al. (2016) and the proposed GMM for the case of inferred and observed V_{S30}

5.2 Incorporating geology into site amplification models

Whilst the linear models fitting $\delta S2S_s$ to either inferred or observed V_{S30} provides an amplification term to the ground motion model that is comparable to those commonly applied in PSHA, we can further build upon this information using the European geology data presented in Chapter 2. This digital dataset provides an additional constraint that is defined across the entire study region of interest. From this

data set each site location within the ESM database is assigned to its corresponding geological unit, for which two qualitative attributes are given: the stratigraphic code and the geological era. A total of eight geological eras are represented in the dataset: Pre-Cambrian, Paleozoic, Mesozoic, Cenozoic, Pleistocene, Holocene, Phanerozoic (eon with unspecified era) and Unknown. Of these Pre-Cambian, Paleozoic, Mesozoic, Pleistocene and Holocene account for nearly all of the mapped geological units and only eight of the 1548 stations in ESM are attributed to other eras. The unspecified Phanerozoic unit is found only in eastern Slovenia, whilst the Unknown units are found in isolated regions mostly in southern Germany or eastern Turkey.

The correlations between $\delta S2S_S$ and V_{S30} for two spectral periods (Sa (0.2 s) and Sa (1.0 s)) are organised by geological era in Figure 30 and Figure 31 for observed and inferred V_{S30} respectively. When subdividing the data set by geological era some important differences in the scaling emerge. Evidently, very few sites in the ESM dataset with observed V_{S30} were located in the oldest rock units (Pre-Cambrian and Paleozoic), thus general trends are difficult to determine for these units. In the case of observed V_{S30} the general scaling of $\delta S2S_S$ with V_{S30} is similar for sites of Mesozoic to Holocene age. This would generally confirm the notion that as a proxy for short period site response itself, the efficiency of V_{S30} is largely consistent from unit to unit. For longer period motion, however, differences are more apparent with stronger scaling between observed V_{S30} and $\delta S2S_S$ found in the younger Pleistocene and Holocene environments than for the older tertiary units (Cenozoic and Mesozoic). This same trend is borne out in the inferred V_{S30} data too, albeit that both the absolute values of $\delta S2S_S$ and the strength of the scaling term with V_{S30} are generally smaller.

Although the partitioning of the data set inevitably results in smaller samples for each geological unit, and given that the geological data is available *to a reasonable degree of uniformity* across Europe, then it is relevant to explore if the inclusion of geology can improve the informative power of V_{S30} in predicting the linear site response. Whilst a lithostratigraphic classification is available for each unit, the proportion of different classes with respect to the size of the data set is so high that very few classes have sufficient data for robust modelling. A better proportion of data within each subclass can be found when partitioning with respect to the geological era. To assess the predictive performance of incorporating geological unit into f_S, the site-to-site term $\delta S2S_S$ is regressed against V_{S30} using the functional form described in Equation 5.2, now using a linear mixed effects regression (Bates et al., 2015) with geological era now held as a random effect such that c_0 and c_1 are conditional upon the geology ($c_{0,g}$ and $c_{1,g}$). The fits of the mixed effects regression for each era are shown for Sa (0.2 s) and Sa (1.0 s) in Figure 30 and Figure 31 for observed and inferred V_{S30} respectively.

In both inferred and observed V_{S30} cases it can be seen that geology seems to have a stronger influence on the shape of the amplification model at longer periods than shorter periods. For the shorter periods, similar gradients ($c_{1,g}$) can be seen for many units, in some cases with the older rock units (Cenezoic and Mesozoic) presenting a slightly stronger amplification than for the younger Holocene and Pleistocene units. By contrast, however, at Sa (1.0 s) a substantially stronger scaling in amplification with V_{S30} can be seen. This would suggest that when considering amplification across the entire response spectrum the geological age of the environment can be seen to play a role. A comparison of the amplification factors with period for the inferred and observed geologically-calibrated V_{S30} to $\delta S2S_S$ model is shown in Figure 32.

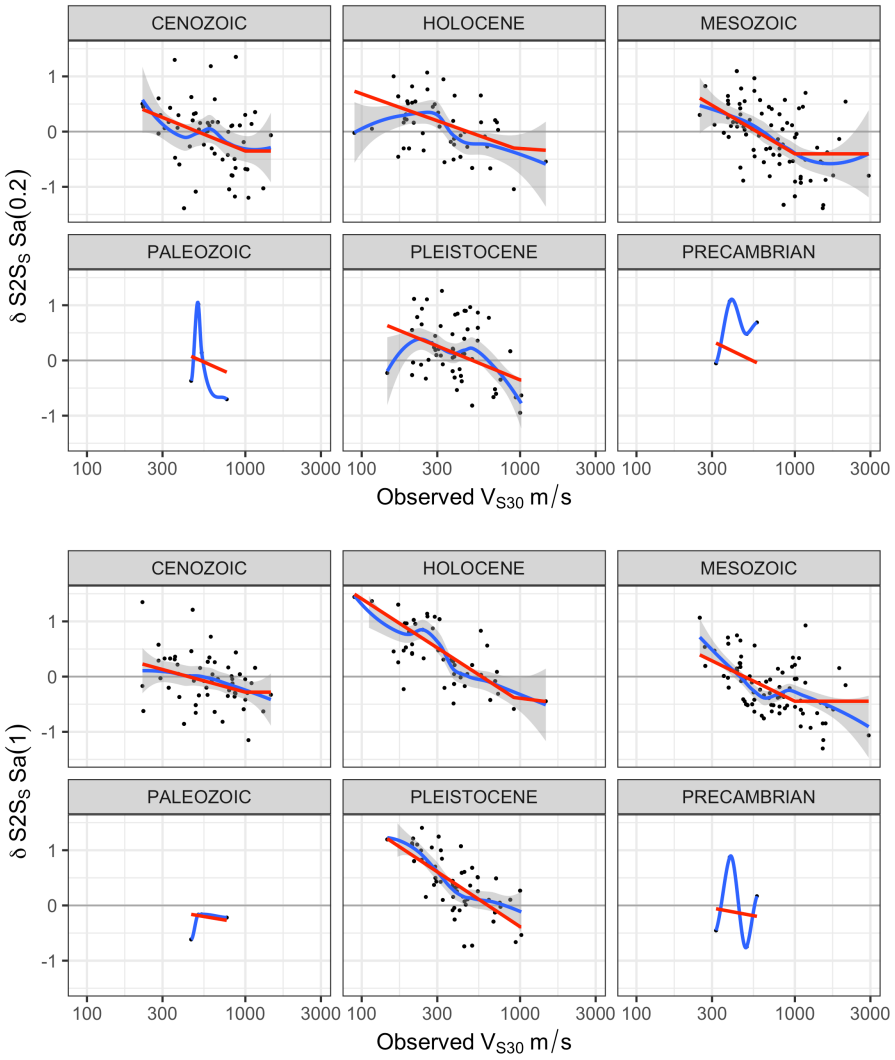

Figure 30: Comparison of site-to-site residual $\delta S2S_S$ against observed V_{S30} by geological era for Sa (0.2 s) (upper) and Sa (1.0 s) lower. Non-parametric LOESS regression lines are shown in blue and the linear mixed effects regression fit in red.

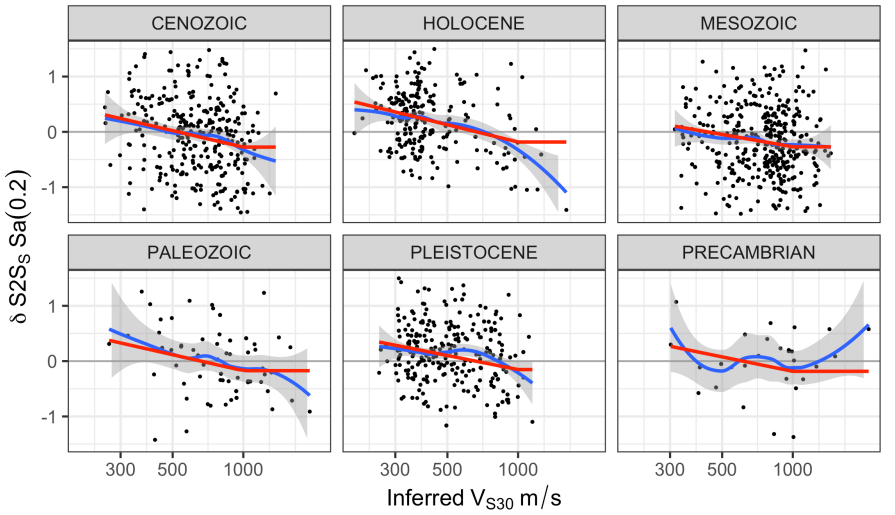

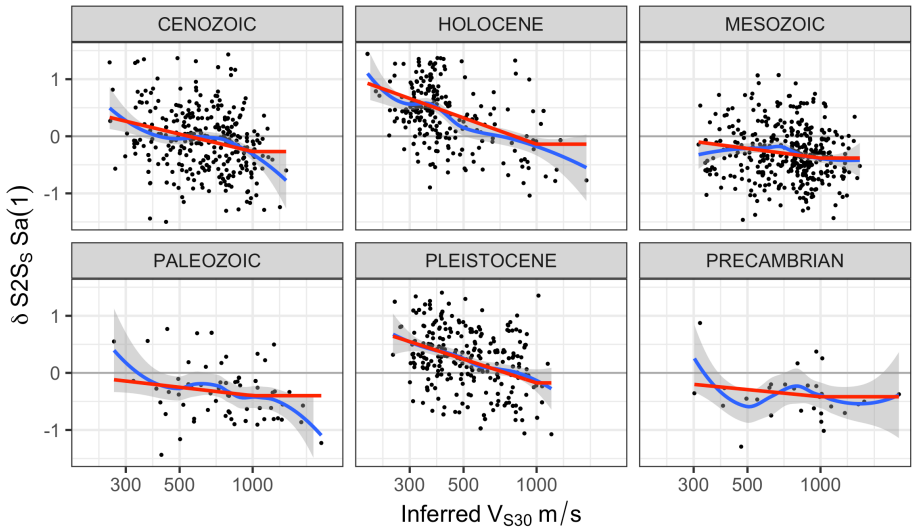

Figure 31: As Figure 30 for inferred V_{S30} using the Wald & Allen (2007) approach.

Contrasting the amplification factors from the observed and inferred V_{S30} models it is evident that inferred V_{S30} from topography does not manage to replicate some of the key trends found in the observed V_{S30} dataset. Arguably the greatest contrast between the two can be seen for older pre-Cambrian to Mesozoic rocks for which substantially higher amplification factors are seen on softer soils for observed V_{S30} than for inferred V_{S30}. This is mostly illustrative of the general limitations of the topographically inferred site conditions, in conjunction with the resolution of the geological data set. The geological information is indicative only of the broader domains to which a region belongs and cannot readily resolve variation in shallower sediments. Naturally, a single geological unit may encompass harder rock outcrops, or rock with only thin layers of sediments, in addition to deeper beds. Large scale sedimentary basins such as the Po Plain or Rhine Graben are well represented, but thinner layers of softer sediments overlaying older rock may account for low V_{S30} values in these domains, illustrating that for short period motion it is the shallowest geology that has the greatest control and for this purpose direct measurement of observed V_{S30} is required. At longer periods the two converge, suggesting that the inferred V_{S30} is in some respects able to characterise facets of the local geology affecting lower frequency motion. It is unclear, however, why a better agreement can be seen at longer periods between observed and inferred V_{S30} amplification factors in Holocene environments than in Pleistocene environments.

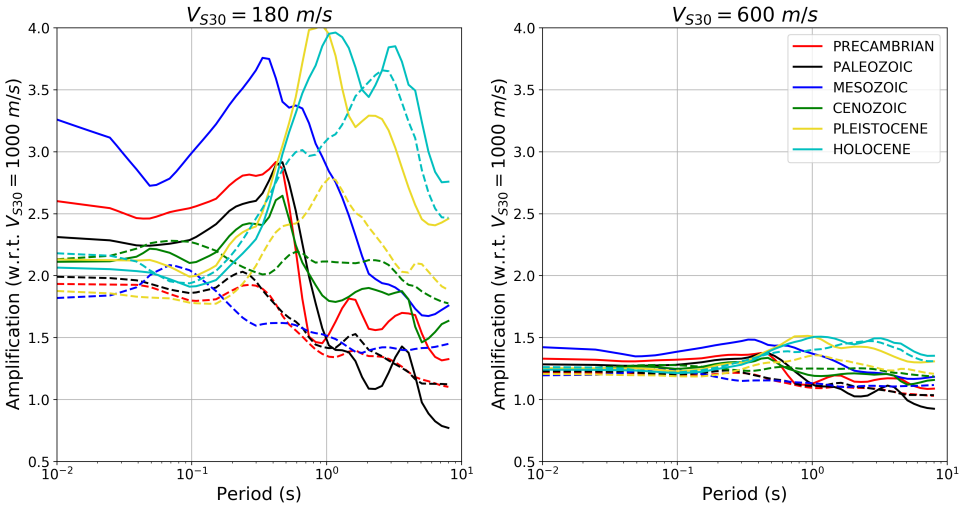

Figure 32: Amplification with period with respect to V_{S30} 1000 m/s for each geological unit for observed V_{S30} (solid lines) and inferred V_{S30} (dashed lines)

5.3 Regional site amplification without V_{S30}

The regression models between $\delta S2S_S$ and V_{S30} demonstrate clearly that with or without the inclusion of geology, inferred V_{S30} does not predict the same degree of amplification as that of observed V_{S30}. When geology is included, however, changes in the amplification can be seen that suggest that it may be relevant in better predicting amplification in certain domains. From this one would conclude that inferred V_{S30} is not an adequate substitute for measured V_{S30}; a result that should be intuitive. But it is important not to lose sight of the fact that inferred V_{S30} is used in the first place not because it is considered the optimal predictor of amplification, but that it is practical from the perspective of being possible to characterise anywhere on the globe. A considerable body of scientific literature has emerged in which many scientists have attempted to refine or improve upon the Wald & Allen (2007) work, either by attempting to calibrate the slope to V_{S30} relations for a particular region, or by refining it using other information, most commonly geology (Thompson et al., 2014; Kwok et al., 2018; Vilanova et al., 2018). Yet this objective seldom challenges the notion that in application it is not the V_{S30} itself that is the target but the ability of the site parameter to predict the amplification.

The $\delta S2S_S$ data set combined with both ESM metadata and the topography and geology data compiled within this work package provides an opportunity to assess to what extent inferred V_{S30} adds predictive value in modelling the amplification when compared to direct usage of slope alone, from which the inferred V_{S30} is derived. Using the 30 arc-second continuous topography and bathymetry data set described in Chapter 2, slope is calculated for each site in the ESM flatfile using the Horn algorithm within the Generic Mapping Tools Software. The correlation between $\delta S2S_S$ and slope, without geology, is shown in Figure 33.

In general, it can be seen that scaling trends of a similar magnitude to that of inferred V_{S30} are found, with a similar degree of scatter. As Wald & Allen (2007) assume a near linear equivalence between the natural logarithm of slope (in m/m) and the natural logarithm of V_{S30} a function can be fit to predict f_S given slope adopting a similar form to that found in equation 5.2:

$$f_S(slope) = \begin{cases} c_0(T) + c_1(T) \cdot \ln slope \\ c_0(T) + c_1(T) \cdot \ln X_C \end{cases} + \varepsilon \quad \begin{matrix} \text{for slope} \leq X_C \\ \text{for } slope > X_C \end{matrix} \qquad [5.3]$$

Where c_0 and c_1 are period dependent coefficients to be fit, and X_C a hinge value found to be period-independent and constant at 0.2 m/m. The fit piecewise-linear models for slope are shown in Figure 33, in addition to the non-parametric LOESS regression.

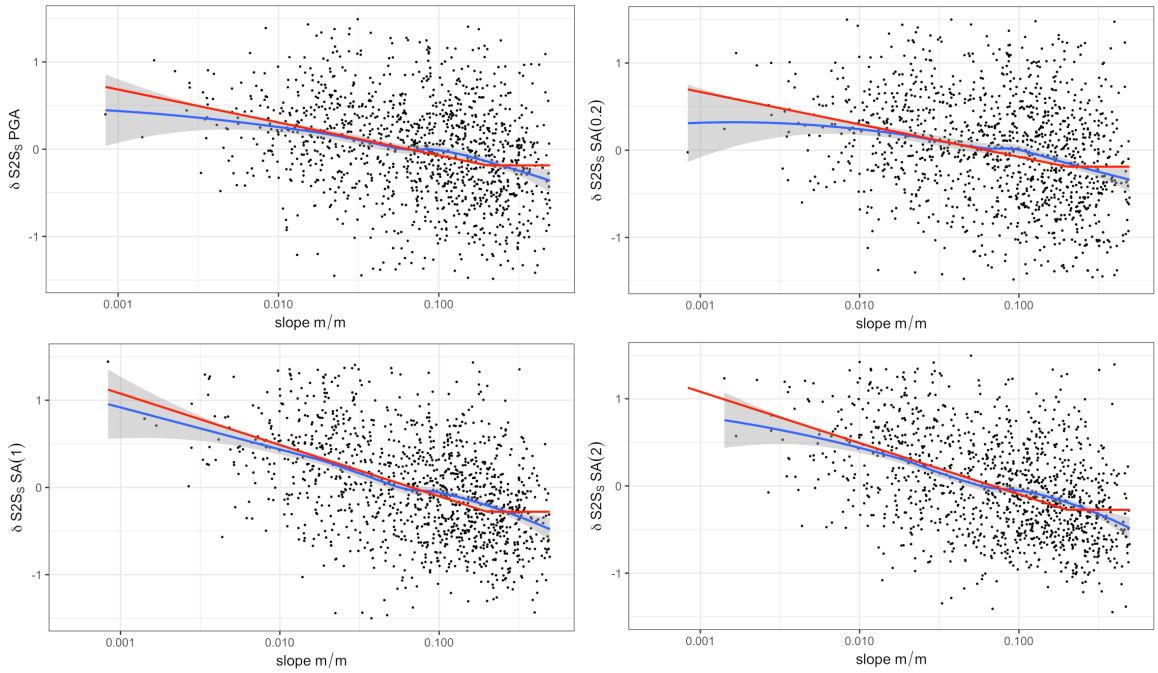

Figure 33: As Figure 26 for the case of topographic slope in m/m.

To determine the efficiency of each of the three variables (observed V_{S30}, inferred V_{S30} and slope) in predicting site response the resulting variability is shown for each (ϕ_S) in Figure 34. These are then integrated with the inter- and single station intra-event variability to give the total standard deviation (σ_T). The definitions of the ergodic, single-station and model total aleatory variability are:

$$\sigma_{SS}^2(\text{single station}) = \tau^2 + \phi_0^2$$

$$\sigma_T^2(\text{ergodic}) = \tau^2 + \phi_0^2 + \phi_{S2S}^2$$

$$\sigma_T^2(\text{model}) = \tau^2 + \phi_0^2 + \phi_S^2$$

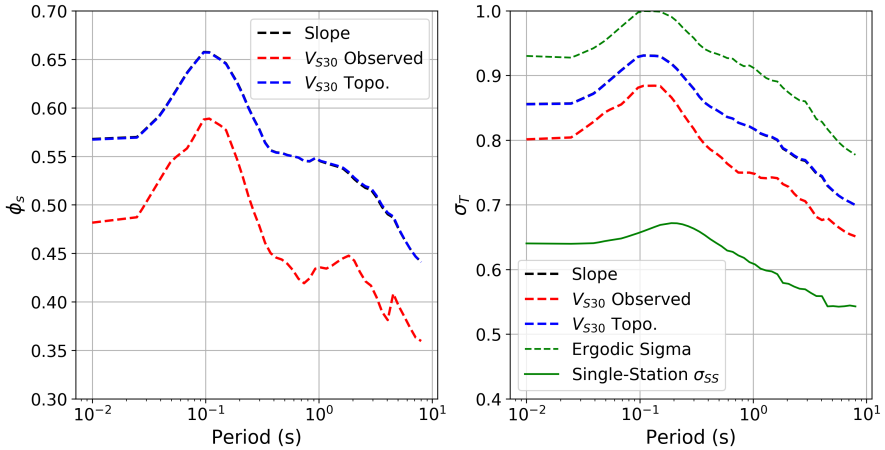

Figure 34: Comparison of the f_S aleatory uncertainty (ϕ_S) (left) and the resulting total aleatory uncertainties of the shallow crustal GMPE (right)

The comparison of the uncertainties shows that the resulting aleatory uncertainty when using inferred V_{S30} and using slope directly are virtually identical. This is not a surprising result given that inferred V_{S30} is a linear function of slope itself. The resulting total aleatory variability, however, when using either slope directly or inferred V_{S30} is between 0.06 – 0.07 log units greater, depending on period, than when using observed V_{S30}.

In the same manner shown in Section 5.2 for V_{S30} we can also assess the impact of incorporating geology into the prediction of amplification. Figure 35 shows the results of implementing a mixed-effects regression methodology to determine $c_{0,g}$ and $c_{1,g}$ dependent upon the geological era. Once again, similar trends can be seen as those in the V_{S30} comparisons, albeit potentially steeper gradients can be seen in the trends between $\delta S2S_S$ and slope for Holocene sites at short periods than was evident for V_{S30}. The resulting amplification trends are illustrated in Figure 36. As with inferred V_{S30}, we find that for slope we observe the largest amplifications at longer periods.

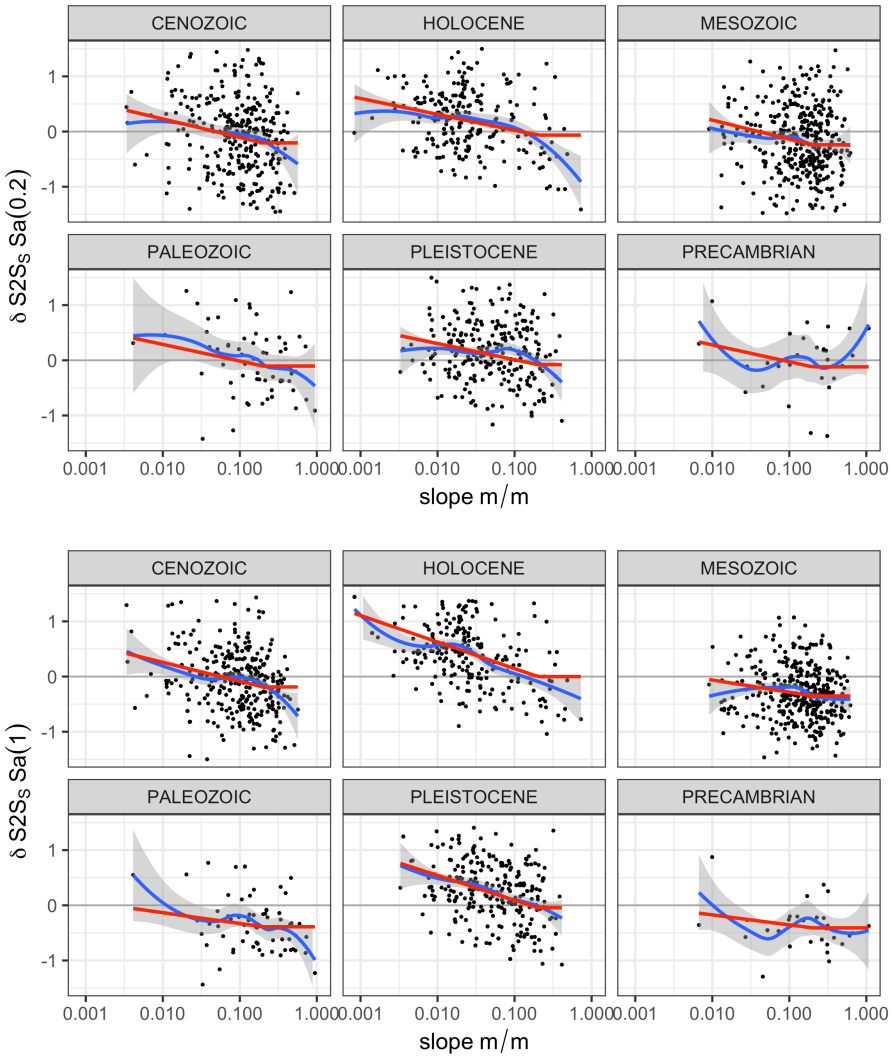

Figure 35: As Figure 30 and Figure 31 for the case of slope as the predictor variable

The resulting changes in aleatory variability when incorporating geology into the regression models can be seen in Figure 37, in which the dashed lines indicate the ϕ_S for each of the three variables when geology is excluded, and the solid lines when it is included. Firstly, it can be seen that the incorporation of geology does have a notable reduction on ϕ_S at spectral periods longer than approximately 0.5 s both for the slope and the inferred V_{S30} model. Somewhat surprisingly, a small improvement can even be found in observed V_{S30} at periods greater than 0.8 s. For short periods, however, the reduction is marginal. It should be emphasised, however, that although ϕ_S may be an indicator of net efficiency of the predictor variable, as small variation in scaling trends from geological era to geological era can be seen in the data then this additional information provides a refined amplification estimate that does not treat different geological environments interchangeably. Therefore, in the current application in the context of the European model, for which geology estimated for each site in Europe from the data

set given in Chapter 2, the inclusion of geology as a site parameter does lead to an improved characterisation of site amplification without additional cost.

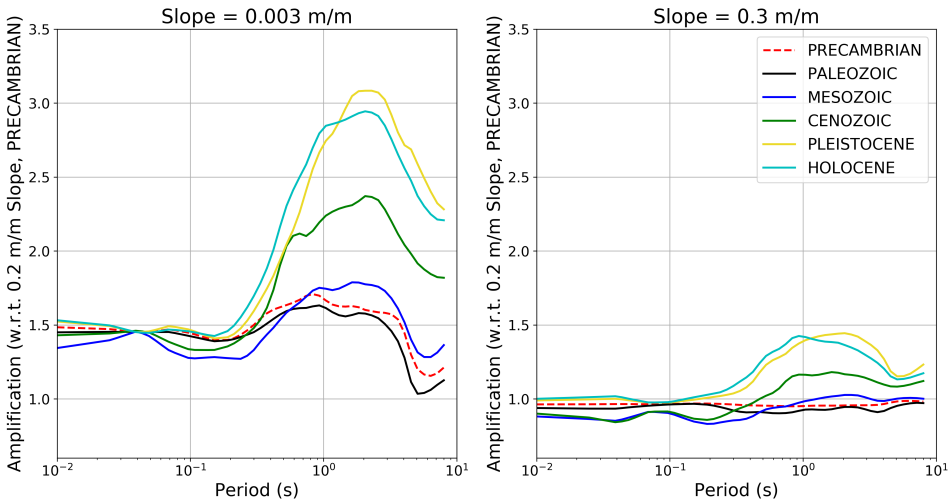

Figure 36: Amplification of ground motion for a slope of 0.003 m/m (left) and 0.3 m/m (right) with each geological class. Amplification is with respect to a site of slope 0.2 m/m on Pre-Cambrian rock

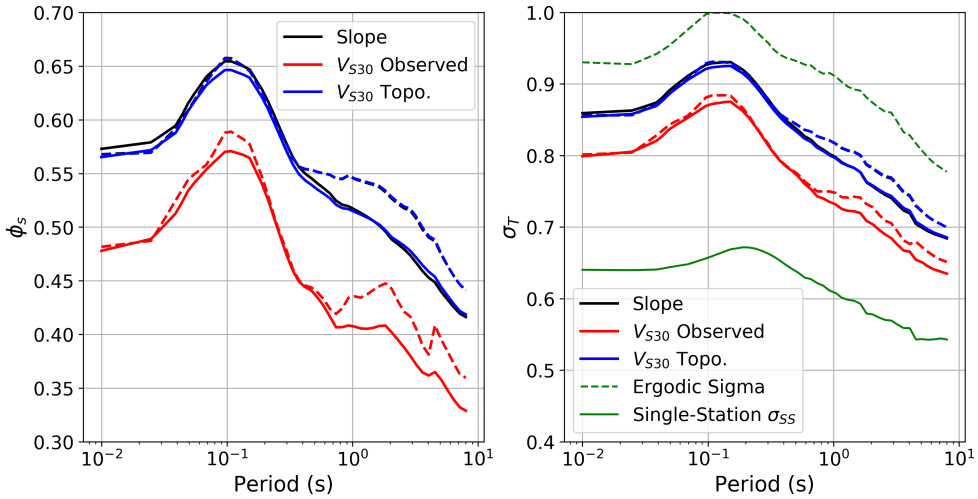

Figure 37: Aleatory uncertainty on the site amplification function, ϕ_S (left), and the total variability, ϕ_T (right), for the different predictor variables when geology is excluded from the regression (dashed lines) and when it is included (solid lines).

5.4 Potential for modelling site amplification at European scale

The development of the $\delta S2S_S$ data set from the shallow crustal GMPE for Europe, in conjunction with the compilation of geological and topographic data described in this deliverable, have provided an opportunity to explore potential pathways for characterising site amplification at a regional level. It cannot be overstated however, that the objectives of regional scale seismic risk analysis are inevitably divergent from those of site-specific analysis. From the outset it is understood that measurement of V_{S30}, or even rapidly obtainable parameters such as f0, is not achievable on a spatial scale and resolution required for the seismic risk model. To achieve the desired spatial coverage compatible with the exposure model, a minimum level of uniformity in the site parameterisation is required, and this inevitably leads to the invocation on a regional scale of proxies in place of measured site parameters.

The topographically-inferred V_{S30} approach introduced by Wald & Allen (2007) (and applied at a European scale in Chapter 4) sought to meet this objective, recognising that correlation exists between broader-scale geomorphological parameters and those factors affecting site response, namely V_{S30}. The analysis within this section illustrates both the benefits and limitations of this approach and calibrates the potential penalty that should be paid in terms of the uncertainty of the ground motion when invoking this proxy in place of the measured V_{S30}. There exists no substitute for better information and detailed site characterisation, so the imposition of a penalty of higher uncertainty when this is absent should be a fundamental component of any seismic risk model. A corollary to this is that given the differences in amplification between inferred and observed V_{S30}, derivation of ground motion models that treat the two interchangeably without penalty, or otherwise take into account uncertainty in V_{S30} within the regression, may be notably underestimating the resulting uncertainty in the model.

The comparisons shown in this chapter also demonstrate that when uncertainty is explicitly accounted for within the total aleatory variability, there is no discernible gain in accuracy for using the inferred proxy V_{S30} in favour of direct adoption of the mapped quantity from which this proxy is derived. Hence, topographically-inferred V_{S30} characterises amplification similarly to direct adoption of topography. Some reduction in uncertainty can be seen when the scaling of site amplification with respect to a mappable parameter is then conditioned upon geology. As this comes at no additional cost then it is recommended that this be considered for inclusion within the seismic risk calculation.

To conclude the analysis, it simply remains to be illustrated that the models derived in this section provide a practical means of characterising site amplification at a European scale. To do so, Figure 38 and Figure 39 present a 30-arc second slope and geology-calibrated site amplification map for Europe for Sa (0.2 s) and Sa (1.0 s) respectively. In this example the “reference” condition to which the amplification refers is for a site on a 30 arc-second slope of 0.2 m/m located within the Pre-Cambrian domain. These maps are not an end-point in themselves and should obviously not be treated as a substitute for site investigation, but instead merely illustrate the spatial extent of regions where local site characteristics may be expected to increase the seismic hazard with respect to a reference rock or site condition. Indeed, the results presented here are intended as complete period-dependent models of amplification that span the range of possible geotechnical, geomorphological and geological conditions found within Europe. Given the characteristics of the slope and geology-based amplification model, higher amplifications are seen at longer periods. Amongst the regions of higher amplification highlighted are the deep recent sedimentary environments of the Po Plain, Pannonian Basin, Rhine Graben and assorted local extensional basins in Greece and Western Turkey.

Naturally, these models contain several caveats that should be taken into consideration. The first is that the accuracy of the model is inevitably dependent on the accuracy of the data from which it is derived. Misclassifications of stations due to inaccuracies in the geological map may account for some of the uncertainty in the process, though variability in shallow surficial geology within a given unit is more likely the predominant factor. The second caveat is that the amplification model is calibrated upon data that are not uniformly distributed across Europe but are instead skewed significantly toward the more active Mediterranean region. In the absence of further data, one is forced to make the assumption that within a given geological unit differences between active and stable regions are minimal. Certain geological units such as Pre-Cambrian rock are far more predominant in the stable regions of Europe than in the small outcrops found close to the Alps. A larger scale, and potentially more geologically homogeneous, Pre-Cambrian domain may very well display different amplification characteristics when compared to the small number of sites sampled within the ESM data set.

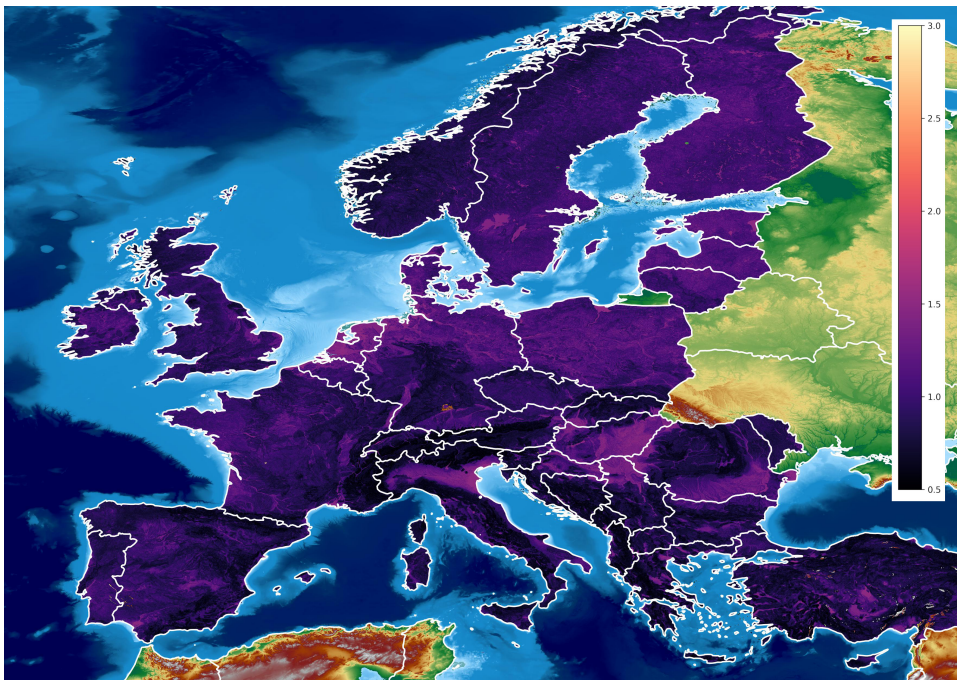

Figure 38: Example of spatial variation in Sa (0.2 s) amplification across Europe, with respect to a site with 0.2 m/m slope on Pre-Cambrian rock derived from slope and geology.

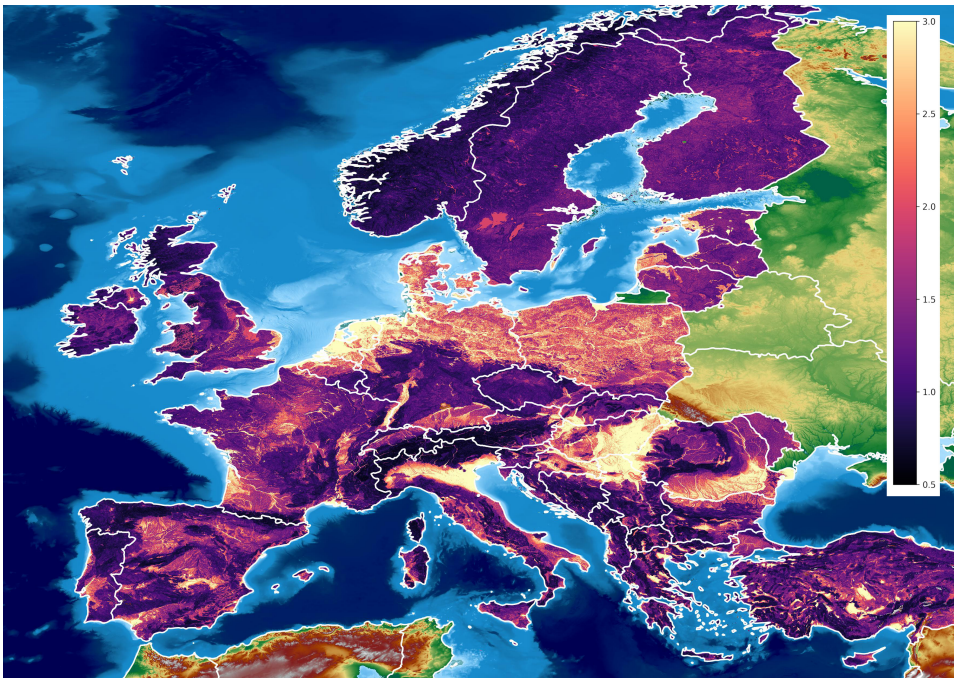

Figure 39: As Figure 38 for Sa (1.0 s)

For application to seismic hazard and risk in Europe the following approaches are recommended on the basis of these comparisons:

1. For calculation of seismic hazard on Eurocode 8 class A rock (V_{S30} 800 m/s) the form of the amplification model dependent only upon *observed/measured* V_{S30} should be used.
2. For seismic risk analysis where local data provide good constraint of the site condition, e.g. microzonation derived site profiles, V_{S30} measurements etc., the corresponding form of the amplification model dependent on *observed/measured* V_{S30} should be adopted.

3. Where no local site data are available to provide an improved constraint (e.g. measured V_{S30}, site profiles etc.) the following options should be considered, in no specific order of priority:
    a. V_{S30} from the Wald & Allen (2007) dataset should be used in conjunction with the geological units, to be implemented using the geologically-calibrated *inferred* V_{S30} amplification model
    b. The 30 arc-second slope data should be used in conjunction with the geological units, to be implemented using the geologically-calibrated *slope* amplification model
    c. A topographically inferred V_{S30} model is derived and calibrated given the geological information for Europe. This *could* be implemented using the general form of the *inferred* V_{S30} amplification model, with ϕ_S taken from the geologically-calibrated inferred V_{S30} amplification model.

A comparison of several of these methods, alongside details of their implementation within the OpenQuake-engine software for seismic hazard and risk calculation will be presented in Chapter 7.

6 Nonlinear site amplification model for site classes

This chapter describes a nonlinear site amplification model that characterises the site using both V_{S30} and T_0 and provides amplification factors that are calibrated using strong motion simulations.

6.1 Site amplification data

For the development of the nonlinear site amplification model by Pitilakis et al. (2018), the experimental data from the SHARE-AUTH database were used (Pitilakis et al., 2013) in combination with results from theoretical analyses of representative models of realistic soil conditions (Pitilakis et al., 2004, 2006).

SHARE-AUTH database is a subset of the strong motion database which was compiled within SHARE (Yenier et al. 2010) and contains records only from sites with very well-known geotechnical information until the seismic rock basement. Profiles of shear wave propagation velocity Vs with depth were collected for as many stations included in the SHARE database as possible, from a number of sources, given in Table 6. The Vs profiles obtained have been measured with a variety of surveying methods. For most of the sites (70% of the total sample), Vs-profiles have been obtained from borehole measurements (e.g. cross-hole, down hole). For the rest of the sites, for example the Turkish stations (24% of the total sample), the Vs-profiles have been evaluated using surface wave inversion surveys. SHARE-AUTH database contains 3,666 strong motion records from 536 stations from Greece, Italy, Turkey, Japan and USA and constitutes a reliable set of empirical measurements for estimation of influence of local site conditions. The geographic distribution of the selected stations and records is presented in Figure 40. The distribution of moment magnitude M_w and geometric mean of the peak ground acceleration values (PGA) of the two horizontal components with epicentral distance R_{epi} for the records of SHARE-AUTH database is illustrated in Figure 41a and Figure 41b respectively. It is observed that there are relatively few records with PGA values exceeding 200cm/s^2 and many weak motion records with peak values less than 20cm/s^2.

For the 536 stations of the database, new site parameters, not included in the original database, were calculated. These include the thickness of the soil deposits H (i.e. depth to "seismic" bedrock - Vs>800m/s), the time-based average shear wave velocity $V_{s,av}$ of the entire soil deposit and the fundamental period T_0 of the soil deposit. In addition, V_{S30} values were recalculated for all sites.

Table 6. Source of the Vs profiles of the stations in SHARE-AUTH database

Station Country	Vs profile source	Number of stations	
Greece	AUTH Research Unit of Soil Dynamics & Geotechnical Earthquake Engineering	20	
Italy	Italian Accelerometric Archive	72	
Japan	Kik-Net	100	Total: 249
	K-Net	149	
Turkey	Turkish National Strong-Motion Database	131	
USA	ROSRINE program	23	Total: 64
	D. Boore's personal webpage	32	
	USGS Open-File Reports	6	
	Nigbor and Steller Rep#9225-6427 (3/11/1993)	2	
	Kajima Corporation	1	

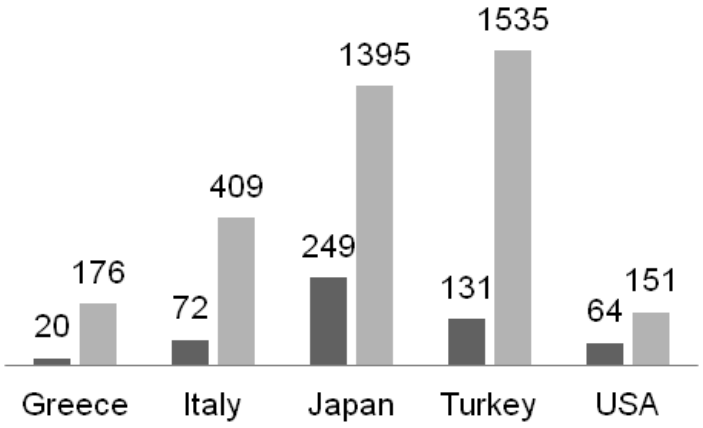

Figure 40: Geographic distribution of selected 536 stations (in dark grey) and 3666 records (in light grey)

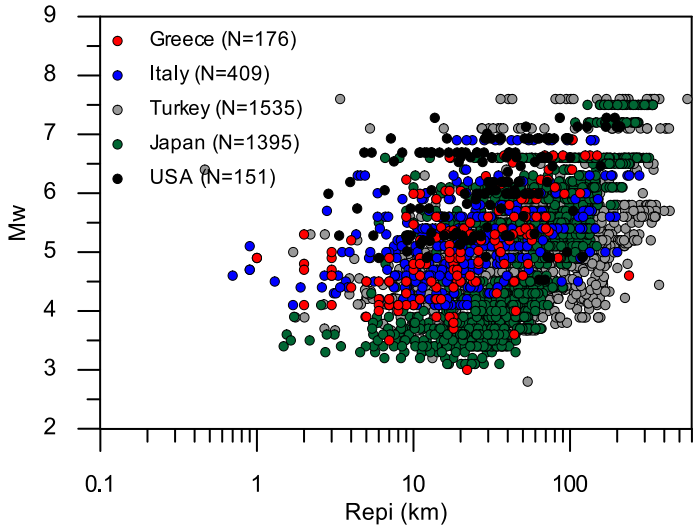

(a)

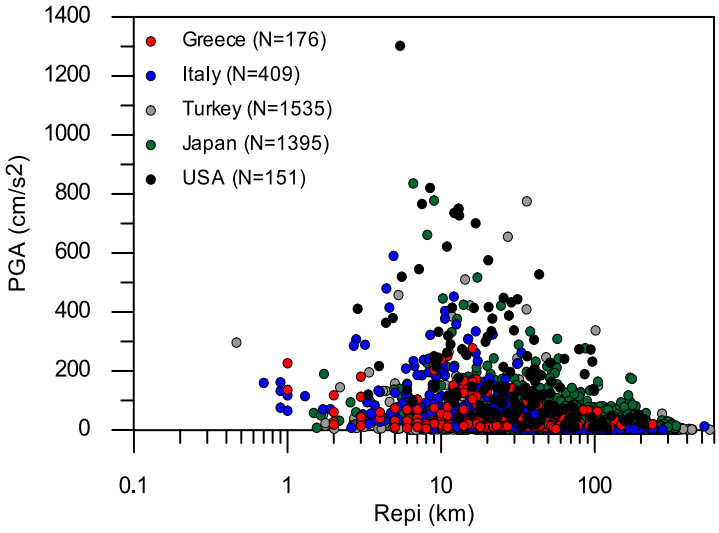

(b)

Figure 41: Data coverage of SHARE-AUTH database records in terms of (a) Moment Magnitude M_w - Epicentral distance R_{epi} and (b) Peak Ground Acceleration (PGA) - Epicentral distance R_{epi}. Different colours are representative for different station countries.

6.2 Description of soil classification scheme

In the framework of the ongoing revision of Eurocode 8, Pitilakis et al. (2018) proposed a new classification scheme and associated intensity dependent soil amplification factors. The new classification scheme, introducing among the main classification parameters the fundamental period T_0 of the site, is an evolution of the recent work by Pitilakis et al. (2013), while the main features of the amplification factors and the new seismic design actions are summarized in the use of two anchoring spectral values, for short (0.2s-0.3s) and intermediate (1.0s) periods, instead of only one of the present version of Eurocode 8 (i.e. effective ground acceleration), and the scalar intensity variation of site amplification factors to account for soil nonlinearity. The work is based on a comprehensive analysis of a worldwide database of the strong ground motion records of SHARE-AUTH database (see Section 6.1).

The proposed classification scheme comprises six main soil classes, i.e. A, B, C, D, E and X, with sub-classes for site class B and C according to Table 7. The main classification parameters are the fundamental period of soil deposit, T_0, the average shear wave velocity of the entire soil deposit to the "seismic bedrock" (defined with Vs>800m/s), $V_{s,av}$, or the average shear wave velocity of the upper 30m of the soil profile, V_{S30}, and the broadly known thickness of the soil deposit, i.e. depth to "seismic" bedrock, H, along with the dominant soil profile description, and average values of standard penetration test blow count, N_{SPT}, plasticity index, PI and undrained shear strength, S_u over broadly estimated depth H. Parameters derived from other field tests like the cone penetration test CPT or pressumeter may be also used. To obtain T_0 and $V_{s,av}$ or V_{S30}, invasive (in-hole measurements) or non-invasive (e.g. surface-waves analysis) techniques at small shear strains are suggested. In case of absence of direct measurement parameters, adequate correlations with SPT and CPT may be applied.

Table 7. Site categorization scheme proposed by Pitilakis et al. (2018)

Site class	Description	T_0	Remarks	
A	Rock formations	≤ 0.2s	Hard rock $Vs_{,av}$ >1500 m/s	
	Slightly weathered/ segmented rock formations (thickness of weathered layer <5.0m)		Rock like formations: $Vs_{,av}$ or $Vs_{,30}$ ≥ 800 m/s	
	Geologic formations resembling rock formations in their mechanical properties and their composition (e.g. conglomerates)		Surface weathered layer (if any with H<5m): $Vs_{,av}$ ≥ 300 m/s	
B	Soft rock formations	0.1-0.3s ≤ 0.3s		B1
	Formations which resemble to soft rock in their mechanical properties (e.g. stiff marls)		$Vs_{,av}$: 350-600 m/s	
	Very dense sand-gravels		$Vs_{,30}$: 400-760m/s	
	Hard and very stiff clays		N-SPT > 50	
	H<30m		S_u> 150 kPa	
	Soil formations of very dense sand –sand gravel and/or very stiff/ to hard clay, of homogenous nature, whose mechanical properties increase with depth	0.3-0.6s ≤ 0.6s	$Vs_{,av}$: 400-550 m/s	B2
			$Vs_{,30}$: 350-500m/s	
			N-SPT > 50	
	30m<H<120m		S_u> 150 kPa	

	Soil formations of dense sand –sand gravel and/or stiff clay, of great thickness (> 60.0m), whose mechanical properties and strength are constant and/or increase with depth H>60m	0.6-1.0s ≤ 1.0s	$Vs_{,av}$: 400-600 m/s $Vs_{,30}$:350-450 m/s N -SPT> 50 S_u > 150 kPa≤ 1.0s	C1
C	Soil formations of medium dense sand – sand gravel and/or medium stiffness clay (PI > 15, fines percentage > 30%) 20m <H< 60m	0.3-0.7s ≤ 0.8s	$Vs_{,av}$: 250-450 m/s $Vs_{,30}$:250-400 m/s N -SPT> 20 150 kPa> S_u>70 kPa	C2
	Like C2 but with great thickness H>60m	0.7-1.4s ≤ 1.4s	$Vs_{,av}$: 300-500 m/s $Vs_{,30}$:200-350 m/s N -SPT> 20 150 kPa> S_u >70 kPa	C3
	Recent soil deposits of substantial thickness (up to 60m), with the prevailing formations being soft clays or/ and clays with a thickness h>3.0m, of high plasticity index (PI>20-30), high water content (W>40%) and low values of strength parameters (S_u<25 kPa)	≤ 1.4s		
D	Recent soil deposits of substantial thickness (up to 60m), with prevailing loose sandy to sandy-silty formations with a substantial fines percentage (not to be considered susceptible to liquefaction)	≤ 1.4s	$Vs_{,av}$: 200-400 m/s $Vs_{,30}$:150-300 m/s N-SPT < 20 S_u < 70 kPa	
	Soil formations of great overall thickness (> 60.0m), interrupted by layers of soft soils of a small thickness (5 – 15m), up to the depth of ~40m, within soils (sandy and/or clayey, category C) of evidently greater strength, with $Vs_{,av}$≥ 300 m/s	1.4-3.0s ≤ 3.0s		
E	Surface soil formations of small thickness (5 - 20m), small strength and stiffness, likely to be classified as category C and D according to its geotechnical properties, which overlie category A formations ($Vs_{,av}$ ≥800 m/s)	0.1-0.5s ≤ 0.5s	$Vs_{,av}$: 160- 300 m/s	
X	Loose fine sandy-silty soils beneath the water table, susceptible to liquefaction (unless a special study proves no such danger, or if the soil's mechanical properties are improved) Soils near obvious tectonic faults Steep slopes covered with loose deposits Loose granular or sot silty-clayey soils, provided they have been proven to be hazardous in terms of dynamic compaction or loss of strength. Recent loose landfills Soils with a very high percentage in organic material Special soils requiring site-specific evaluations			

Ranges of T_0, H, V_{S30} and $V_{s,av}$ for site classes of Table 7 were derived based on experimental data from the SHARE-AUTH database (Pitilakis et al., 2013) and when needed from theoretical analyses of representative models of realistic soil conditions (Pitilakis et al., 2004, 2006) applying classical statistics. Figure 42 illustrates the median, 16th and 84th percentile values of T_0, H, $V_{s,av}$ and V_{S30} for the sites of SHARE-AUTH database classified according to the site categories of Table 7. The classification of the sites of SHARE-AUTH database according to the classification scheme proposed by Pitilakis et al. (2018) as well as the one of the current version of EC8 (CEN, 2004) is shown in Figure 43.

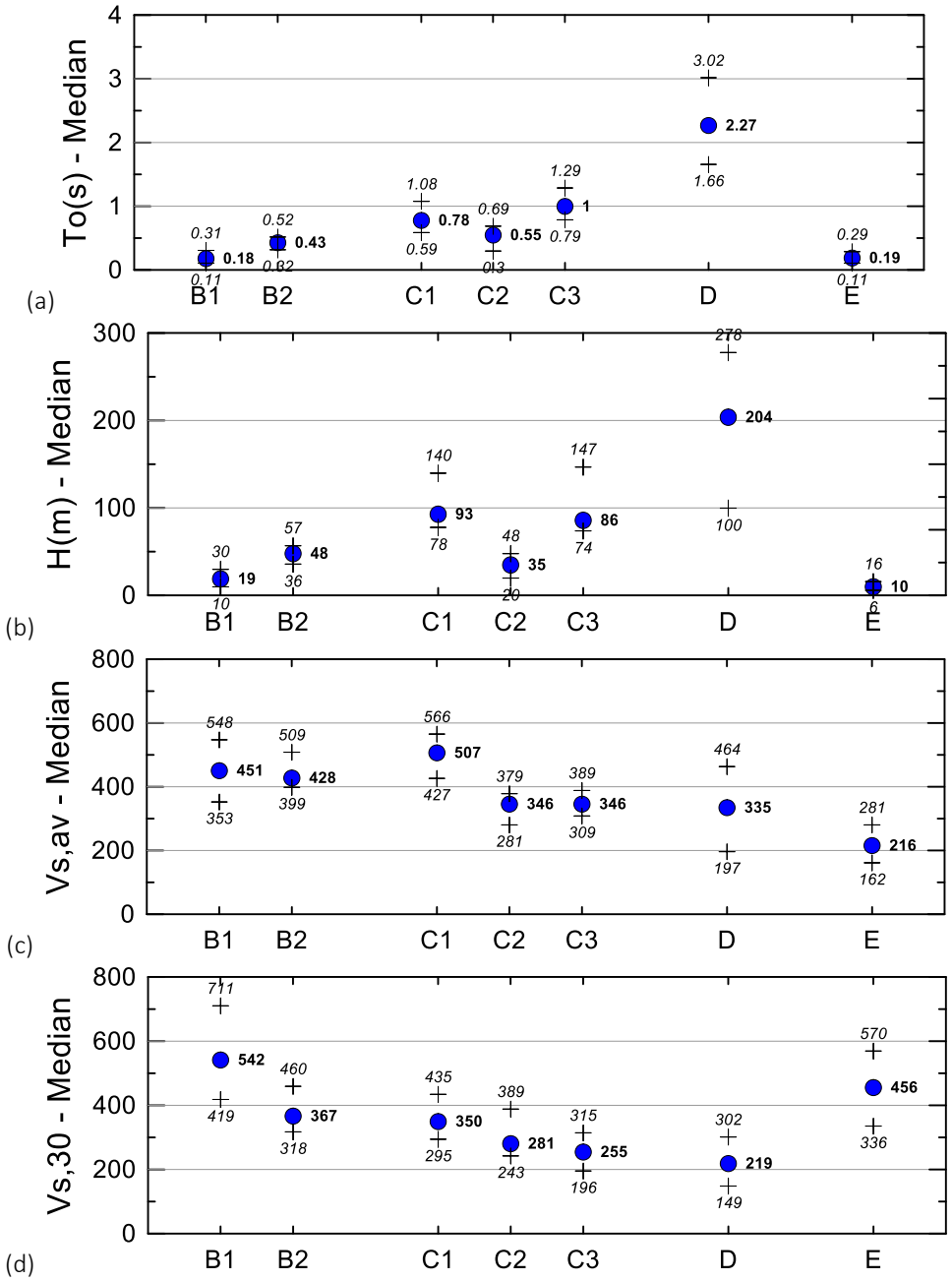

Figure 42: Median, 16th and 84th percentile values of (a) fundamental period of soil deposit, T_0 (in s), (b) depth to seismic bedrock, H (in m), (c) average shear wave velocity of the soil deposit, $V_{s,av}$ (in m/s) and (d) average shear wave velocity of the upper 30m of the soil profile, V_{S30} (in m/s) of the sites of SHARE-AUTH database classified according to the site categories of Table 7.

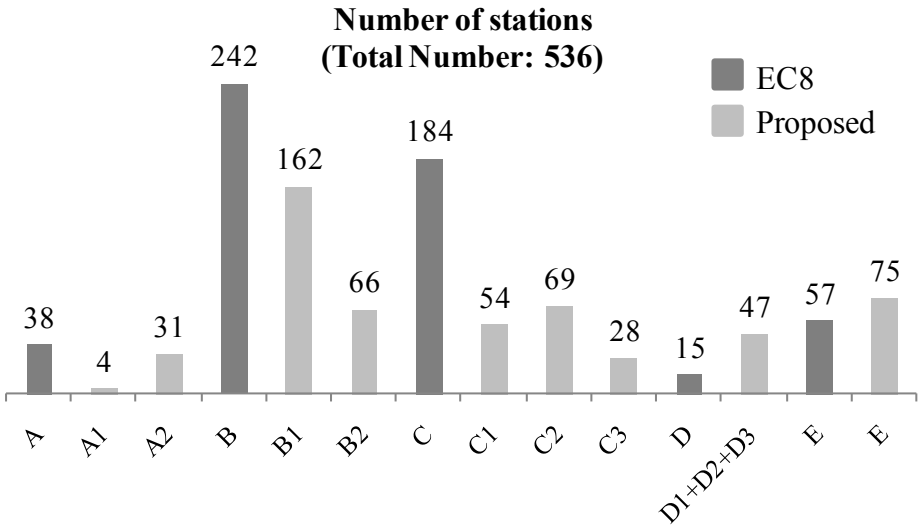

Figure 43: Classification of the sites of SHARE-AUTH database according to EC8 (in dark grey) and the classification scheme by Pitilakis et al. (2018) (in light grey)

6.3 Elastic response spectra and nonlinear soil amplification factors

In line with the present practice in modern international seismic codes (e.g. NEHRP, BSSC 2015), the seismic hazard in Pitilakis et al. (2018) is proposed to be described in terms of two parameters, namely S_{sRP} (i.e. the reference maximum spectral acceleration, corresponding to the constant acceleration branch of the horizontal 5% damped elastic response spectrum on site class A) and S_{1RP} (i.e. the reference spectral acceleration at the vibration period T = 1 s of the horizontal 5% damped elastic response spectrum on site class A) instead of only one, a_g (i.e. the effective ground acceleration on site class A). S_{sRP} and S_{1RP} should be provided in the National Annex of each European country for the reference return period T_{ref} (e.g. 475 years), depending also on the local seismic hazard. For the horizontal components of the seismic action, the elastic response spectrum $S_e(T)$ for 5% damping is defined by the following expressions:

$$0 \le T \le T_A : \; S_e(T) = \frac{S_S}{F_0} \qquad [6.1]$$

$$T_A \le T \le T_B : \; S_e(T) = \frac{S_S}{T_B - T_A}\left[\eta \cdot \left(T - T_A\right) + \frac{T_B - T}{F_0}\right] \qquad [6.2]$$

$$T_B \le T \le T_C : S_e(T) = \eta \cdot S_S \qquad [6.3]$$

$$T_C \le T \le T_D : S_e(T) = \eta \cdot \left[\frac{S_1 \cdot T_1}{T}\right] \qquad [6.4]$$

$$T \ge T_D : S_e(T) = \eta \cdot T_D\left[\frac{S_1 \cdot T_1}{T^2}\right] \qquad [6.5]$$

where T is the vibration period of a linear single-degree-of-freedom system; S_s is the maximum response spectral acceleration (5% damping) corresponding to the constant acceleration range of the elastic response spectrum; S_1 is the 5% damping response spectral acceleration at the vibration period

T_1=1s; T_A is the short-period cut-off associated to the effective ground acceleration; F_0 is the ratio of S_s with respect to the effective ground acceleration; $T_C=S_1 \cdot T_1/S_s$ is the upper corner period of the constant spectral acceleration range; $T_B=T_C/\kappa$ is the lower corner period of the constant spectral acceleration range, with $0.05 \leq T_B \leq 0.1$s, whatever value of T_C; κ is the ratio of T_C and T_B; T_D is the corner period at the beginning of the constant displacement response range of the spectrum; η is the damping correction factor, with a reference value of η = 1 for 5% viscous damping. Table 8 presents generic values for parameters T_A, κ, F_0 and T_D.

Table 8. Recommended values for seismic hazard parameters defining the elastic response spectrum

T_A (s)	κ	F_0	T_D (s)
0.03	5	2.5	2 if $S_{1RP} \leq 0.1$g $1+10 \cdot S_{1RP}$ if $S_{1RP} > 0.1$g

The spectral accelerations S_s and S_1 are defined as follows:

$$S_s = F_s \cdot S_{sRP} \quad [6.6]$$

$$S_1 = F_1 \cdot S_{1RP} \quad [6,7]$$

where F_s is the short period site amplification factor and F_1 is the intermediate period (T_1=1s) site amplification factor.

To account for soil nonlinearity, site amplification factors F_s and F_1 for the different soil classes are proposed for distinct values of S_{sRP} (reference maximum spectral acceleration at rock site conditions). Following the rationale of the Boore et al. (2014) GMPE, amplification factors F_i (i=s,1) are considered to comprise two additive terms, i.e. a linear component, $F_{i,lin}$, which is practically independent of the amplitude of shaking, and a nonlinear component, $F_{i,nl}$, which modifies the linear term in order to decrease amplification for increasing shaking intensity:

$$F_i = \ln(F_{i,lin}) + \ln(F_{i,nl}), \quad i = s,1 \quad [6.8]$$

For the linear component, $F_{i,lin}$, soil amplification factors proposed by Pitilakis et al. (2013) for Type 2 (low seismicity) were adopted, which were estimated using a subset of the SHARE-AUTH database, consisting of 715 strong-motion records with surface wave magnitude $M_s \geq 4$, PGA≥20cm/s^2 and usable spectral period T≥2.5s. For the nonlinear term, the formulation developed by Seyhan and Stewart (2014) and adopted in the Boore et al. (2014) GMPE was applied:

$$\ln(F_{i,nl}) = f_1 + f_2 \ln\left(\frac{a_g + f_3}{f_3}\right) \quad [6.9]$$

where a_g is the median effective horizontal acceleration for reference rock and f_1, f_2, f_3, f_4, f_5 are model coefficients defined in Seyhan and Stewart (2014) as follows: f_1=0, f_2=0.1, f_4 and f_5 are period-dependent coefficients and f_2 is a function of period and $Vs_{,30}$ as follows:

$$f_2 = f_4\left[\exp\left\{f_5\left(\min\left(V_{s,30},760\right)-360\right)\right\} - \exp\left\{f_5\left(760-360\right)\right\}\right] \quad [6.10]$$

The adopted procedure to estimate site amplification factors F_s and F_1 for the soil classes of Table 7 is summarized in the following. First, the Type 2 period-dependent soil amplification factor according to Pitilakis et al. (2013) is estimated for each soil class by normalizing the Type 2 elastic response spectrum of the specific soil class by the Type 2 spectrum for soil class A. The values of the period-dependent amplification factor corresponding to the constant acceleration branch of the spectrum and to T=1s are then identified, to obtain the linear terms for the short period site amplification factor, $F_{s,lin,}$ and

intermediate period site amplification factor, $F_{1,lin,}$ respectively. The nonlinear terms of amplification factors are calculated for distinct levels of a_g (= S_{sRP} /F_0), using Equations (6.9) and (6.10). In Equation (6.10) the average values of $Vs_{,30}$ of the sites of the SHARE-AUTH database (PItilakis et al., 2013) classified in each site category are used. Applying Equation (6.8), site amplification factors F_s and F_1 were finally estimated for distinct values of S_{sRP}, equal to 0.125, 0.25, 0.5, 0.75, 1.0 and 1.25g. The proposed values for F_s and F_1 (Table 9 and Table 10) were obtained after adequate rounding. For intermediate values of S_{sRP}, straight line interpolation of the values of F_s and F_1 of Table 9 and Table 10 is suggested. For the computation of site amplification factors of site class X and for buildings of importance classes III or IV based on the current version of EC8 (CEN, 2004) located on sites classified as D or E, site-specific geotechnical investigation and dynamic site response analyses should be performed.

Table 9: Proposed values for short period site amplification factor F_s

Site class	S_{sRP} (maximum response spectral acceleration at short period on site class A in g)					
	S_{sRP}<0.25	S_{sRP}=0.25	S_{sRP}=0.5	S_{sRP}=0.75	S_{sRP} =1.0	S_{sRP} ≥1.25
A	1.00	1.00	1.00	1.00	1.00	1.00
B1	1.30	1.30	1.20	1.20	1.20	1.20
B2	1.40	1.30	1.30	1.20	1.10	1.10
C1	1.70	1.60	1.40	1.30	1.30	1.20
C2	1.60	1.50	1.30	1.20	1.10	1.00
C3	1.80	1.60	1.40	1.20	1.10	1.00
D	2.20	1.90	1.60	1.40	1.20	1.00
E	1.70	1.60	1.60	1.50	1.50	1.50
X	-	-	-	-	-	-

Table 10. Proposed values for intermediate period site amplification factor F_1

Site class	S_{sRP} (maximum response spectral acceleration at short period on site class A in g)					
	S_{sRP}<0.25	S_{sRP}=0.25	S_{sRP}=0.5	S_{sRP}=0.75	S_{sRP} =1.0	S_{sRP} ≥1.25
A	1.00	1.00	1.00	1.00	1.00	1.00
B1	1.40	1.40	1.40	1.40	1.30	1.30
B2	1.60	1.50	1.50	1.50	1.40	1.30
C1	1.70	1.60	1.50	1.50	1.40	1.30
C2	2.10	2.00	1.90	1.80	1.80	1.70
C3	3.20	3.00	2.70	2.50	2.40	2.30
D	4.10	3.80	3.30	3.00	2.80	2.70
E	1.30	1.30	1.20	1.20	1.20	1.20
X	-	-	-	-	-	-

7 Implementation and Comparison of Site Amplification Models

The implementation of the methods described within this report into a seismic risk calculation software is critical to their deployment for application at any scale, be it municipal, national or regional. For the new European Seismic Hazard and Risk model the preferred calculation engine is the OpenQuake-engine (Silva et al., 2014; Pagani et al., 2014). This is an open source seismic hazard and risk calculation software developed by the Global Earthquake Model, which has found application across the globe, including previous European seismic hazard and risk assessments (Wössner et al., 2015). As an open software it has been possible to adapt the code to consider, and ultimately compare, the different site amplification approaches being presented in this report. Within the implementation there are several key requirements:

1. The parameterisation of the site must allow for categorical variables (such as Eurocode 8 site class, geological era etc.) in addition to the conventional quantitative parameters, such as V_{S30}
2. The methods should be feasible to implement at a regional scale providing that the input site parameters can be constrained at that scale.
3. Distinction should be made between site parameters that are measured and those that are inferred from proxies, with the capability to adjust the uncertainty accordingly.
4. The implementation should be compatible with the ground motion logic tree proposed within the SERA project (Weatherill et al., 2019b)

Whilst efforts are made to address the four requirements, it will be seen in due course that some new practical and theoretical challenges emerge when considering deployment of certain methods in this manner. What follows is a brief overview of the OpenQuake implementations for different approaches to site response for seismic risk in Europe, followed by a comparison of the different models for i) a scenario earthquake, and ii) seismic hazard curves for selected case study sites.

7.1 OpenQuake-engine implementations

7.1.1 Technical Considerations in the OpenQuake-engine implementation

The OpenQuake-engine adopts a modular approach to calculation of seismic hazard and risk, building on an object-oriented framework first explained in Field et al., (2003). In simpler terms, each component of the hazard and risk calculation, such as an earthquake source, a ground motion model, a vulnerability function etc, is represented by an object that holds both the attributes (e.g. for an earthquake rupture: magnitude, rake, geometry etc.) and associated methods/functions (e.g. calculation of distance to a site). This architecture facilitates the addition of new calculation features such as GMPEs, fragility/vulnerability functions etc., without the need to make substantial changes to the broader architecture of the engine; effectively a “plug and play” system.

At the time of writing work is underway to expand OpenQuake’s capabilities toward a more advanced site amplification calculator tailored more toward site-specific PSHA, including new logic tree models for epistemic uncertainty in site properties. Whilst it is hoped that such a calculator will greatly enhance the practice of site-specific seismic hazard assessment it cannot be applied on the spatial scale required for a European risk model, for which hundreds of thousands of sites, if not millions, may need to be considered within the calculation run.

The preferred approach for the current implementations is to enhance/expand the ground shaking intensity model (GSIM) objects to allow them to return amplified ground motion. A GSIM object describes the general framework for any GMPE, defining as attributes the list of required rupture,

distance and site parameters, and implementing two functions: `get_mean_and_stddevs`, which returns the mean and standard deviation of the logarithm of the ground motion from a single rupture at a given set of sites, and `get_poes` which determined the probability of exceeding specified levels of ground shaking given the logarithmic mean and standard deviation of the ground motion. To implement the site amplification methods we implement a "MetaGSIM", an object that behaves in exactly the same manner as a GSIM, but acting as a wrapper around another GSIM object to modify its outputs ground motions before then returning the modified outputs in the same format as the GSIM itself. This relatively simple approach means that amplification models can be implemented in the same manner as an ordinary GMPE, with the only additional requirement being that the choice of GMPE around which the MetaGSIM will wrap can be specified by the user.

Fortunately, recent enhancements of OpenQuake have made the deployment of MetaGSIM objects much easier. These include changes in the logic tree syntax that allow the user to pass additional configuration parameters the selected ground motion models, which in the past would have required hard coding, as well as simplification of the procedure for adding of new site parameters to the calculator. A comparison of a conventional logic tree syntax and the enhanced syntax for MetaGSIM (now site amplification) application is shown in Figure 44.

```
<?xml version="1.0" encoding="UTF-8"?>

<nrml xmlns:gml="http://www.opengis.net/gml"
      xmlns="http://openquake.org/xmlns/nrml/0.4">
    <logicTree logicTreeID='lt1'>
<!-- 1.0 Logic Tree for Active Shallow Crust -->
        <logicTreeBranchingLevel branchingLevelID="bl1">
            <logicTreeBranchSet uncertaintyType="gmpeModel"
                                branchSetID="Active Shallow"
                                applyToTectonicRegionType="Shallow Crust">

                <logicTreeBranch branchID="AkkarBommer2010">
                    <uncertaintyModel>AkkarBommer2010</uncertaintyModel>
                    <uncertaintyWeight>0.35</uncertaintyWeight>
                </logicTreeBranch>

                <logicTreeBranch branchID="CauzziFaccioli2008">
                    <uncertaintyModel>CauzziFaccioli2008</uncertaintyModel>
                    <uncertaintyWeight>0.35</uncertaintyWeight>
                </logicTreeBranch>

                <logicTreeBranch branchID="ChiouYoungs2008">
                    <uncertaintyModel>ChiouYoungs2008</uncertaintyModel>
                    <uncertaintyWeight>0.20</uncertaintyWeight>
                </logicTreeBranch>

                <logicTreeBranch branchID="ZhaoEtAl2006Asc">
                    <uncertaintyModel>ZhaoEtAl2006Asc</uncertaintyModel>
                    <uncertaintyWeight>0.10</uncertaintyWeight>
                </logicTreeBranch>
            </logicTreeBranchSet>
        </logicTreeBranchingLevel>
    </logicTree>
</nrml>
```

```
<?xml version="1.0" encoding="utf-8"?>
<nrml
xmlns="http://openquake.org/xmlns/nrml/0.5"
xmlns:gml="http://www.opengis.net/gml"
>
    <logicTree
    logicTreeID="LT1"
    >
        <logicTreeBranchingLevel
        branchingLevelID="SetOfMetaGSIMs"
        >
            <logicTreeBranchSet
            applyToTectonicRegionType="Active Shallow Crust"
            branchSetID="SiteAmplificationModels"
            uncertaintyType="gmpeModel"
            >
                <logicTreeBranch
                branchID="AmpModel1"
                >
                    <uncertaintyModel>
                        [AmplificationModel1]
                        gmpe_name = "KothaEtAl2019SERA"
                        another_argument = 12345.6789
                    </uncertaintyModel>
                    <uncertaintyWeight>
                        0.5
                    </uncertaintyWeight>
                </logicTreeBranch>
                <logicTreeBranch
                branchID="AmpModel2"
                >
                    <uncertaintyModel>
                        [AmplificationModel2]
                        gmpe_name = "KothaEtAl2019SERA"
                        another_argument = -12345.6789
                        [AmplificationModel2.nested_argument]
                        'PGA' = 0.123
                        'SA(0.2)' = 0.456
                        'SA(1.0)' = 0.789
                    </uncertaintyModel>
                    <uncertaintyWeight>
                        0.5
                    </uncertaintyWeight>
                </logicTreeBranch>
            </logicTreeBranchSet>
        </logicTreeBranchingLevel>
    </logicTree>
</nrml>
```

Figure 44: Conventional syntax for describing a ground motion logic tree using multiple GMPEs (left) and enhanced syntax for application to MetaGSIMs (right)

7.1.2 Site Amplification According to Design Code Factors

Whilst a majority of ground motion models include a site amplification term (usually based on V_{S30}), which can be used directly within a risk calculation, an alternative approach in seismic risk analysis could be to use design code amplification factors themselves. This has some advantages for regional scale application as it may be sufficient only to parameterise the site in terms of the design code class, and it may inherit some aspects of the design code amplification factors that are calibrated upon strong motions simulations and not necessarily just on data, such as nonlinearity. For this purpose, we introduce three amplification models that can take ordinary ground motion models as inputs and apply the amplification factors according to a *design code* style application: i) Amplification factors based on the new generation Eurocode 8 for the case when the site properties ($V_{S,H}$ and H_{800}) are known, ii) Amplification factors based on the new generation Eurocode 8 for the case when only the site class is

known (i.e. the default factors), iii) Amplification factors proposed by Pitilakis et al., (2018) for application to their site classification schema (called EC8-P18 hereafter) adopting the next generation Eurocode design spectrum definition.

Each of the three methods works in a similar fashion, with the user defining the preferred ground motion model for calculation of seismic hazard on the reference rock site (taken as V_{S30} = 800 m/s as the default, but configurable by the user if necessary). The logarithmic mean of the ground motion is then calculated for the S_S and the S_1 (i.e. Sa(1.0 s)) term. It should be noted that the S_S term of Eurocode 8 describes the effective peak of the acceleration spectrum, but Eurocode 8 does not prescribe a particular spectral period at which this occurs. This potentially deliberate ambiguity means that we do not determine S_S from a given spectral acceleration (such as Sa (0.2 s)), but recognising that Eurocode 8 also indicates that the effective peak of the spectrum should be 2.5 times greater than the high frequency limit of the spectrum we instead determine S_S to be $2.5 \times PGA$. With S_S and S_1 determined for V_{S30} 800 m/s the amplification factors are then determined and corresponding design code spectrum constructed to then return the mean ground motion at the spectral period desired by the user.

There are two theoretical caveats to this approach, which do not prevent implementation but should be taken into consideration when interpreting the results. The first, and most important, is the implied aleatory variability in the amplified ground motion. The design code amplification factors do not provide an uncertainty in the amplification factor, and are in that sense deterministic. Rather than attempting to assign and propagate amplification uncertainties, the logarithmic standard deviation output from the ground motion model is taken as the standard deviation of the original ground motion model at the desired spectral period of interest. It is hoped that this would provide an equivalence (in terms of aleatory variability) to the approach of calculating hazard on the "rock" site class and applying the deterministic code factors *a posteriori*.

The second caveat is that no explicit consideration is given to the joint distribution of PGA and Sa (1.0). The term explicit is used here because there is a fundamental difference between this approach and the conventional application of the design code amplification factors to the uniform hazard spectrum (UHS). In the UHS it is the probability of exceedance of S_S and S_1 that is uniform, meaning that the controlling scenarios will likely differ. In the MetaGSIM approach here, PGA and Sa (1.0) are generated from the same scenario for each earthquake and potential conditional dependences are neglected, these include: i) the probability of the spectral acceleration on rock at 1.0 s taking or exceeding a particular value given the PGA on rock and the scenario $P(Sa_{ROCK}(1.0) \geq x_2 | PGA_{ROCK} = x_1, M, R)$, and ii) the probability of the spectral acceleration on soil at the desired period T taking or exceeding a certain value given the PGA, and Sa (1.0) on rock, $P(Sa_{SOIL}(T) \geq x_T | Sa_{ROCK}(1.0) = x_2, PGA_{ROCK} = x_1, M, R)$. In both cases, period-to-period correlation both in terms of the rock motion and the amplified motion would need to be captured. To explicitly account for these dependencies would require additional numerical integration over multiple conditional distributions, which would drastically increase computational time and render the process impractical at regional level.

7.1.3 Site amplification from generalised amplification models

An alternative to code-based amplification factors is the adoption of amplification models (both linear or nonlinear) from studies published in the literature (e.g. Choi & Stewart, 2005; Kamai et al., 2014; Seyen & Stewart; 2014 etc.). These approaches can provide a useful counterpoint to the design code approaches, as the amplification factors in the literature are derived empirically from data and/or simulations but are not tied to the design code shape. Additionally, most empirical models from the literature provide the uncertainty in the amplification factors explicitly, meaning that propagation of this uncertainty may be necessary.

Whilst many models appear in the literature, currently only one is implemented here for illustrative purposes, and that is the shallow crustal ground motion amplification model of Sandikkaya & Dinsever

(2018). As with the design code amplification factors, the MetaGSIM object is used in order to allow the user to specify the preferred GMPE for calculation on the reference rock, which in this case is V_{S30} 760 m/s rather than the 800 m/s of Eurocode 8. The general form of the Sandikkaya & Dinsever (2018) model is as follows:

$$\ln(Amp) = (b_1 + c_k)\ln\left[\frac{\min(V_{S30},1000)}{760}\right] + b_2 \ln z_1 + b_3 \ln\left[\frac{\exp\left(ln\left(Sa_{ROCK}(T)\right)+\eta_i\right)+0.1g}{0.1g}\right] \cdot \exp(-exp[b_4\, ln(V_{S30}) - b_5]) \quad [7.1]$$

Where b_1, b_2 and b_3 are period-dependent coefficients, b_4 and b_5 are period-independent coefficients fixed at 2.0 and 11 respectively, $z_1$the depth (m) to the 1.0 km/s shearwave velocity layer) and η_i the inter-event residual term from earthquake i (set to 0.0 in a PSHA calculation). Sandikkaya and Dinsever (2018) also explore regional variation in the linear amplification, and this is expressed in the parameter c_k, a regional parameter to modify the linear scaling term. The aleatory uncertainty of the amplification model is given by:

$$\sigma(Sa_{ROCK}(T), V_{S30}) = \sigma_s \cdot c_0 \cdot (c_1 \ln(Y_{sig}) + c_2 \ln(V_{sig})) \quad [7.2]$$

where $Y_{sig} = \max\left(\min\left(0.35, Sa_{ROCK}(T)\right), 0.005\right)$, $V_{sig} = \max(min(600, V_{S30}), 150))$ and σ_s, c_0, c_1 and c_2 are period-dependent coefficients.

The implementation of this model, which would be followed in other amplification models of the same nature, uses the user-selected GMPE to define the ground motion at the reference V_{S30} (Sa_{ROCK}(T)), before then applying equation 7.1 to determine the amplification factor which is then added to the logarithmic mean of the ground motion.

The uncertainty in the site amplification model should be integrated into the total aleatory uncertainty according to:

$$\sigma_T(T) = \sqrt{\eta_i^2(T) + \phi_0^2(T) + \sigma(Sa_{ROCK}(T), V_{S30})^2} \quad [7.3]$$

Where $\phi_0^2(T)$ is the site-corrected within event residual term. Whilst some GMPEs, including Kotha et al. (2019), define the site-corrected within-event residual explicitly, not all GMPEs do and this has not become a mandatory parameter for existing GMPEs in OpenQuake. In light of both this and the emerging trend of adopting common aleatory uncertainty models across many GMPEs, the user is given the option of specifying $\phi_0^2(T)$ for the desired GMPE in the logic tree file. If absent, a default value will be taken as 0.85 multiplied by the existing within-event standard deviation of the GMPE.

7.1.4 Site amplification from inferred proxy models for Europe

The final family of models to be implemented is more directly linked with the GMPE logic tree being selected for the 2020 European Seismic Hazard Model. As described in Chapter 5, depending on the approach finally adopted the European site amplification model may be based upon either the use of a regional V_{S30} model inferred from proxies, or a slope and geology based amplification model. In contrast to the design code approach, or to the generalised amplification model approach, the proxy-based amplification models are explicitly tied to the GMPE selection adopted within the ground motion logic tree. The key requirements here are the ability to distinguish between inferred and measured V_{S30}, thus adjusting the uncertainty accordingly, and the capacity to define new site terms (e.g. geology). The latter is easily added into the calculation via the site model input file. An example definition of the site model characterisation for a site whose properties are inferred from proxy data is given below:

```
<?xml version="1.0" encoding="utf-8"?>
<nrml xmlns="http://openquake.org/xmlns/nrml/0.5"
      xmlns:gml="http://www.opengis.net/gml">
    <siteModel>
```

```
        <site geology="CENOZOIC" lat="40.675" lon="22.938" slope="0.012431"
vs30="314.1" vs30Type="inferred"/>
        <site geology="HOLOCENE" lat="40.672" lon="22.942" slope="0.026859"
vs30="314.2" vs30Type="inferred"/>
        <site geology="HOLOCENE" lat="40.669" lon="22.946" slope="0.026859"
vs30="471.1" vs30Type="inferred"/>
...
    </siteModel>
</nrml>
```

OpenQuake has always had as a configurable site option the term vs30Type, which switches between measured or inferred. This was previously applied in NGA West 2 models that made such a distinction and it used here again as a primary classifier to determine which sites should be assigned a given aleatory uncertainty model. Slope must always be define in terms of m/m, and V_{S30} m/s. The introduction of the categorial geology parameter allows the user to input the geological era to which the site is assigned. As a note of warning, however, this must always be implemented in upper case and correspond to the geology types for which the amplification model is applied, which in this case are: PRECAMBRIAN, PALEOZOIC, MESOZOIC, CENOZOIC, PLEISTOCENE and HOLOCENE. As a small number of other units can be found in Europe, for those sites either unclassified or not classified to one of these six categories, the fixed effects part of the amplification model will be applied without the geological adjustments.

7.2 Comparison of models – scenario earthquake

A preliminary comparison of the degree of amplification predicted by the different models for different site conditions can be made using scenario earthquakes. In this example two scenarios are considered: i) a M_W 6.5 strike-slip earthquake recorded at a Joyner-Boore distance of 12.5 km, and ii) a M_W 5.0 strike-slip earthquake recorded at the same distance. The spectral period range considered is from 0.015 s to 3 s. Seven different amplification models are compared each using the Kotha et al., (2019) shallow crustal GMPE as the input for ground motion on rock:

1. Pitilakis et al., (2018) design code amplification
2. Eurocode 8 amplification for the case in which $V_{S,H}$ and H_{800} are known
3. Eurocode 8 amplification for the "default" (i.e. $V_{S,H}$ and H_{800} are unknown)
4. Sandikkaya & Dinsever (2018) empirical nonlinear amplification model dependent on V_{S30} and depth to the 1 km/s velocity layer ($Z_{1.0}$)
5. Kotha et al. (2019) empirical linear amplification model for the case in which V_{S30} is measured
6. Kotha et al., (2019) empirical linear amplification model for the case in which V_{S30} is inferred
7. Slope and geology empirical linear amplification model

Small differences in site classification are present between the models, e.g. Pitilakis et al. (2018) classification versus the Eurocode 8 classification, use of $Z_{1.0}$ or h_{800} etc., therefore a set of site conditions are proposed in Table 11 to try to capture the different subclasses within the main Eurocode 8 classification depending on the depth to the bedrock. As the Sandikkaya & Dinsever (2018) model uses depth to the 1 km/s layer rather than 800 m/s a relation between the two was sought using the Kiknet site profiles. Though the distribution is strongly censored, with the majority of sites reporting $h_{800} = Z_{1.0}$ when the shallowest bedrock layer has $V_S \geq 1000$ km, the modal difference for those sites with differing values was found to be around 12.5 m. It could be argued that the two may be used interchangeably, and the difference is trivial for the comparisons being undertaken here, nevertheless we offset the $Z_{1.0}$ values to be 12.5 m deeper than h_{800}.

Table 11: Site conditions assumed in the comparison studies

Eurocode 8 Site Class	Pitilakis et al. (2018) Site Class	VS30 (m/s)	H800 (m)	Z1.0 (m)
A	A	800	0.	12.5
B	B1	700	15.0	27.5
B	B2	600	50.	62.5
B	C1	500	120.	132.5
C	C2	400	30.	42.5
C	C3	300	80.	92.5
D	D	250	35.	47.5
D	D	200	80.	92.5
E	E	180	20.	32.5

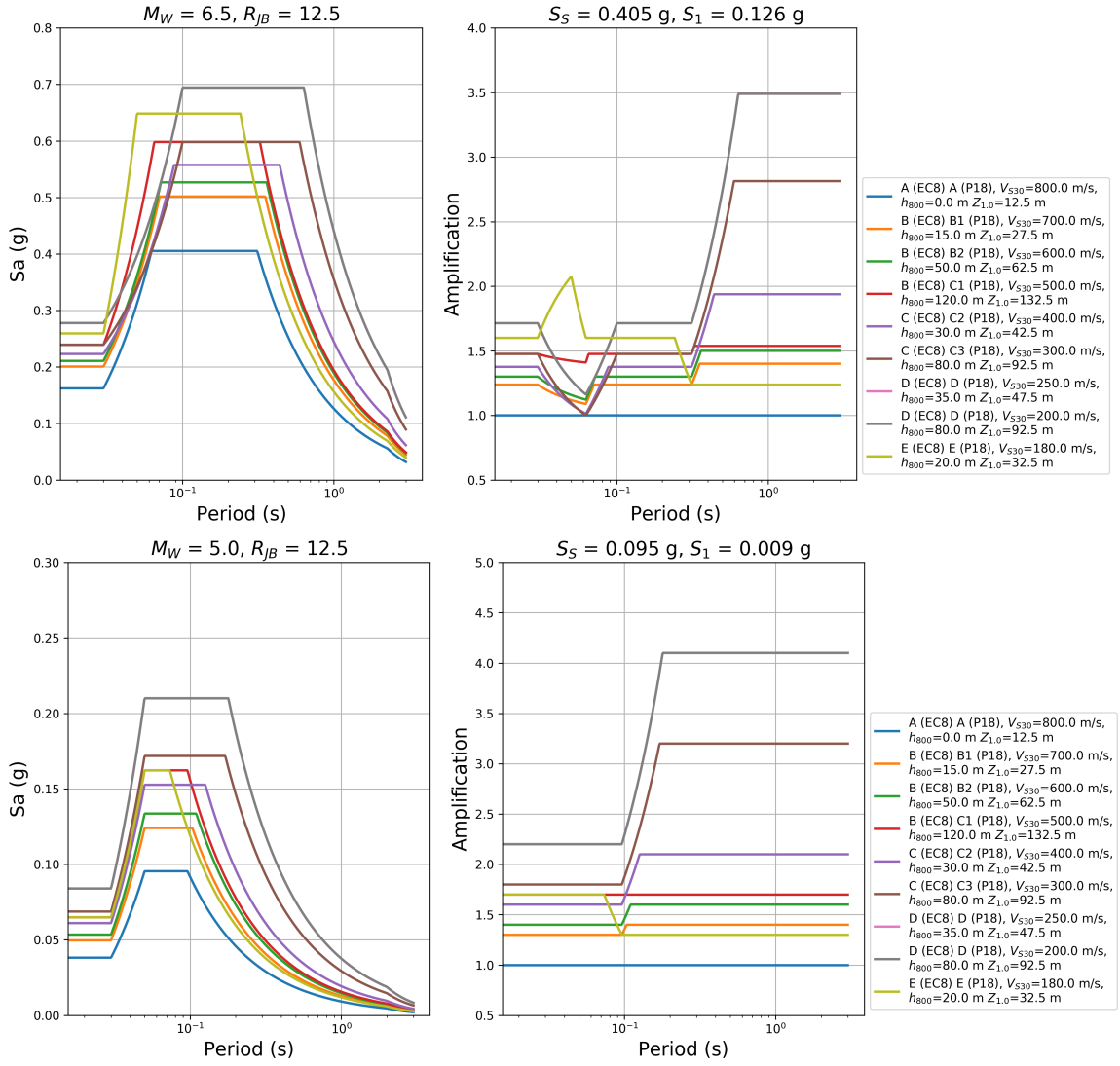

Figure 45: Comparison of scenario spectra (left) and amplification with respect to Eurocode 8 class A rock (V_{S30} 800 m/s, h_{800} 0 m) using the Pitilakis et al. (2018) model, for the M_W 6.5 scenario (upper) and M_W (5.0) scenario (lower)

The comparison between the Pitilakis et al. (2018) amplification model (Figure 45) and that of Eurocode 8 for the known site properties (Figure 46) indicates a substantially greater amplification on thick soil layers (type D) at intermediate-to-long periods compared to that of Eurocode 8. This is even more pronounced in the case of weaker rock motion for the M_W 5.0 scenario. The behaviour of site E for the larger rock acceleration scenario in the T_A to T_C range is somewhat unusual, but may represent a case of limited soil damping due to the thinness of the soil respect to the bedrock (see Table 7) resulting in higher amplification within a narrow period range. The default Eurocode 8 factors shown in Figure 47, whilst notably more conservative than the other Eurocode 8 case, do increase the amplification for the shallow sites, but obviously do not take into account longer period amplification on deep soils.

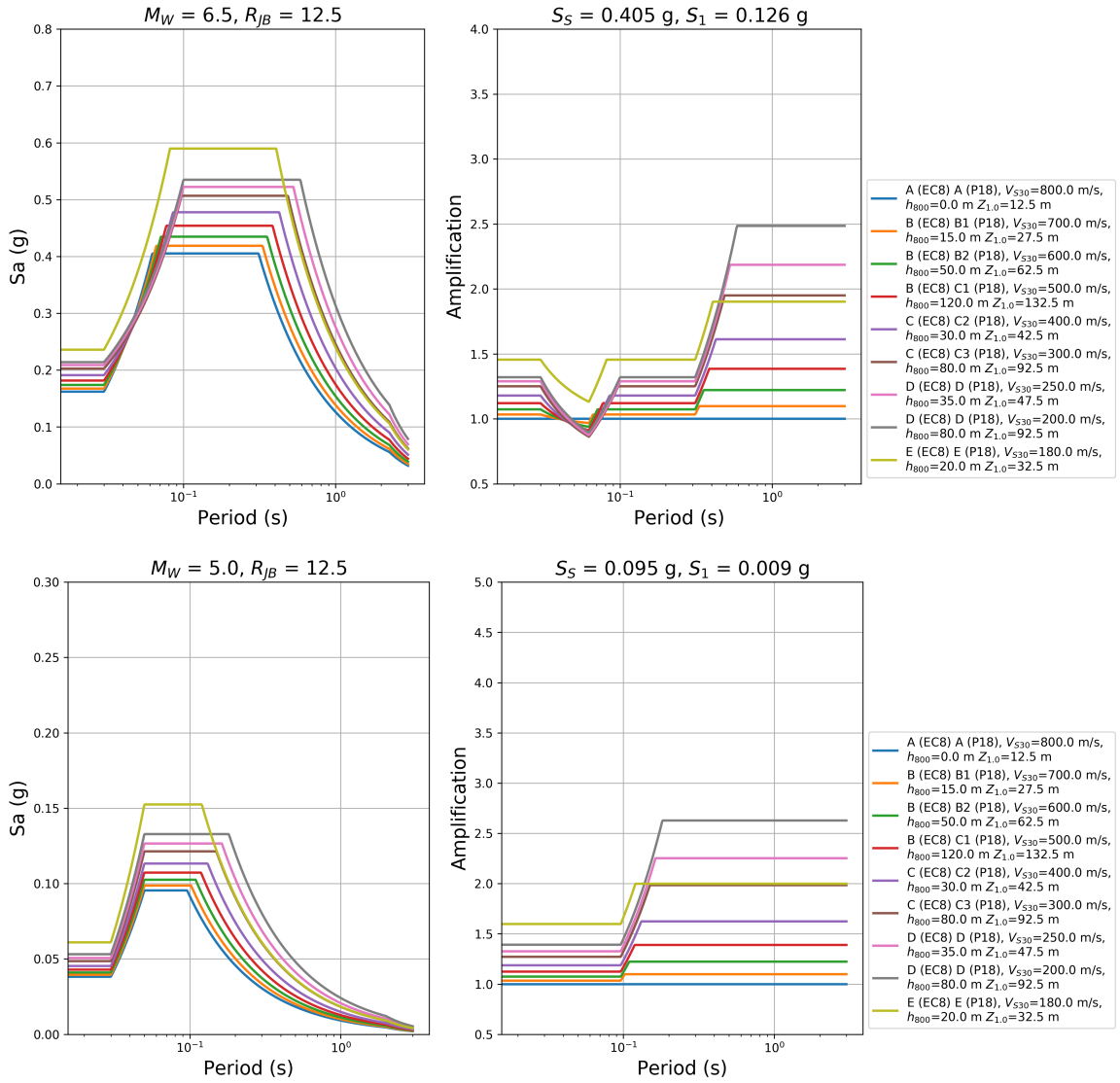

Figure 46: As Figure 45 using the Eurocode 8 model for the case when $V_{s,H}$ and H_{800} are known.

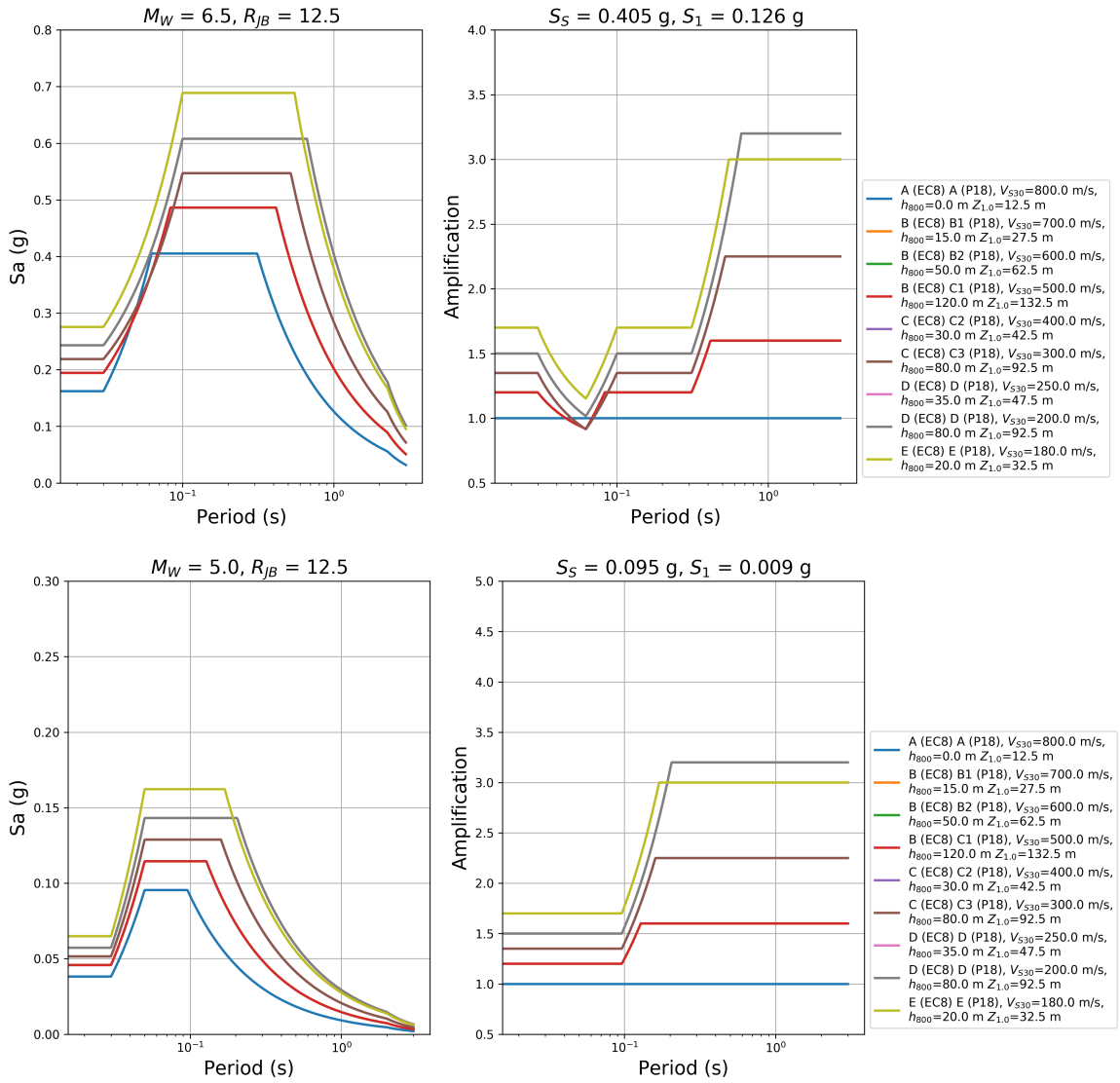

Figure 47: As Figure 45 using the Eurocode 8 model for the case when $V_{s,H}$ and H_{800} are unknown.

The Sandikkaya and Dinsever (2018) model (Figure 48) naturally reflects more the underlying shape of the GMPE spectrum but predicts the highest level of amplification with respect to the rock case, and over a broader period range. There does not appear to be a strong depth dependence, though we note that the b_2 coefficient was adjusted with respect to the values published in the paper due to some clearly erroneous depth scaling.

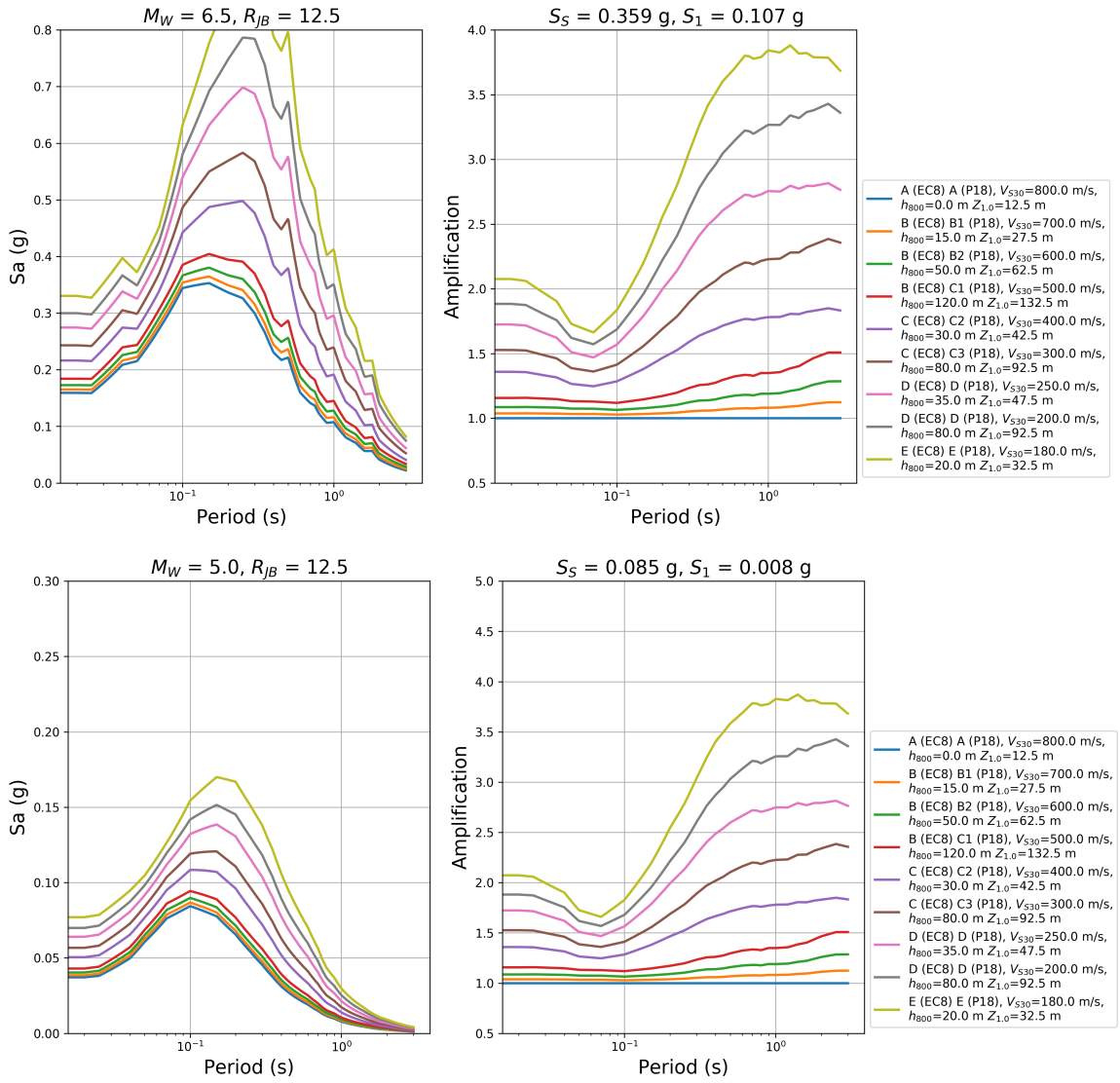

Figure 48: As Figure 45 using the Sandikkaya & Dinsever (2018) model

For the Kotha et al. (2019) GMPE in which the scaling with measured V_{S30} is assumed to follow a linear model (Figure 49), it can firstly be seen that the amplification is unaffected by the strength of rock shaking (as expected), and that the level of amplification is smaller overall. This suggests that the overall mean amplification is smaller based on the ESM $\delta S2S_S$ values than for the global amplification data set used in Sandikkaya & Dinsever (2018). This may reflect the influence from many factors such as the high degree of variability found in the observed $\delta S2S_S$ or the implicit differences in the reference rock conditions.

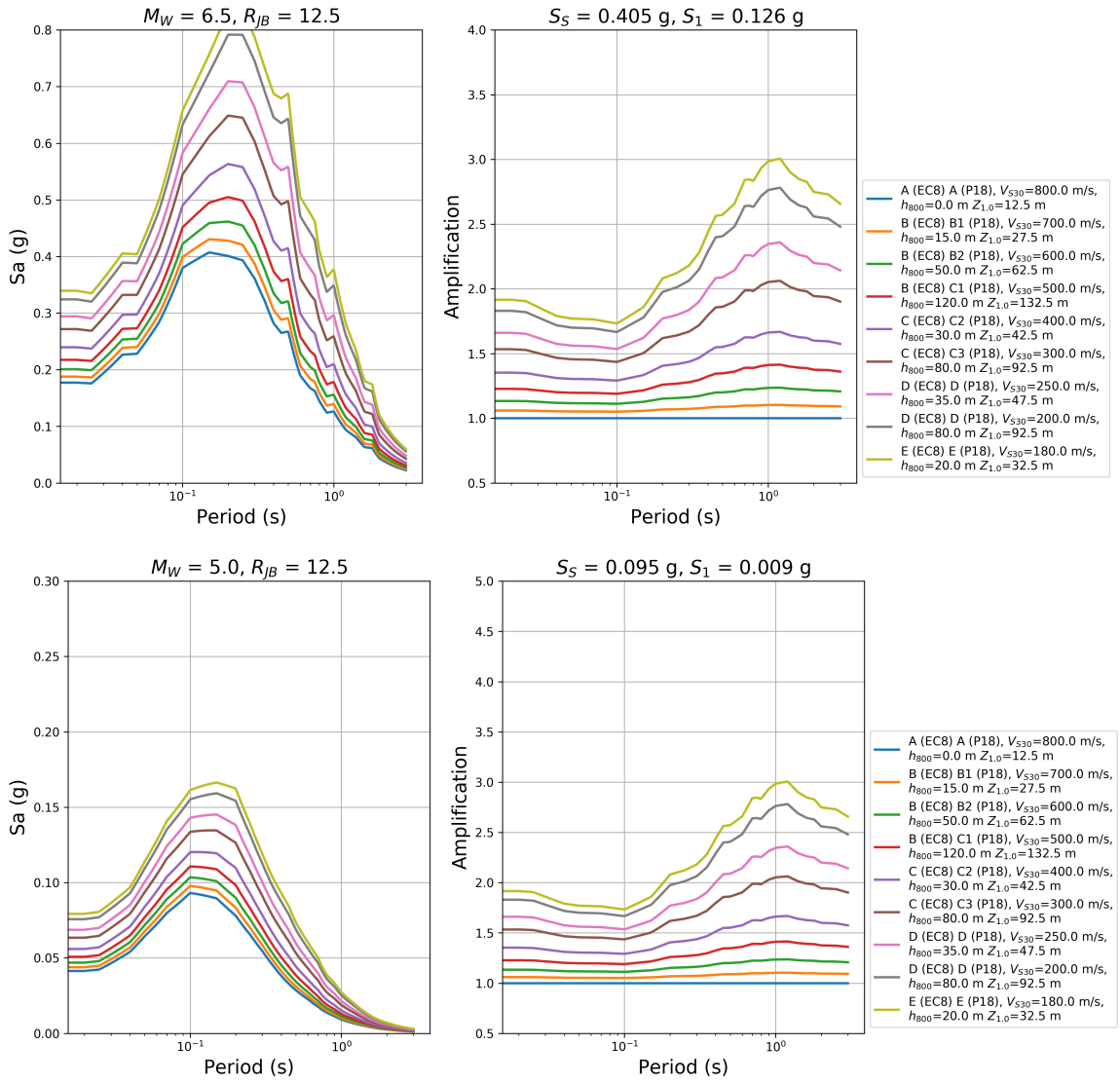

Figure 49: As Figure 45 using the measured V_{S30} site amplification model from the SERA GMPE

Finally, Figure 50 and Figure 51 show the implied amplification for the inferred V_{S30} model from the SERA ground motion model and for the slope + geology amplification respectively. Whilst it is difficult to compare the latter with the other models because of the contrasting difference in the definition of the reference, we find that defining amplification with respect to a site with a slope of 0.2 m/m on Precambrian rock gives a similar level of amplification as the inferred V_{S30} model with respect to a V_{S30} 800 m/s reference site. In both cases the expected amplification is smaller than the other models considered, which is due to the slightly weaker scaling of $\delta S2S_S$ with the inferred site properties.

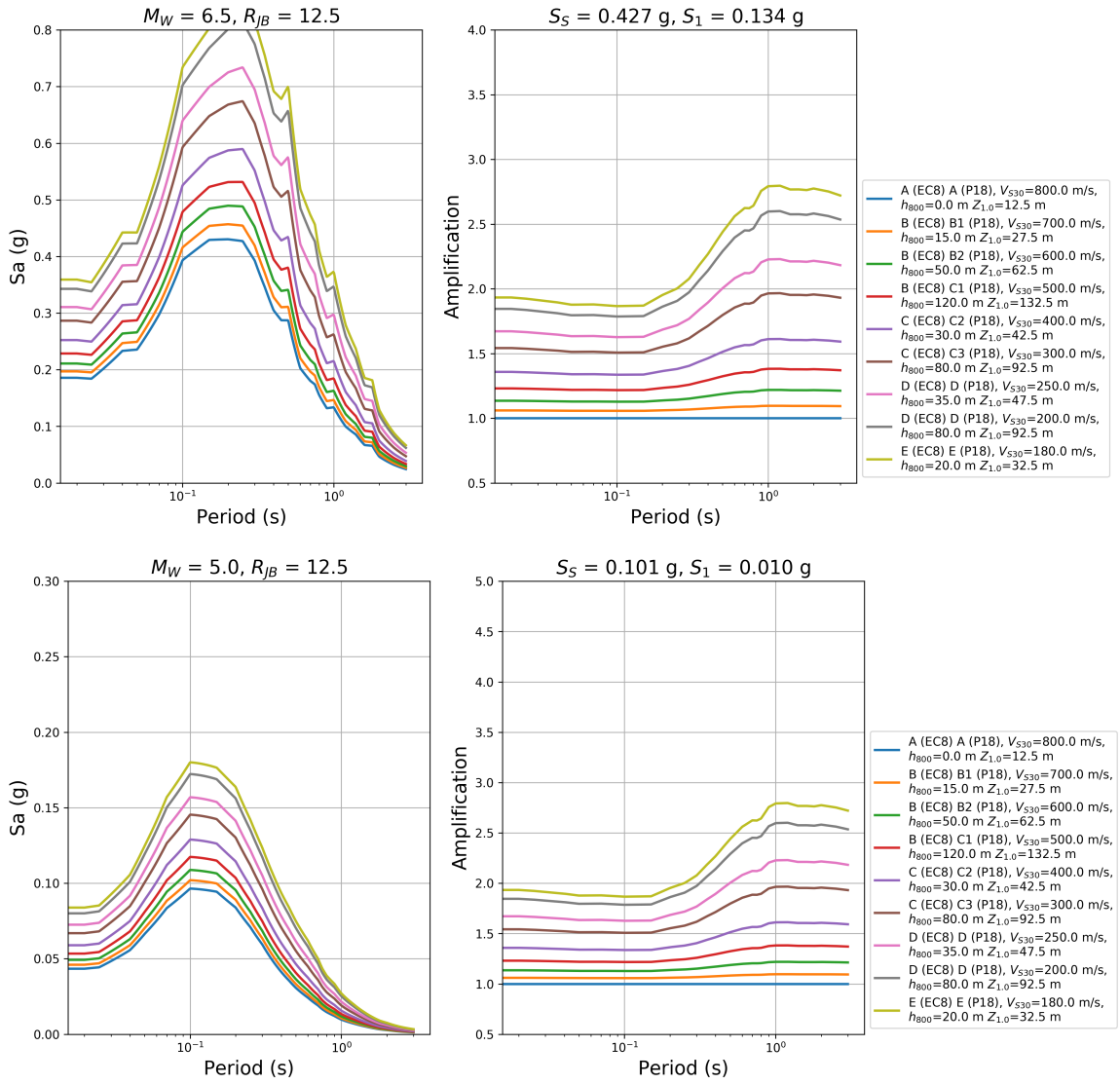

Figure 50: As Figure 45 for the inferred site amplification model from the SERA GMPEs

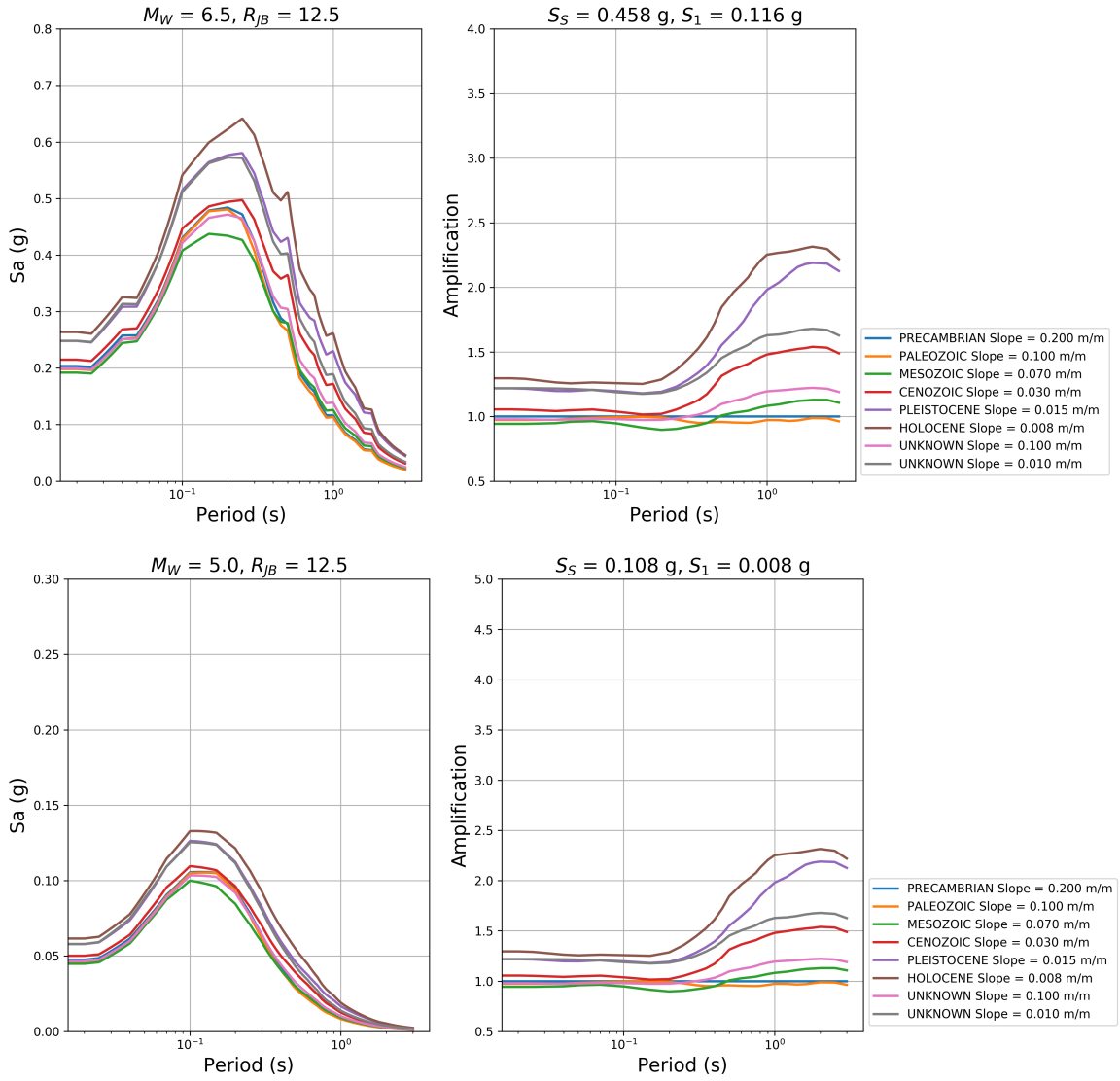

Figure 51: As Figure 45 for the slope + geology amplification model, with amplification given with respect to a site of slope 0.2 m/m on Precambrian rock

7.3 Comparison of models – PSHA

Whilst the scenario comparisons can provide some indication of the expected level of amplification from each model, a more insightful comparison can be made by applying them in a PSHA calculation. The hazard context is important because it incorporates not only the amplification factors themselves but also their respective uncertainties, the comparative influence of which is not necessarily intuitive. This is particularly important when considering the potential consequences in terms of hazard (and ultimately risk) of adopting simplified proxies for site characterisation and tolerating a higher level of aleatory variability (as discussed in Chapter 5).

For the purposes of a seismic hazard comparison we consider sites from a case study application: Thessaloniki. A detailed microzonation of the city was undertaken by Anastasiadis et al. (2001), and from this seismic zonations in terms of Eurocode 8 site class and Pitilakis et al., (2018) site class have been constructed (see Figure 52). Additionally, V_{S30} and h_{800} measurements have been made for over 250 sites across the metropolitan region. This data is then supplemented with site observations from regional databases, including the Wald & Allen (2007) inferred V_{S30}, topographic slope and geology.

Assignments of the Eurocode 8 and Pitilakis et al. (2018) site classes to the 250 sites is done on the basis of the location of the site with respect to the polygons shown, and do not necessarily indicate a direct assignment based on measurement of the site itself.

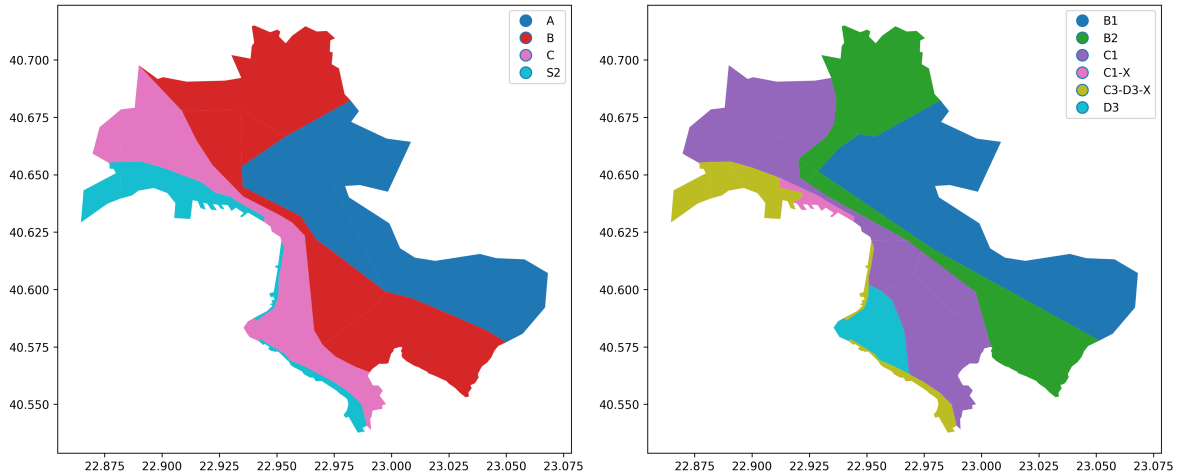

Figure 52: Microzonation for Thessaloniki in terms of Eurocode 8 site class (left) and Pitilakis et al., (2018) classification (right)

Using the ESHM2013 seismic source model, PSHA calculations are undertaken for over 250 sites around the city. Seismic hazard maps are not produced at this juncture as the objective is to understand the potential influence of the different amplification models, and a proportion of sites are assigned to classes for which no amplification model is indicated by either Eurocode 8 or Pitilakis et al. (2018) as they would require special investigation (e.g. very soft soils, high water table etc.). Instead Figure 53 to Figure 55 show the seismic hazard curves for selected sites that are representative of the typical geological and geotechnical conditions encountered in Thessaloniki itself: i) stiff soil (soft rock) (EC8 class B) on a Cenozoic formation (Figure 53), ii) soft rock of intermediate thickness on a Holocene formation (Figure 54), and iii) soft rock of larger thickness on a Holocene formation (Figure 55). Once again, seven models are compared including the three design code spectra (Eurocode 8, Eurocode 8 Default and Pitilakis et al., 2018), the nonlinear empirical amplification model of Sanikkaya & Dinsever (2018) and the built in site amplification models for the Kotha et al., (2019) GMPE for measured V_{S30}, inferred V_{S30} (Wald & Allen,2007) and slope + geology.

For the stiff soil on Cenozoic formation (Figure 53) all seven of the models give a reasonable agreement with only the Sandikkaya & Dinsever (2018) model indicating a lower hazard at short return periods. The slope plus geology form of the SERA ground motion model gives values close to Sandikkaya & Dinsever (2018) at the 1 second spectral period, making it slightly lower than the design code models. Both this and the inferred V_{S30} model seem to agree well in the hazard curves with the design code amplifications despite giving lower amplifications within the scenarios. This may require further investigation; however, it may be indicative of the competing influence of the higher aleatory uncertainty for the inferred V_{S30} and slope+geology models compared to those of design codes, for which no additional uncertainty is added.

For the two Holocene sites (Figure 54 and Figure 55) differences do emerge, though overall it could be argued that the range of hazard outcomes remains relatively well constrained. On the intermediate thickness formation (Figure 54) the higher aleatory uncertainty of the inferred V_{S30} and slope+geology methods is more visible in the form of the flatter seismic hazard curves. For shorter periods, however, there is good agreement between these and the other models for the range of annual probabilities of

exceedance typically considered for design codes. At Sa (1.0 s) in fact the hazard is toward the higher end of the range, again reflecting the role of the increased uncertainty.

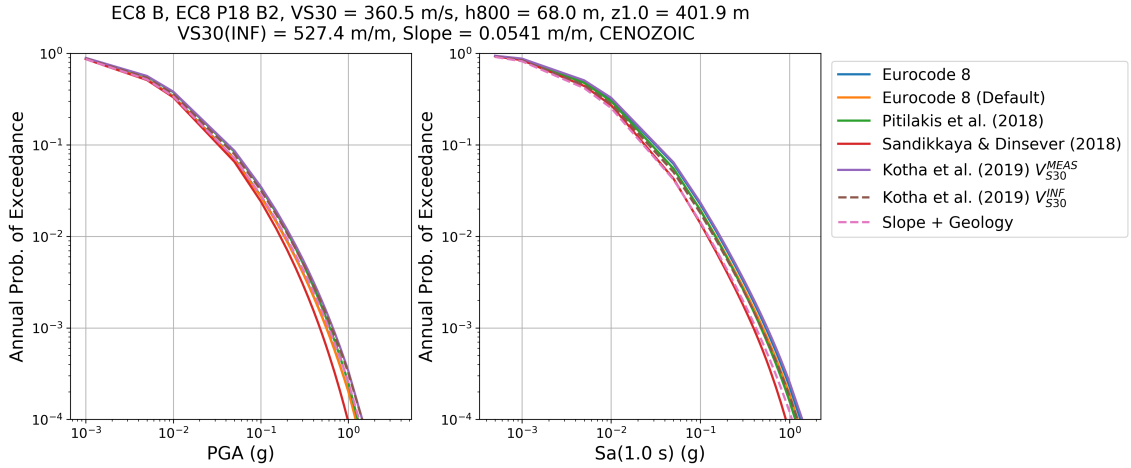

Figure 53: Comparison of seismic hazard curves for PGA (left) and Sa (1.0 s) right for the stiff soil Ceneczoic site.

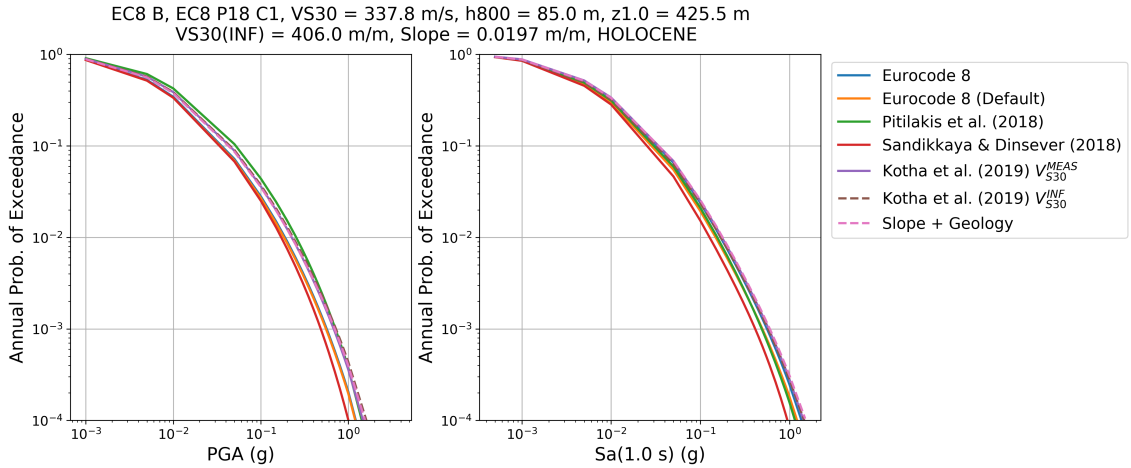

Figure 54: As Figure 53 for the intermediate thickness soft soil Holocene site

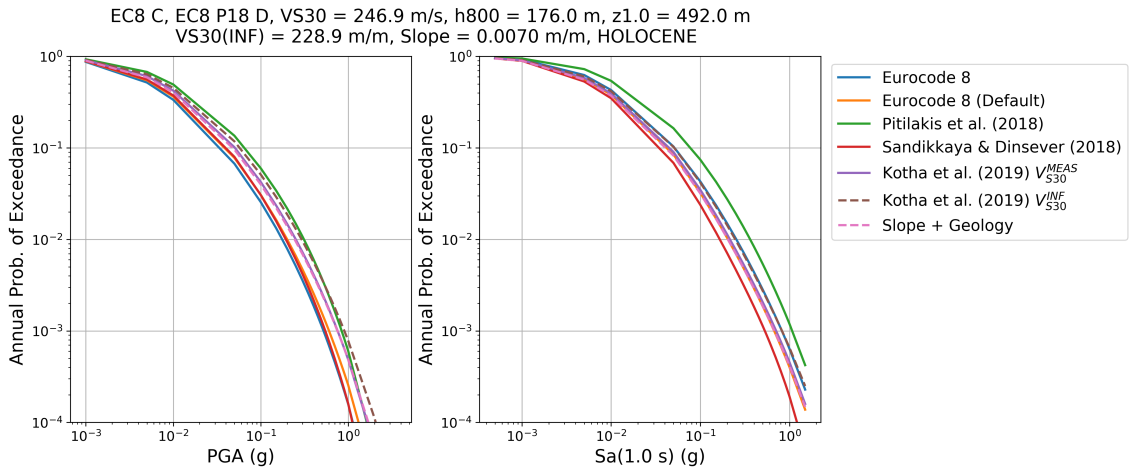

Figure 55: As Figure 53 for the deep soft soil Holocene site

For the thick, soft soil Holocene site (Figure 55) the divergence of the models is at its greatest, with the Pitilakis et al. (2018) model generally producing the highest hazard, the Sandikkaya & Dinsever (2018) model the lowest and the Eurocode 8 amplification models toward the middle. The inferred V_{S30} and slope+geology methods fall within the middle of the range, tending slightly toward the higher end. This clearly reflects the difference between the methods in terms of how they characterise deeper basin effects. It is notable, however, that those models that are explicitly absent a basin term fall within the middle of the range, suggesting that the aleatory variability may be capturing well the possible distribution of amplification function from both deep and shallow basins. However, as discussed in Weatherill et al. (2019) given that slope itself, and therefore inferred V_{S30}, is correlated with basin depth on soft soils an implicit basin amplification may be contained within these models.

The seismic hazard curve comparisons for Thessaloniki, though not necessarily indicative of the range of geological and geotechnical conditions across Europe, may provide some insights into the potential outcomes of a European site response model. The agreement not only between the various design methods themselves but also between the inferred vs. measured site properties would seem to imply that the additional uncertainty in the inferred V_{S30} or slope+geology model offsets, partially at least, the under-prediction of the expected value. A more important test, however, will need to be made in the risk domain, comparing the total losses across a region such as Thessaloniki under the different conditions, which will be facilitated by recent efforts to set up the components of a seismic risk model for Thessaloniki (Riga et al., 2019). Such tests can also potentially be extended to other test sites including Lisbon and Istanbul as part of Task 26.6 (Testing and Verification).

8 Conclusions

This deliverable has proposed methods to address site amplification within seismic risk assessments from local to continental (European) scale.

At the European scale, the following options are currently available for implementing site amplification within a probabilistic seismic risk assessment with the OpenQuake-engine:

- V_{S30} from the Wald & Allen (2007) approach (see Section 4.1) can be implemented using the *inferred* V_{S30} amplification model (see Section 5.1);
- V_{S30} from the Wald & Allen (2007) dataset can be used in conjunction with the geological units and implemented using the geologically-calibrated *inferred* V_{S30} amplification model (see Section 5.2);
- The 30 arc-second slope data can be used in conjunction with the geological units, to be implemented using the geologically-calibrated *slope* amplification model (see Section 5.3).

With future research, the following options could also be added to the list of methods:

- V_{S30} from a geological model (e.g. Vilanova et al., 2018) (see Section 4.2) could be implemented using an associated *inferred* V_{S30} amplification model (not yet developed);
- A new topographically inferred V_{S30} model could be derived and calibrated given the geological information for Europe.

It is clear that for further improvement of all of the above methods, and in particular the last one, it will be necessary to significantly extend the database of measured V_{S30} across Europe. Further research to develop a map of harmonised superficial geology at European scale would also be extremely beneficial.

At the local scale a nonlinear site amplification method has been proposed and implemented within the OpenQuake-engine. This approach should be implemented with a ground motion amplification model dependent on observed/measured V_{S30} (see Section 5.1). This model has been developed primarily for use in seismic design codes, but it could be revisited in the future to explicitly model and propagate the uncertainty in the amplification within a local scale risk assessment.

The different approaches proposed herein have been implemented within the OpenQuake-engine and some preliminary comparisons in terms of response spectra and hazard curves have been undertaken. An important activity for future research will be to extend these tests to the risk domain, which will fit well within the proposed activities of Task 26.6 (Testing and Verification) which is the focus of the last 12 months of the JRA4 work package.

9 Acknowledgements

The authors would like to acknowledge a number of researchers that have contributed to the work presented herein. The following attendees of the first site amplification meeting that took place in Pavia in September 2017 as well are the NA5/JRA4 meeting that took place in December 2018 in Thessaloniki are acknowledged for their input through presentations, feedback and discussions: Sinan Akkar, Pierre Yves Bard, Miriam Belvaux, Cecile Cornou, Laurentiu Danciu, Lucia Luzi, Donat Fäh, Abdullah Sandikkaya, Nikos Theodulidis. Finally, the following have provided data that has either contributed to the development of the methods or is being / has been used used in the tests: Donat Fäh (Basel case study data), Susana Vilanova (V_{S30} data for Portugal), Sinan Akkar and Mustafa Tolga Yilmaz (V_{S30} data for Turkey and Iran), Pauline Kruiver (V_{S30} data from Groningen) and Nikos Theodulidis (V_{S30} data from Greece).

10 References

Ahdi, S. K., Stewart, J. P., Ancheta, T. D., Kwak, D. Y., & Mitra, D. (2017). Development of VS Profile Database and Proxy-Based Models for VS 30 Prediction in the Pacific Northwest Region of North America. *Bulletin of the Seismological Society of America*, *107*(4), 1781-1801.

Akkar S., Sandikkaya M. A., Bommer J. J. (2014) "Empirical ground-motion models for point- and extended-source crustal earthquake scenarios in Europe and the Middle East", *Bulletin of Earthquake Engineering,* 12(1): 359 - 387

Allen T. I. and Wald D. J. (2009) "On the Use of High-Resolution Topographic Data as a Proxy for Seismic Site Conditions (V_{S30})", *Bulletin of the Seismological Society of America,* 99(2A): 935-943

Bates D., Mächler M., Bolker B.M., S. Walker S. C. (2015) "Fitting Linear Mixed-Effects Models Using lme4." *Journal of Statistical Software,* 67(1): doi:10.18637/jss.v067.i01.

Becker, J. J., Sandwell, D. T., Smith, W. H. F., Braud, J., Binder, B., Depner, J. L., ... & Ladner, R. (2009). Global bathymetry and elevation data at 30 arc seconds resolution: SRTM30_PLUS. *Marine Geodesy*, *32*(4), 355-371.

Bindi D., Massa M., Luzi L., Ameri G., Pacor F., Puglia R., Augliera P. (2014) "Pan-European ground-motion prediction equations for the average horizontal component of PGA, PGV and 5%-damped PSA at spectral periods up to 3.0 s using the RESORCE dataset", *Bulletin of Earthquake Engineering,* 12: 391 – 430

Boore D.M., Stewart J.P., Seyhan E., Atkinson G.M. (2014) "NGA-West2 Equations for Predicting PGA, PGV, and 5% Damped PSA for Shallow Crustal Earthquakes", Earthquake Spectra, 30(3):1057-1085.

BSSC (Building Seismic Safety Council). (2015) "NEHRP Recommended Seismic Provisions for New Buildings and Other Structures", FEMA P-1050-1/2015 Edition 2015.

CEN (2004) "Eurocode 8: Design of structures for earthquake resistance - Part 1: General rules, seismic actions and rules for buildings", European Standard EN 1998-1:2004.

Corbane C., Hancilar U., Ehrlich D., De Groeve T. (2017) "Pan-European seismic risk assessment: a proof of concept using the Earthquake Loss Estimation Routine (ELER)," *Bulletin of Earthquake Engineering*, 15(3): 1057-1083

Delavaud, E., Cotton, F., Akkar, S., Scherbaum, F., Danciu, L., Beauval, C., ... & Segou, M. (2012). Toward a ground-motion logic tree for probabilistic seismic hazard assessment in Europe. *Journal of Seismology*, *16*(3), 451-473.

Derras B., Bard P. -Y., Cotton F. (2014) "Towards fully data driven ground-motion prediction models for Europe", *Bulletin of Earthquake Engineering*, 12: 495 - 516

Di Capua, G., Peppoloni, S., Amanti, M., Cipolloni, C., & Conte, G. (2016). Site classification map of Italy based on surface geology. *Geological Society, London, Engineering Geology Special Publications*, *27*(1), 147-158.

Farr, T. G., & Kobrick, M. (2000). Shuttle Radar Topography Mission produces a wealth of data. *Eos, Transactions American Geophysical Union*, *81*(48), 583-585.

Farr, T. G., Rosen, P. A., Caro, E., Crippen, R., Duren, R., Hensley, S., ... & Seal, D. (2007). The shuttle radar topography mission. *Reviews of geophysics*, *45*(2).

Forte, G., Fabbrocino, S., Fabbrocino, G., Lanzano, G., De Magistris, F. S., & Silvestri, F. (2017). A geolithological approach to seismic site classification: an application to the Molise Region (Italy). *Bulletin of Earthquake Engineering*, *15*(1), 175-198.

Garofalo F., Foti S., Hollender F., Bard P.Y., Cornou C., Cox B.R., Ohrnberger Sicilia D., Asten M., Di Giulio G., Forbriger T., Guillier B., Hayashi K., Martin A., Matsushima S., Mercerat D., Poggi V., Yamanaka H. (2016). "InterPACIFIC project: Comparison of invasive and non-invasive methods for seismic site characterization. Part I: Intra-comparison of surface wave methods", *Soil Dynamics and Earthquake Engineering*, 82: 222-240.

Garofalo F., Foti S., Hollender F., Bard P.Y., Cornou C., Cox B.R., Dechamp A., Ohrnberger M., Perron V., Sicilia D., Teague D. Vergniault C. (2016). "InterPACIFIC project: Part II: Inter-comparison between surface-wave and borehole methods".*Soil Dynamics and Earthquake Engineering*, 82: 241-254.

Gehl P., Bonilla F., Douglas J. (2011) "Accounting for Site Characterization Uncertainties when Developing Ground Motion Prediction Equations", *Bulletin of the Seismological Society of America,* 101(3): 1101 – 1108

Iwahashi, J., & Pike, R. J. (2007). Automated classifications of topography from DEMs by an unsupervised nested-means algorithm and a three-part geometric signature. *Geomorphology*, *86*(3-4), 409-440.

Kotha S. R., Bindi D., Cotton F. (2016) "Partially non-ergodic region-specific GMPE for Europe and Middle-East", *Bulletin of Earthquake Engineering,* 14: 1245 - 1263

Kotha S. R., Weatherill G., Bindi D., Cotton F. (2019) "A Revised Ground-Motion Prediction Equation for Shallow Crustal Earthquakes in Europe and the Middle-East", *in preparation*

Kuehn N. and Abrahamson N. A. (2018) "The effect of uncertainty in predictor variables on the estimation of ground-motion prediction equations", *Bulletin of the Seismological Society of America,* 108(1): 358 – 370

Kwok O. L., Stewart J. P., Kwak D. Y., Sun P. L. (2018) "Taiwan-specific Model for V_{S30} Prediction Considering Between-Proxy Correlations", *Earthquake Spectra,* 34: 1973-1993

Lee, C. T., & Tsai, B. R. (2008). Mapping Vs30 in Taiwan. *TAO: Terrestrial, Atmospheric and Oceanic Sciences*, *19*(6), 6.

Lemoine, A., Douglas, J., & Cotton, F. (2012). Testing the applicability of correlations between topographic slope and vs 30 for Europe. *Bulletin of the Seismological Society of America*, *102*(6), 2585-2599.

Luzi L, Puglia R, Russo E & ORFEUS WG5 (2016a). Engineering Strong Motion Database, version 1.0. Istituto Nazionale di Geofisica e Vulcanologia, Observatories & Research Facilities for European Seismology. doi: 10.13127/ESM

Luzi, L., Puglia, R., Russo, E., D'Amico, M., Felicetta, C., Pacor, F., et al. (2016b). The Engineering Strong-Motion Database: A Platform to Access Pan-European Accelerometric Data. *Seismological Research Letters*, *87*(4), 987–997. http://doi.org/10.1785/0220150278

McPherson, A., & Hall, L. (2013). Site classification for earthquake hazard and risk assessment in Australia. *Bulletin of the Seismological Society of America*, *103*(2A), 1085-1102.

Noorlandt, R., Kruiver, P. P., de Kleine, M. P., Karaoulis, M., de Lange, G., Di Matteo, A., ... & Bommer, J. J. (2018). Characterisation of ground motion recording stations in the Groningen gas field. *Journal of seismology*, *22*(3), 605-623.

Pitilakis K., Gazepis C., Anastasiadis A. (2004) :Design response spectra and soil classification for seismic code provisions", In: Proceedings of 13th World Conference on Earthquake Engineering, paper n. 2904, Vancouver, B.C., Canada

Pitilakis K., Gazepis C., Anastasiadis A. (2006) "Design response spectra and soil classification for seismic code provisions", In: Proceedings of geotechnical evaluation and application of the seismic Eurocode EC8 2003-2006, ETC-12 Workshop, NTUA Athens, pp. 37-52

Pitilakis K., Riga E., Anastasiadis A. (2013) "New code site classification, amplification factors and normalized response spectra based on a worldwide ground-motion database", Bulletin of Earthquake Engineering,11(4):925–966

Pitilakis, K., Riga, E., Anastasiadis, A., Fotopoulou, S., Karafagka, S. (2018) "Towards the revision of EC8: Proposal for an alternative site classification scheme and associated intensity dependent spectral amplification factors", Soil Dynamics and Earthquake Engineering, https://doi.org/10.1016/j.soildyn.2018.03.030

Riga E., Fotopoulou S., Karatzetzou A., Apostolaki S., Ntafloukas K., Pitilakis K. (2019) "Towards the development of a seismic risk model for Greece," Proceedings of 2nd International Conference on Natural Hazards and Infrastructure, Chania, Greece.

Roullé, A., Auclair, S., Dewez, T., Hohmann, A., Lemoine, A., & Rey, J. (2010). Cartographie automatique des classes de sol à l'échelle régionale à partir d'un modèle numérique de terrain ou de surface. Rapport final. BRGM/RP-58853-FR.

Seyhan, E., & Stewart, J. P. (2014). Semi-empirical nonlinear site amplification from NGA-West2 data and simulations. *Earthquake Spectra*, *30*(3), 1241-1256.

Stafford P. J. (2014) "Crossed and Nested Mixed-Effects Approaches for Enhanced Model Development and Removal of the Ergodic Assumption in Empirical Ground-Motion Models", *Bulletin of the Seismological Society of America,* 104(2): 702-719

Stewart, J. P., Klimis, N., Savvaidis, A., Theodoulidis, N., Zargli, E., Athanasopoulos, G., ... & Margaris, B. (2014). Compilation of a local VS profile database and its application for inference of VS 30 from geologic-and terrain-based proxies. *Bulletin of the Seismological Society of America*, *104*(6), 2827-2841.

Thompson E. M., Wald D. J., Worden C. B. (2014) "A V_{S30} Map for California with Geological and Topographic Constraints", *Bulletin of the Seismological Society of America,* 104: 2313-2321

Vilanova, S. P., Narciso, J., Carvalho, J. P., Lopes, I., Quinta-Ferreira, M., Pinto, C. C., ... & Nemser, E. S. (2018). Developing a Geologically Based VS 30 Site-Condition Model for Portugal: Methodology and Assessment of the Performance of Proxies. *Bulletin of the Seismological Society of America*, *108*(1), 322-337.

Wald D. J. and Allen, T. I. (2007) "Topographic Slope as a Proxy for Seismic Site Conditions and Amplification", *Bulletin of the Seismological Society of America*, 97: 1379-1395

Weatherill G. W., Kotha S. R., Cotton F. (2019a) "Re-thinking Site Amplification in Regional Seismic Risk Assessment", *Earthquake Spectra*, Submitted.

Weatherill G. W., Kotha S. R., Cotton, F., Bindi, D. (2019b) "D25.4 Updated GMPE Logic Tree and Rock/Soil Parameterisation for ESHM20", SERA Deliverable.

Wessel, P., and W. H. F. Smith, Free software helps map and display data, *EOS Trans. AGU*, 72(41), 445–446, 1991. doi:10.1029/90EO00319.Wills, C. J., & Clahan, K. B. (2006). Developing a map of geologically defined site-condition categories for California. *Bulletin of the Seismological Society of America*, *96*(4A), 1483-1501.

Wills CJ, Clahan KB (2006) "Developing a map of geologically defined site-condition categories for California," Bulletin of the Seismological Society of America 96:1483–1501

Woessner J., Danciu L., Giardini D., Crowley H., Cotton F., Grünthal G., Valensise G., Arvidsson R., Basili R., Demircioglu M. B., Hiemer S., Meletti C., Musson R. M. W., Rovida A. N., Sesetyan, K., Stucchi M., and The SHARE Consortium. 2015. "The 2013 European Seismic Hazard Model: Key Components and Results." *Bulletin of Earthquake Engineering* 13(12):3553–96.

Yenier E., Sandikkaya M.A., Akkar S. (2010) "Report on the fundamental features of the extended strong motion databank prepared for the SHARE project (v1.0)"

Yilmaz M.T., Ansari A., Harmandar E. (2014). "Simple geological categories as proxies to VS30 in Turkey and Iran. *Second European Conference on Earthquake Engineering and Seismology*, Istanbul August 25-29, 2014.

Zevenbergen L. W. and Thorne, C. R. (1987) "Quantitative Analysis of Land Surface Topography", *Earth Surface Processes and Landforms*, 12: 47-56

Contact

Project lead	ETH Zürich
Project coordinator	Prof. Dr. Domenico Giardini
Project manager	Dr. Kauzar Saleh
Project office	ETH Department of Earth Sciences

Sonneggstrasse 5, NO H62, CH-8092 Zürich

sera_office@erdw.ethz.ch

+41 44 632 9690

Project website www.sera-eu.org